Developments in the Chemistry of Stibine and Bismuthine Complexes

Victoria K. Greenacre, William Levason*, Gillian Reid

School of Chemistry, University of Southampton, Southampton SO17 1BJ, UK.

Abstract

New findings in the coordination chemistry of neutral stibine and bismuthine ligands are reviewed. The article describes new ligand syntheses, coordination complexes of d-block and p-block elements with halostibines, halobismuthines, tertiary monostibines, tertiary bismuthines, distibines and hybrid polydentates containing antimony or bismuth. Current views on the nature of the M-Sb(Bi) bonds based upon X-ray structural studies and DFT calculations are discussed. The new work distinguishing metal stibine complexes from the chemistry of lighter phosphorus or arsenic ligands including, μ^2- and μ^3-bridging stibines, hypervalency and the oxidation of metal-coordinated stibines to stiboranyl or stiborane complexes, is also presented. Emerging applications of metal stibine complexes in catalysis, as reagents for the deposition of electronic materials and as anion sensors are illustrated. Literature coverage is from 2006 - early 2020.

Keywords: antimony ligands; stibines; bismuthines; distibines; hypervalency, non-innocent stibines.

Abbreviations

R = alkyl or aryl; acac = acetylacetonate; dmso = dimethylsulfoxide; DMF = N,N-dimethylformamide; dba = dibenzylideneacetone; Cp = cyclopentadienyl; Cp* = pentamethylcyclopentadienyl; CpMe = methylcyclopentadienyl; Fc = ferrocenium; COD = cyclooctadiene; COE = cyclooctene; CyNC = cyclohexylisonitrile; thf = tetrahydrofuran; tmeda = tetramethylethylenediamine; NHC = N-heterocyclic carbene; nbd = norbonadiene; Htpym = 2-thio-1,3-pyrimidine; pip = piperidine; S-Phoz = 2-(2-thiophenyl)-4,4-dimethyloxazoline; [9]aneS_3 = 1,4,7-trithiacyclononane; tht = tetrahydrothiophene; R_3-tacn = 1,4,7-R_3-1,4,7-triazacyclononane.

* Corresponding author. E.mail wxl@soton.ac.uk

Contents

1. Introduction

2. Ligand synthesis

3. Monodentate halopnictine complexes

3.1 Halostibine complexes

3.2 Halobismuthine complexes

4. Monodentate stibine complexes

5. Monodentate bismuthine complexes

6. Distibine complexes

7. Mixed donor polydentates containing stibine or bismuthine donor groups

7.1 Ligands containing neutral O, S or N donor atoms

7.2 Ligands containing neutral P donor atoms

8. Systematics of structures and bonding

9. Applications

10. Conclusions and outlook

References

1. Introduction

For most of the twentieth century neutral organoantimony ligands were viewed as rather softer and more weakly binding, but generally similar to other pnictines ER_3 (E = P, As or Sb) [1,2]. The majority of the complexes were with the later d-block metals in medium or low oxidation states, or with metal carbonyls. The synthesis of other than the simplest bidentate stibines was challenging, due both to the relative weakness of the C-Sb bond and the tendency of certain linkages, such as $-CH_2CH_2-$ and -CH=CH- to eliminate $CH_2=CH_2$ or HC≡CH, respectively, forming Sb-Sb bonds [3]. Polystibines were largely unknown and antimony incorporation into mixed N/Sb, O/Sb hybrid multidentates little explored. The first indication that stibines could behave very differently to their lighter analogues, came from the studies of Werner *et al* [4] who synthesised the first examples of complexes containing bridging pnictines, for example, $[XRh(\mu\text{-}Sb^iPr_3)(\mu\text{-}CPh_2)_2RhX]$ (X = Cl, acac). Although these could be converted by metathesis into analogues with bridging PR_3 and AsR_3, the direct synthesis of analogues with the lighter ligands adopting a bridging mode was not possible. Studies of stibine chemistry in the twenty-first century has revealed more examples, which have few or no analogues with phosphines or arsines, including hypervalent interactions, where a stibine functioning as a σ-donor towards a metal centre simultaneously behaves as a σ-acceptor to other neutral or anionic groups [5] (hypervalent interactions also occur in some antimony multidentate ligands with pendant arm donor groups [6]). Oxidation of metal-coordinated stibine donor groups with retention of the Sb-M bond and conversion of the Sb centre to an electron acceptor from the metal has also been identified [7].

The older coordination chemistry of bismuthine ligands, BiR_3 was very limited, most accounts involving only $BiPh_3$ and often reporting the failure to isolate complexes analogous to those formed by the lighter pnictines [1,2]. The few attempts to develop dibismuthines or to incorporate Bi into polydentates often foundered on the weakness of the Bi-C bond [2,3]. Although the volume of work remains small, recent studies have included detailed characterisation of some trialkylbismuthine complexes (Section 5), incorporation of bismuth donors into hybrid polydentate ligands, and the identification of hypervalent interactions in some systems [5].

The previous review of the area [2] covered work published up to the end of 2005, and the present article covers work published between then and mid-2020. Whilst we have aimed to include all new stibine and bismuthine complexes reported in that period, the new types of behaviour identified, including hypervalency, oxidation of metal-coordinated stibine groups, and applications in catalysis and anion sensing are also described.

2. Ligand synthesis

The synthetic routes to the simple SbR_3 and BiR_3 have been discussed previously [3] and mostly involve reaction of $SbCl_3$ or $BiCl_3$ with Grignard or organolithium reagents; $SbR_{3-n}R'_n$ and $BiR_{3-n}R'_n$ are obtained similarly using $SbR_{3-n}Cl_n$ and $BiR_{3-n}Cl_n$, although for bismuth the tendency for the R group scrambling hinders the preparation of unsymmetrical bismuthines. The structures of BiR_3 (R = Me, ^{i}Pr), which are liquids at room temperature, have been determined by low temperature X-ray crystallography [8]. Distibinoalkanes, $R_2Sb(CH_2)_nSbR_2$ (n = 1, 3, 4, etc., $\neq 2$), are readily made by reaction of $NaSbR_2$ with $Cl(CH_2)_nCl$, usually in liquid NH_3 [3], but other inter-donor linkages are more challenging to incorporate. The ligand, *o*-$C_6H_4(SbMe_2)_2$, which is the most strongly coordinating distibine, combining small steric demands with pre-organisation for chelation, still lacks a high yield route that would facilitate detailed studies of its metal ion chemistry. However, despite producing a seven-membered chelate ring, the *o*-xylyl linked *o*-$C_6H_4(CH_2SbMe_2)_2$, which is formed in high yield from the diGrignard *o*-$C_6H_4(CH_2MgCl)_2$ and $SbMe_2Cl$, forms chelates even to 3d metal halides [9]. Concentrated solutions of the diGrignard *o*-$C_6H_4(CH_2MgCl)_2$ in thf result in coupling to form $\{CH_2(o\text{-}C_6H_4CH_2MgCl)\}_2$, which in turn affords the wide-angle distibine, $\{CH_2(o\text{-}C_6H_4CH_2SbMe_2)\}_2$, upon reaction with $SbMe_2Cl$; this too can function as a bidentate ligand, to produce 11-membered chelate rings [10].

The 1,8-bis$(R_2Sb)_2$-naphthalenes (R = Me, Ph) (I) (Scheme 1) were prepared in ~ 50% yields from 1,8-dibromonaphthalene, lithium foil and SbR_2Cl in diethyl ether [11]. Similarly, treatment of 2,2'-dibromo-1,1'-binaphthyl with ^{n}BuLi in Et_2O, followed by addition of SbR_2Cl, gave racemic mixtures of 2,2'-$(R_2Sb)_2$-1,1'-binaphthyl (II) [11]. The ^{1}H and $^{13}C\{^{1}H\}$ NMR spectra of the dimethylstibino ligand showed two methyl resonances, the X-ray crystal structure (Fig. 1) shows one methyl group on each antimony pointing towards the aryl ring and the other pointing away. Enantiopure samples of the DIOP-based distibines (III) were obtained from $NaSbR_2$ (R = Me, Ph) and the *D*- or *L*-form of 4,5-bis(bromomethyl)-2,2'-dimethyl-1,3-dioxolane [11]. The enantiomeric pairs are indistinguishable by NMR spectroscopy, but were identified by their optical rotation.

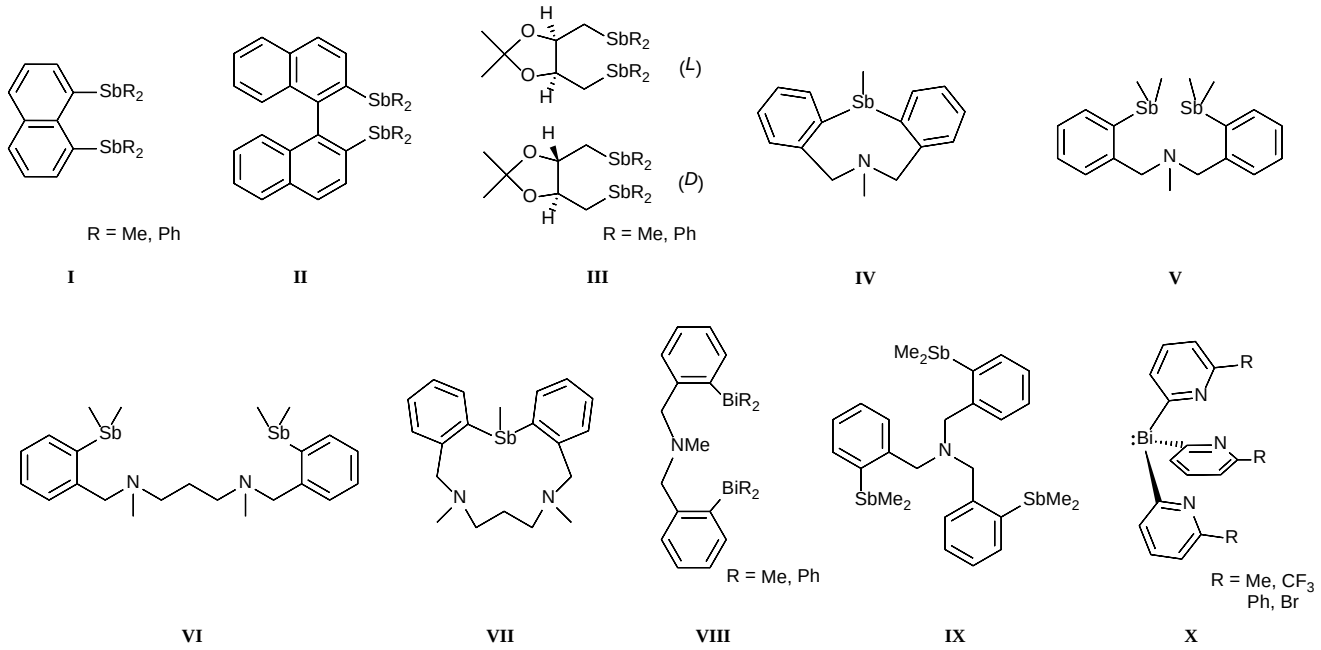

Scheme 1: New stibine and bismuthine ligands.

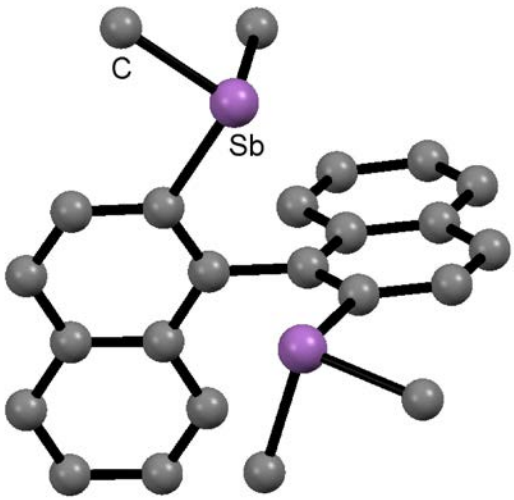

Fig. 1: X-ray structure of 2,2'-bis(Me_2Sb)-1,1'-binaphthyl, redrawn from Ref. 11.

The reaction of $NaSbR_2$ (R = Me, Ph) with $O(CH_2CH_2Br)_2$ in liquid ammonia gave $O(CH_2CH_2SbR_2)_2$ as yellow air-sensitive oils [12]. Despite the presence of dimethylene links, the oils are stable if protected from dioxygen (contrasting with $R_2SbCH_2CH_2SbR_2$, which are unknown); curiously, the arsine analogue $O(CH_2CH_2AsMe_2)_2$ decomposes to $Me_2AsCH_2CH_2OH$ under some conditions. The bismuthine, $O(CH_2CH_2BiPh_2)_2$, was obtained in good yield from $O(CH_2CH_2I)_2$ and $NaBiPh_2$ in liquid ammonia; corresponding reactions using $O(CH_2CH_2X)_2$ (X = Cl or Br) gave incomplete substitution of the halide, reflecting the poor nucleophilicity of the bismuthide anion [13]. The structure of

$O(CH_2CH_2BiPh_2)_2$ (Fig.2) revealed pyramidal bismuth centres and hypervalent interaction between the ether oxygen and both bismuth centres. Attempts to isolate $O(CH_2CH_2BiMe_2)_2$ failed, with the production of metallic bismuth and a mixture of organic products [13].

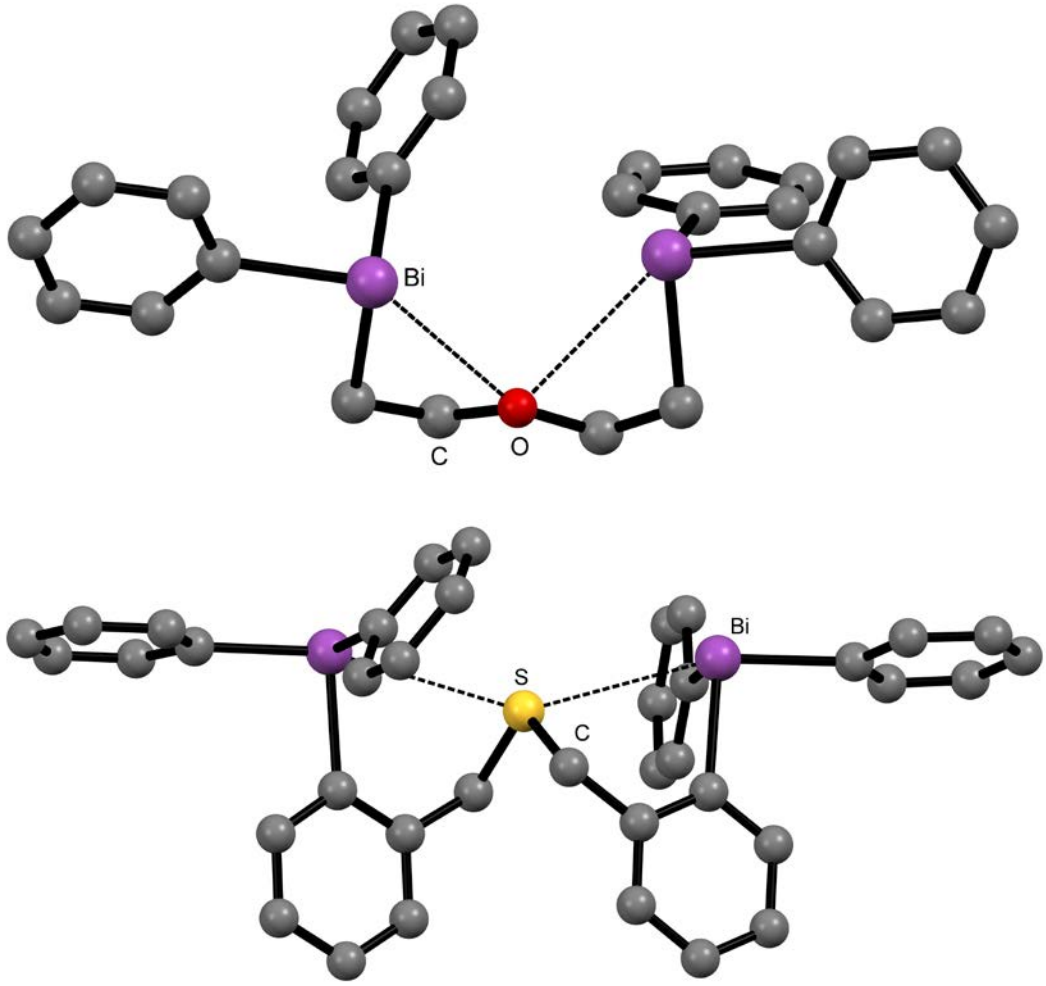

Fig. 2 X-ray structures of $O\{(CH_2)_2BiPh_2\}_2$ and $S(CH_2\text{-}2\text{-}C_6H_4BiPh_2)_2$ with hypervalent interactions, redrawn from Ref. 13.

New tridentates with Sb_2S- and Bi_2S-donor sets, $S(CH_2\text{-}2\text{-}C_6H_4SbMe_2)_2$ and $S(CH_2\text{-}2\text{-}C_6H_4BiR_2)_2$ (R = Me, Ph), have been prepared by reaction of $S(CH_2\text{-}2\text{-}C_6H_4Br)_2$ with ^nBuLi and the appropriate ER_2Br (E = Sb, R = Me; E = Bi; R = Me, Ph). While the methyl-based ligands are air-sensitive oils, $S(CH_2\text{-}2\text{-}C_6H_4BiPh_2)_2$ is a white crystalline solid, the structure of which (Fig. 2) reveals hypervalent S···Bi interactions (3.33, 3.30 Å) to both bismuth atoms [13].

New mixed Sb/N-donor ligands (IV-VII) [14] and some bismuth analogues (VIII) [13] have also been described. Addition of a solution of $N(CH_2\text{-}2\text{-}C_6H_4Li)_3$ to $SbMe_2Cl$ in diethyl ether at –78°C afforded $N(CH_2\text{-}2\text{-}C_6H_4SbMe_2)_3$ (IX) in high yield, a very rare example of a ligand containing three stibine donor atoms [15]. Tripodal tetradentates containing bismuthine and pyridyl donors, $Bi(6\text{-}R\text{-}C_5H_3N)_3$ (R = Me, CF_3, Ph, Br), were obtained straightforwardly from 2-Li-6-R-C_5H_3N and $BiCl_3$ (X) [16].

The new P_2Sb-donor tridentate, $PhSb(o\text{-}C_6H_4P^iPr_2)_2$ (XI), was obtained by reaction of $o\text{-}BrC_6H_4P^iPr_2$, ^nBuLi and $PhSbCl_2$ in thf [17]. A similar reaction using $SbCl_3$ produced the tripodal tetradentate, $Sb(o\text{-}C_6H_4P^iPr_2)_3$ (XII) [17]. Comproportionation of $PhSb(o\text{-}C_6H_4P^iPr_2)_2$ and $SbCl_3$ gave the halostibine $ClSb(o\text{-}C_6H_4P^iPr_2)_2$ (XIII). The bismuthine analogues, $Bi(o\text{-}C_6H_4P^iPr_2)_3$ (XIV) [17], $ClBi(o\text{-}C_6H_4PPh_2)_2$ (XV) [18] and $ClBi(o\text{-}C_6H_4P^iPr_2)_2$ (XVI) [19], were also obtained; the $ClBi(o\text{-}C_6H_4P^iPr_2)_2$ being produced from substituent scrambling between $Bi(o\text{-}C_6H_4P^iPr_2)_3$ and [AuCl(tht)] (the other product is $[\{Au(o\text{-}C_6H_4P^iPr_2)\}_2]$) [19]. The $ClBi(o\text{-}C_6H_4PPh_2)_2$ is converted to $RBi(o\text{-}C_6H_4PPh_2)_2$ (R = Me or C_6F_5) by treatment with RLi [20]. New halobismuthines, $XBi(o\text{-}C_6H_4PPh_2)_2$ (X = Br or I) (XVII), were also made, formed from $BiBr_3$ and $o\text{-}LiC_6H_4PPh_2$ for X = Br and from $ClBi(o\text{-}C_6H_4PPh_2)_2$ and NaI for X = I [21].

Although strictly falling outside the subject of this article in that it coordinates as a monoanion, the rare example of incorporation of antimony donors into the PNSb diarylamido pincer (XVIII) is notable [22].

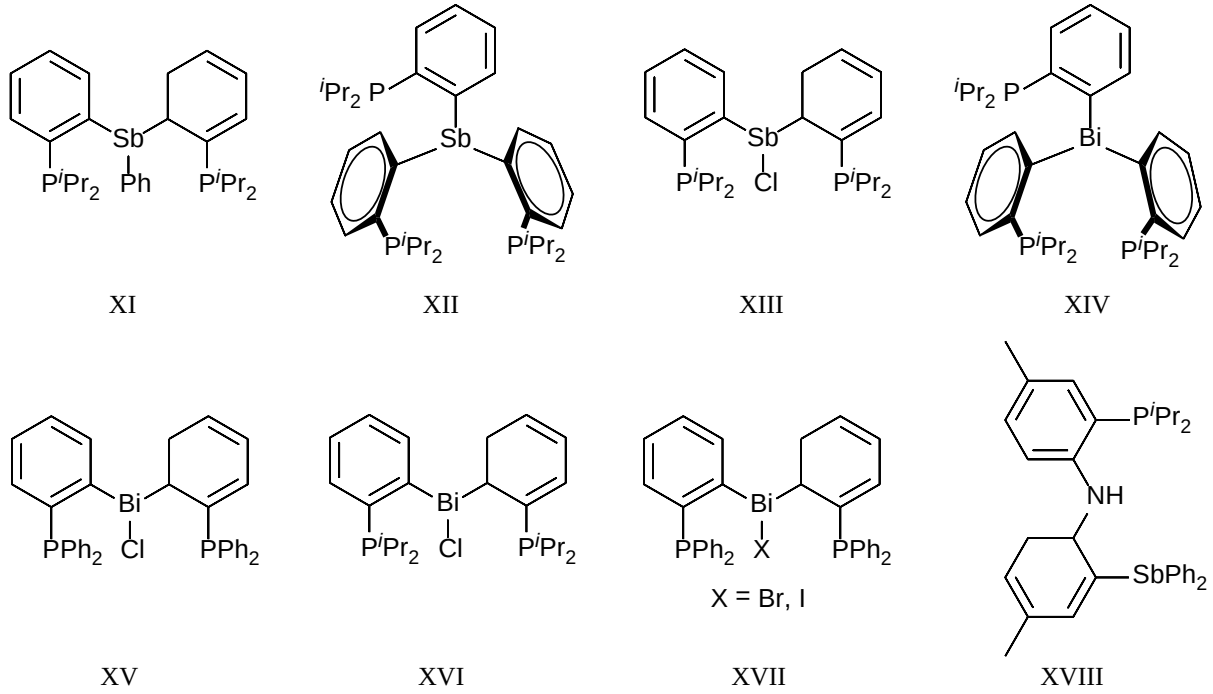

XI XII XIII XIV

XV XVI XVII XVIII

Scheme 2: Phosphorus-antimony and phosphorus-bismuth multidentate ligands.

3. Monodentate halopnictine complexes

Antimony(III) halides, SbX_3 (X = Cl, Br, I), are modest Lewis acids that form complexes with many neutral bases [23]. A much small number of complexes of SbF_3 with hard neutral N– or O–donors have been characterised [24,25]. Since triorganostibines, SbR_3, are Lewis bases, the behaviour of organohalostibines is of particular interest (Lewis acid or Lewis base?), although relatively little studied until recently. In fact, Lewis acidity by organohalostibines is rather rare, and (as anticipated)

is more prevalent for $SbRX_2$ than SbR_2X types [5]; only the Lewis basic behaviour is considered here.

3.1 Halostibine complexes

Group 6 carbonyls form $[M(CO)_5(L)]$ (M = W: L = $SbMe_2Br$, $SbMeBr_2$ [26], Sb^tBu_2Cl [27], $SbPh_2X$, X = Cl, Br, I [28]; M = Cr: L = $SbMe_2Br$ [26], $SbMeCl_2$ [29]) complexes by reaction of $[M(CO)_5(thf)]$ with the halostibine. Notably, attempts to obtain $[W(CO)_5(SbBr_3)]$ by a similar route were not successful [26]. Comparison of the spectroscopic data with that of SbR_3 analogues shows that in the IR spectra, υ(CO) generally falls along the series: $[M(CO)_5(SbRX_2)] \rightarrow [M(CO)_5(SbR_2X)] \rightarrow [M(CO)_5(SbR_3)]$ for fixed M, whilst in the NMR spectra $\delta(^{13}C)$ of the carbonyl groups shift to high frequency along the same series [26], both consistent with more electron density on the metal centre in this order. The X-ray crystal structures show that for a fixed M (either Cr or W) d(M-Sb) also increases with the number of R groups on the antimony [26]. The structures reveal the angles at the coordinated antimony have increased significantly compared to the free halostibine [26,28] and also show weak hypervalent interactions between the carbonyl groups and the stibine centres on neighbouring molecules, M-C-O···Sb-M, leading to chain structures (Fig 3) [26]. Base hydrolysis (NaOH) of $[W(CO)_5(Sb^tBu_2Cl)]$ in a mixture of H_2O and Et_2O produced $[W(CO)_5(Sb^tBu_2OH)]$, whilst from $[W(CO)_5(SbPh_2Cl)]$ the product was $[\{W(CO)_5\}_2(\mu\text{-}Ph_2SbOSbPh_2)]$; the crystal structures of both were determined [27]. The $[W(CO)_5(SbMe_2Br)]$ is cleanly alkylated to $[W(CO)_5(SbMe_2R)]$ by the appropriate RLi (R = Me, ^nBu) [26].

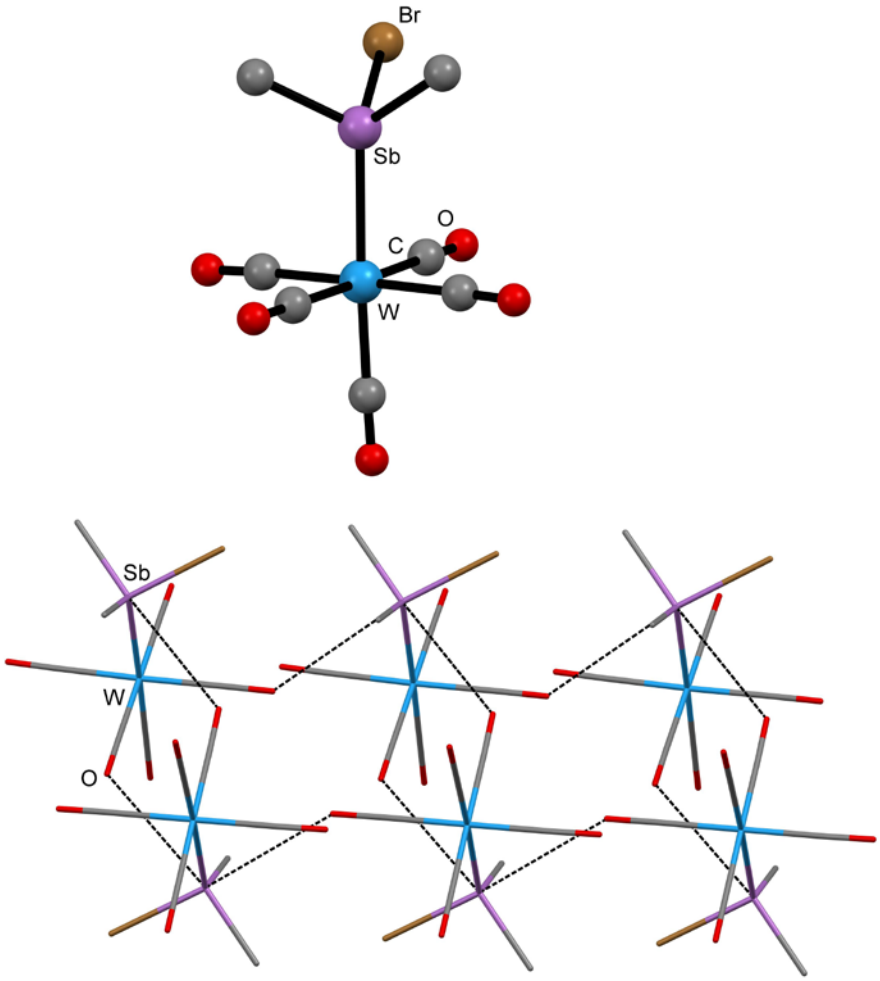

Fig. 3: View of $[W(CO)_5(SbMe_2Br)]$ showing the hypervalent interactions, redrawn from Ref. 26.

The $[CpFe(CO)_2(SbMe_2Br)]Y$ (Y = BF_4, CF_3SO_3) were prepared from $[CpFe(CO)_2(thf)]Y$ and $SbMe_2Br$; the X-ray structures of both show a strong hypervalent interaction between the anion and the iron coordinated antimony [30]. On standing for several days, the reaction mixture from the synthesis of $[CpFe(CO)_2(SbMe_2Br)]CF_3SO_3$ deposited crystals of a second complex, identified by its X-ray crystal structure as [CpFe(CO)(Me_2BrSb-μ-Br-$SbMe_2$Br)] [Fig. 4]. Treatment of $[Mn(CO)_5(CF_3SO_3)]$ or $[Mn(CO)_3(Me_2CO)_3]CF_3SO_3$ with appropriate quantities of $SbMe_2Br$ produced $[Mn(CO)_5(SbMe_2Br)]CF_3SO_3$ or *fac*-$[Mn(CO)_3(SbMe_2Br)_3]CF_3SO_3$, the latter is the first example of a complex containing three halostibine ligands [26]. The structure of the former shows a strong hypervalent O···Sb interaction (2.70 Å), which significantly distorts the geometry at the antimony centre. The structure of *fac*-$[Mn(CO)_3(SbMe_2Br)_3]CF_3SO_3$ reveals similar hypervalent interactions, producing a chain structure [26].

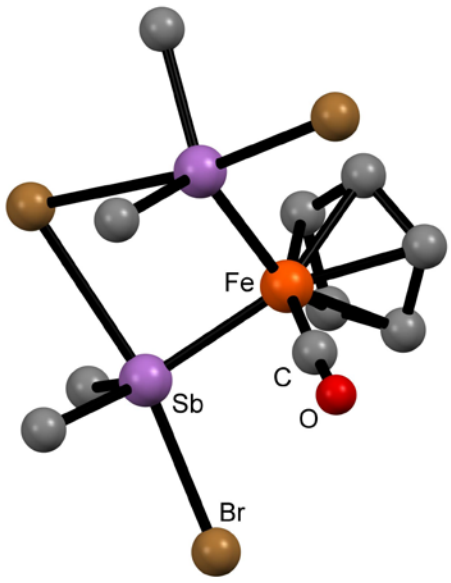

Fig. 4: X-ray crystal structure of [CpFe(CO)(Me_2BrSb-μ-Br-SbMe_2Br)], redrawn from Ref. 30.

The reaction of [$Os_3(CO)_{11}$(MeCN)] with $SbPh_2Cl$ produces [$Os_3(CO)_{11}(SbPh_2Cl)$] containing the $SbPh_2Cl$ ligand coordinated to one osmium centre [31,32], which on standing in polar solvents rearranges into various Os_3 clusters formed by oxidative addition of the Sb-Cl bonds. Base hydrolysis of [$Os_3(CO)_{11}(SbPh_2Cl)$] leads to a mixture of Os_3 and Os_6 clusters with bridging μ^2-$SbPh_2$ groups. Use of $SbPhCl_2$ resulted in clusters containing μ^3-SbPh groups. Attempts to isolate a complex of $SbPh_2Cl$ with $Ru_3(CO)_{12}$ failed, but reduction of $Ru_3(CO)_{12}$ with the benzophenone ketyl radical, followed by addition of $SbPh_2Cl$, gave [$Ru_6(CO)_{20}(\mu^2$-$SbPh_2)_2$], which has a raft structure [32]. Carbonyl clusters containing Ru_3 and Ru_6 units with μ^2-$SbPh_2$ groups result from reaction of $Na[HRu_3(CO)_{11}]$ with $SbPh_2Cl$ [33]. The reaction of [$Ru_3(CO)_{10}(\mu^2$-$SbPh_2)_2$] with $SbPh_2Cl$ in CH_2Cl_2 produced [$Ru_3(CO)_8(\mu^2$-$SbPh_2)_3Cl(SbPh_2CH_2Cl)$], containing the tertiary stibine, $SbPh_2CH_2Cl$ formed by reaction with the solvent [33].

A highly unusual series of five complexes, $Pd(SbMe_2Cl)_nCl_2$ (n = 1-5), have been prepared by reaction of [$Pd(MeCN)_2Cl_2$] with various ratios of $SbMe_2Cl$ in toluene; the X-ray structures of all five have been determined [34,35]. The dark green, $[Pd(SbMe_2Cl)_5]Cl_2$, which crystallises from a toluene solution of [$Pd(MeCN)_2Cl_2$] and excess $SbMe_2Cl$ at -18°C, contains a unique square pyramidal cation, the first example of an $PdSb_5$ moiety. It dissociates in solution at ambient temperatures with loss of $SbMe_2Cl$ to form the complex with n = 3. The other four complexes all contain square planar palladium centres: for n = 1 the structure is a chloride-bridged tetramer [$Pd_4Cl_8(SbMe_2Cl)_4$]; for n = 2, a dimer [$Pd_2Cl_4(SbMe_2Cl)_4$]; n = 3, a polymer [$PdCl(SbMe_2Cl)_2(SbMe_2Cl_2)]_n$; and n = 4, a weakly associated dimer [$Pd_2(SbMe_2Cl)_8]Cl_4$ (Fig. 5). Each structure contains further interactions between the coordinated Sb and coordinated or anionic

chlorides. The case of n = 3 also contains a coordinated $[SbMe_2Cl_2]^-$ ligand resulting from insertion of the halostibine into a Pd-Cl bond. The structural data and DFT calculations are consistent with the secondary bonding at antimony involving a lone pair on the chlorine atom *trans* to the covalent Sb-Cl bond, which donates into the low lying Sb-Cl σ* orbital of the chlorostibine. The $[Pd_2Cl_4(SbMe_2Cl)_4]$ is alkylated by MeLi to form $[Pd_4(SbMe_3)_4(\mu^3\text{-}SbMe_3)_4]$ (Section 4).

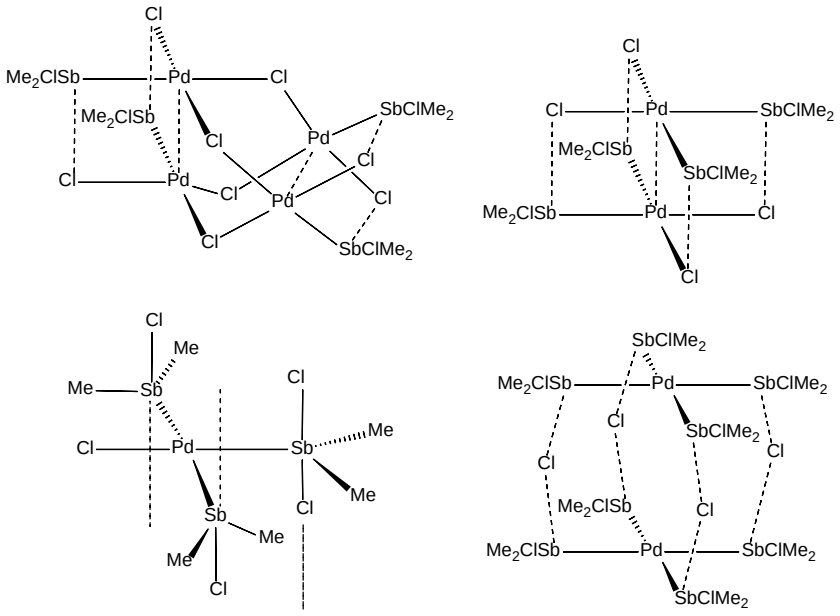

Fig 5: Palladium complexes, $[Pd(SbMe_2Cl)_nCl_2]$ (n = 1-4), formed using various ratios of $SbMe_2Cl$ [35].

3.2 Halobismuthine complexes

The coordination chemistry of halobismuthines is rather different to that of the antimony analogues described in Section 3.1 and far fewer compounds have been characterised. The $BiMeX_2$ (X = Cl, Br) behave as Lewis acids towards common N-donor ligands (2,2'-bipy, 1,10-phen, tmeda), but the same ligands cause disproportionation upon reaction with $BiMe_2X$, with complexes of $BiMeX_2$ being isolated [36].

The reaction of $BiMe_2Br$ with $[M(CO)_5(thf)]$ (M = Cr, W) in thf solution resulted in scrambling of the groups on the bismuth to give a mixture of $[M(CO)_6]$, $[M(CO)_5(BiMe_3)]$ and unidentified carbonyl-free products [36]. The carbonyl species, which after recrystallisation from hexane were isolated with yields of 25-30%, were identified by comparison of their IR, ^1H and $^{13}C\{^1H\}$ NMR spectra with samples prepared directly from $BiMe_3$ [37]. Reaction of $[Mn(CO)_5(CF_3SO_3)]$ with $BiMe_2Br$ gave $[Mn(CO)_5Br]$ as the only carbonyl species, again contrasting with the results using $SbMe_2Br$ [36]. $BiPh_2Cl$ and $[Re_3(CO)_{12}(\mu\text{-}H)_2]^-$ gave $[Re_3(CO)_{12}(\mu\text{-}H)_2(\mu^2\text{-}BiPh_2)]$ [38]. Reaction of $[HIr_4(CO)_{11}]^-$ and $BiPh_2Cl$ also results in cleavage of the Bi-Cl bond to give $[\{Ir_4(CO)_{10}(\mu\text{-}H)(\mu^2\text{-}BiPh_2)\}_2]$, in which the $BiPh_2$ groups bridge between the two Ir_4 clusters [39].

4. Monodentate tertiary stibine complexes

4.1 Groups 1-7

There are no reports of stibine complexes of Group 1-3 metals or of the f-block elements. In Group 4, no new complexes have been described, and the few old reports [1] lack convincing characterisation data. Similarly, although substituted vanadium carbonyl complexes are known [1], no new examples have appeared, and no studies with vanadium halides are reported. The stable niobium hydride, $[Nb(\eta^5\text{-}C_5H_4SiMe_3)_2H(SbPh_3)]$, has been prepared from $[Nb(\eta^5\text{-}C_5H_4SiMe_3)_2(H)_3]$ and $SbPh_3$ [40]. Low temperature protonation with CF_3CO_2H gave the dihydrogen complex $[Nb(\eta^5\text{-}C_5H_4SiMe_3)_2(\eta^2\text{-}H_2)(SbPh_3)][CF_3CO_2]$, which upon warming rearranged into $[Nb(\eta^5\text{-}C_5H_4SiMe_3)_2(H)_2(SbPh_3)]$ $[CF_3CO_2]$. The reported complexes of $SbPh_3$ with $NbCl_5$, $[NbCl_5(SbPh_3)_n]$ (n = 1, 2), were identified only by microanalysis [1]. Since $NbCl_5$ and $TaCl_5$ complexes of $TeMe_2$ (not normally thought to be a good ligand for high valent metals) have been fully characterised recently [41], formation of trialkylstibine complexes seems quite possible and worth investigation. However, attempts to prepare complexes of $SbMe_3$ with NbF_5 or TaF_5 in Et_2O solution, a route which successfully produced analogues with PMe_3 and $AsMe_3$, failed, with the $[MF_5(Et_2O)]$ complexes being isolated [42].

The synthesis and crystal structures of several trialkylstibine complexes, $[Cr(CO)_5(Sb^tBu_3)]$ [43], $[M(CO)_5(SbMe_3)]$ (M = Cr, W), and *cis*-$[Mo(CO)_4(SbMe_3)_2]$ (Fig. 6) [37] have been described. The structures reveal the expected increase in C-Sb-C angles upon coordination; DFT calculations were used to simulate the structures and to explore the Sb-M bonding [37]. The kinetics of substitution of pyridine or piperidine (L) in $[M(CO)_4(L)(SbPh_3)]$ (M = Mo, W) by phosphines and phosphites have been determined [44]. Various Fischer carbene (L') complexes of types $[Mo(CO)_4(SbPh_3)(L')]$ [45,46] and $[W(CO)_4(SbPh_3)(L')]$ [47] have been synthesised and their structures and electrochemical properties explored.

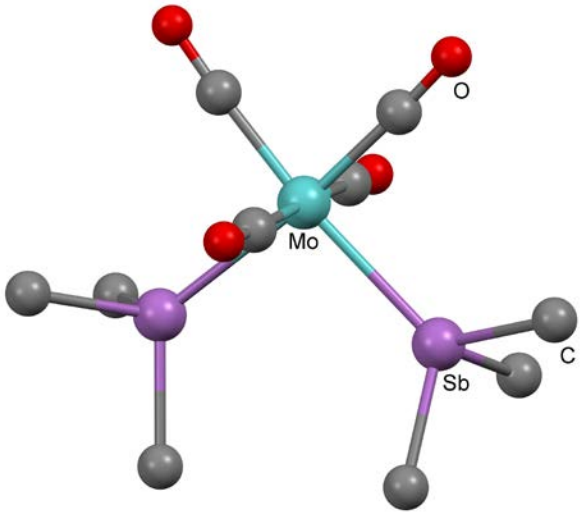

Fig. 6: Structure of *cis*-[$Mo(CO)_4(SbMe_3)_2$], redrawn from Ref. 37.

As in earlier Groups, the chemistry of stibines with molybdenum and tungsten chlorides is unexplored and although seven-coordinate, 1:1 complexes of WF_6 with PMe_3 and $AsMe_3$ have been obtained, the reaction of $SbEt_3$ with WF_6 gave only black decomposition products [48].

Orange [$CpMn(CO)_2(SbMe_3)$] was made by photolysis of [$CpMn(CO)_3$] in thf to form [$CpMn(CO)_2$(thf)], followed by addition of $SbMe_3$ [49]. Photolysis of $Re_2(CO)_{10}$ and $SbPh_3$ in benzene produced [$Re_2(CO)_8(SbPh_3)(Ph)(\mu^2\text{-}SbPh_2)$], along with small amounts of [$ReH(CO)_4(SbPh_3)$], [$Re(CO)_4(Ph)(SbPh_3)$], and *fac*-[$Re(CO)_3(Ph)(SbPh_3)_2$] [50]. The *mer* isomer of [$Re(CO)_3(Ph)(SbPh_3)_2$] is formed from treatment of [$Re_2(CO)_8(SbPh_3)(Ph)(\mu^2\text{-}SbPh_2)$] with more $SbPh_3$. The reactions of [$Pt(P^tBu_3)_2$] with [$ReH(CO)_4(SbPh_3)$] using various conditions gave Pt-Re cluster complexes, mostly containing μ^2-$SbPh_2$ or less commonly μ^3-SbPh bridges resulting from Sb-C bond cleavage [51]. A few complexes with intact $SbPh_3$ also resulted, including [$PtRe_2(CO)_8(SbPh_3)(Ph)(\mu^2\text{-}SbPh_2)_2(\mu\text{-}H)$], [$Re_2Pt(P^tBu_3)(Ph)(CO)_8(SbPh_3)(\mu^3\text{-}SbPh)(\mu\text{-}H)$] and [$Re(CO)_4(Ph)(SbPh_3)$] [51,52].

Octahedral rhenium clusters, *trans*-[$Re_6S_8(SbPh_3)_4Br_2$] and *trans*-[$Re_6Se_8(SbPh_3)_4Br_2$], were obtained by heating $Cs_4[Re_6S_8Br_6]\cdot 2H_2O$ or $Cs_3[Re_6Se_8Br_6]\cdot 2H_2O$ with excess $SbPh_3$ at 200°C in sealed tubes. The structures contain the one $SbPh_3$ coordinated to each of the four Re centres in the equatorial plane, with the bromines coordinated to the Re atoms in the axial positions [53].

4.2 Groups 8-10

New stibine complexes of iron are all substituted carbonyl species. The structure of [$CpFe(CO)_2(SbMe_2Ph)$]BF_4 has been determined [13]. The [$Fe_4(CO)_{16}(\mu^4\text{-}Sn)$] reacts with Me_3NO and $SbPh_3$ in CH_2Cl_2 to form red [$Fe_4(CO)_{15}(\mu^4\text{-}Sn)(SbPh_3)$] [54]. The reaction of [$Fe_3(\mu^3\text{-}Te)_2(CO)_9$] with SbR_3 (R = Ph, ^{i}Pr) at 0 °C in CH_2Cl_2 form red [$Fe_3(\mu^3\text{-}Te)_2(CO)_9(SbR_3)$], which have an 'open' structure (Fig 7) [55]. On warming to ambient temperatures the $SbPh_3$ complex loses one carbonyl group with formation of a new Fe-Fe bond in [$Fe_3(\mu^3\text{-}Te)_2(CO)_8(SbPh_3)$], but the Sb^iPr_3 analogue seems stable under these conditions.

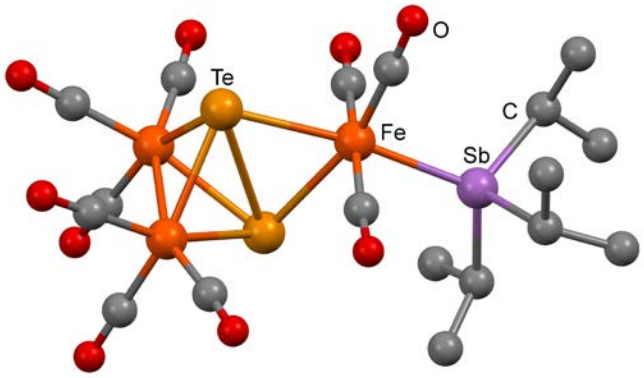

Fig 7: Structure of $[Fe_3(\mu^3\text{-}Te)_2(CO)_9(SbR_3)]$, redrawn from Ref. 55.

The $[Fe_3(\mu^3\text{-}Se)_2(CO)_9]$ cluster does not react with stibine ligands at room temperature, but on heating in hexane solution with $SbPh_3$, gave black $[Fe_3(\mu^3\text{-}Se)_2(CO)_8(SbPh_3)]$ [55]. The ethane dithiolate complex, $[Fe_2(CO)_6(SCH_2CH_2S)]$, reacted with one equivalent of $SbPh_3$ in MeCN with Me_3NO to form red, air-stable $[Fe_2(CO)_5(\mu\text{-}SCH_2CH_2S)(SbPh_3)]$, whilst excess stibine afforded $[Fe_2(CO)_4(\mu\text{-}SCH_2CH_2S)(SbPh_3)_2]$ [56]. The structures of both complexes reveal the stibine lying *trans* to the Fe-Fe bond (Fig. 8).

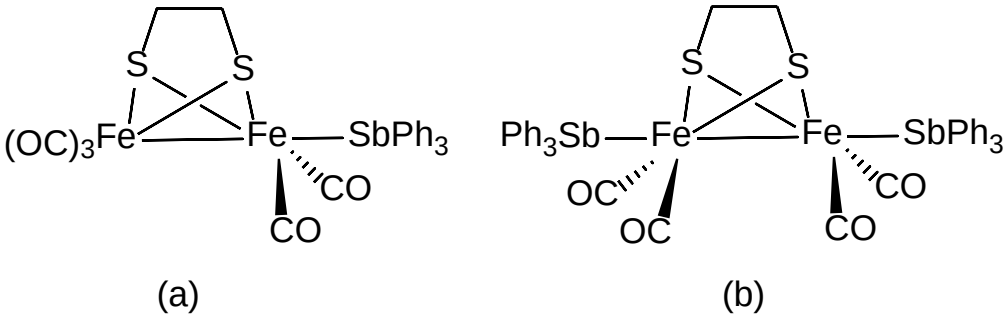

Fig. 8: Structures of $[Fe_2(CO)_5(\mu\text{-}SCH_2CH_2S)(SbPh_3)]$ (a) and $[Fe_2(CO)_4(\mu\text{-}SCH_2CH_2S)(SbPh_3)_2]$ (b) from Ref. 56.

Whilst reacting PPh_3 and $AsPh_3$ (L') with $[Fe_2(CO)_6(\mu\text{-}Cl_2\text{-}bdt)]$ ($\mu\text{-}Cl_2\text{-}bdt$ = 3,6-dichloro-1,2-benzenedithiolate) in thf with added Me_3NO simply substitutes one carbonyl group to form $[Fe_2(CO)_5(\mu\text{-}Cl_2\text{-}bdt)(L')]$, using $SbPh_3$ gave a red product in high yield, which was identified by an X-ray crystal structure as $[Fe_2(CO)_5(\mu\text{-}Cl_2\text{-}bdt)(Sb(O)Ph_3)]$ (Fig. 9) [57]. The antimony is coordinated to the iron, but has been oxidised, presumably by the Me_3NO, to Sb(V). Conducting the reaction in the absence of Me_3NO gave $[Fe_2(CO)_4(\mu\text{-}Cl_2\text{-}bdt)(SbPh_3)_2]$, whose structure reveals one stibine ligand on each iron.

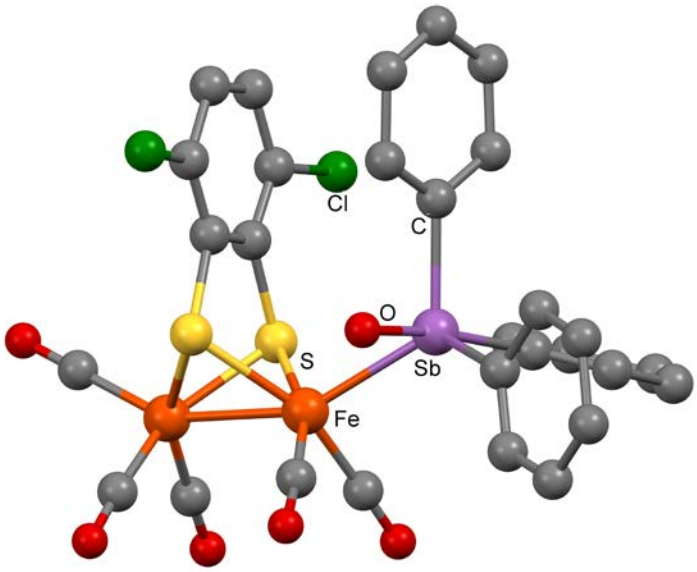

Fig. 9: Structure of $[Fe_2(CO)_5(\mu\text{-}Cl_2\text{-}bdt)(Sb(O)Ph_3)]$, redrawn from Ref. 57.

Photolytic substitution of the iron selenosulfonate complexes, $[CpFe(CO)_2SeSO_2R]$ (R= C_6H_5, 4-$CH_3C_6H_4$, 4-$CH_3OC_6H_4$), with $SbPh_3$ produces the monosubstituted complexes $[CpFe(CO)(SbPh_3)SeSO_2R]$ [58]. A large range of complexes of $SbPh_3$ with $CpFe(CO)_x$ centres coordinated to S- or Se-donor ligands has been described: $[CpFe(CO)(SbPh_3)(SeC(O)R)]$ [59]; **[**$CpFe(CO)(SbPh_3)SeC(O)OPh]$, $[CpFe(CO)(SbPh_3)SeC(O)SPh]$, $[CpFe(CO)(SbPh_3)SeC(S)SPh]$ [60]; $[CpFe(CO)(SbPh_3)SC(O)SEt)]$ [61]; $[CpFe(CO)(SbPh_3)SeC(O)SEt]$ [62]; $[CpFe(CO)(SbPh_3)SC(O)OR)]$ and $[CpFe(CO)(SbPh_3)SC(S)SR)]$ [63,64].

Substituted ruthenium and osmium carbonyl and mixed ruthenium-osmium carbonyl clusters remain an active area of research. The X-ray crystal structures of two mixed ligand complexes, $[Ru_3(CO)_9(L\text{-}L)(SbPh_3)]$ (L-L = $Ph_2P(CH_2)_2PPh_2$, $Ph_2AsCH_2AsPh_2$) have been determined, both containing the L-L bridging one edge of the Ru_3 triangle, with $SbPh_3$ on the third Ru and with the Group 15 donor ligands occupying equatorial sites [65,66]. The $[Ru_6(\mu^5\text{-}Sb)(\mu\text{-}H)_3(CO)_{18}(SbPh_3)]$ cluster was formed in very poor yield by reaction of $[HRu_3(CO)_{11}]^-$ with $SbPh_3$ in thf, and contains two triangular Ru_3 units linked by the bridging antimony atom and one Ru-Ru bond; the formation of the (μ^5-Sb) unit by degradation of $SbPh_3$ is notable [67]. The carbido cluster anion, $[Ru_{10}(\mu^6\text{-}C)(\mu\text{-}H)(CO)_{24}]^-$, reacts with $SbPh_3$ in acetone at room temperature to give $[Ru_{10}(\mu^6\text{-}C)(\mu\text{-}H)(CO)_{24\text{-}x}(SbPh_3)_x]^-$ (x = 1-3) [68]. The structures are illustrated in Fig 10.

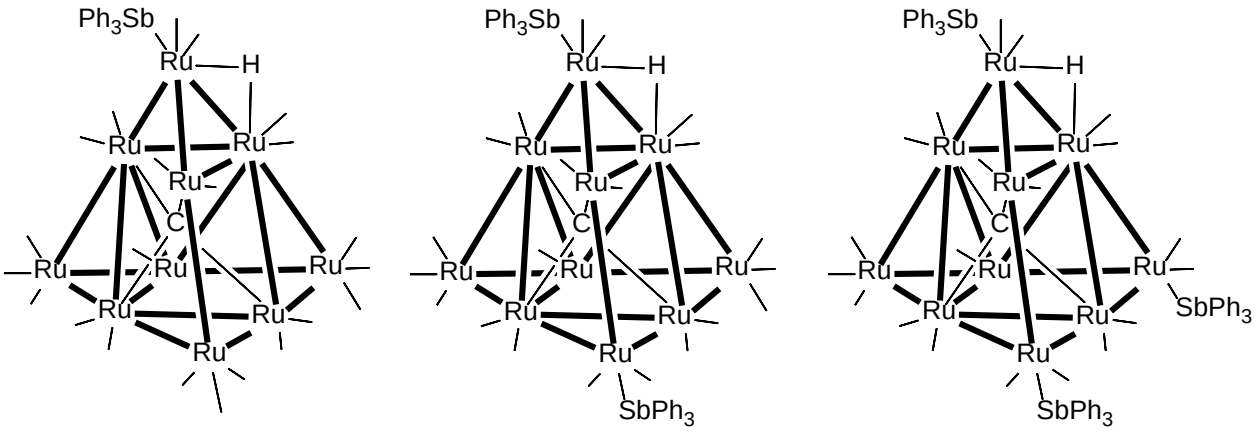

Fig. 10: Cores structures of $[Ru_{10}(\mu^6\text{-}C)(\mu\text{-}H)\ (CO)_{24\text{-}x}(SbPh_3)_x]^-$ (x = 1-3), redrawn from Ref. 68.

The half-sandwich compounds, $[Ru(\eta^6\text{-}C_6H_6)(L\text{-}L)(SbPh_3)]$ (L-L = cyclometallated 2-phenylpyridine, N,N-dimethylbenzylamine) (Fig 11), have been prepared [69].

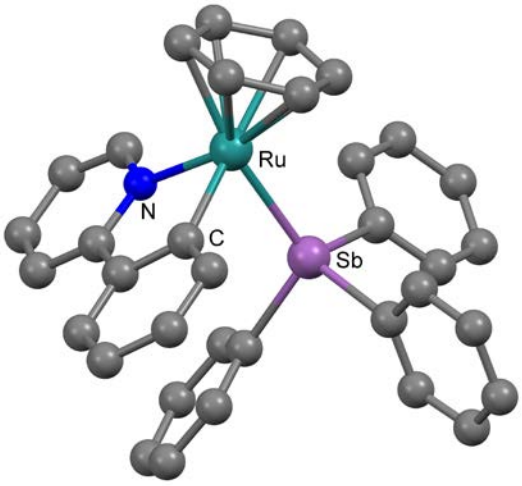

Fig. 11: Structure of $[Ru(\eta^6\text{-}C_6H_6)(L\text{-}L)(SbPh_3)]$; L-L = cyclometallated 2-phenylpyridine, redrawn from Ref. 69.

The reaction of $SbPh_2H$ with $[Os_3(CO)_{11}(MeCN)]$ results in oxidative addition of the Sb-H bond to form $[Os_3(CO)_{11}(H)(\mu^2\text{-}SbPh_2)]$ and $[Os_3(CO)_{11}(\mu\text{-}H)(\mu^2\text{-}SbPh_2)Os_3(CO)_{11}]$ [70]. Using the stibines, SbR_3 (R_3 = $SbMe_2Ph$, $SbMePh_2$, $SbMe_2$(*o*-tolyl), $SbMe_2$(*p*-tolyl), $SbMe_2(3,5\text{-}Me_2C_6H_3)$), gave the mono-substituted clusters, $[Os_3(CO)_{11}(SbR_3)]$ [71]; an example is the structure of $[Os_3(CO)_{11}(SbMe_2Ph)]$ shown in Fig 12. Thermolysis results in cleavage of Sb-C bonds and formation of a range of μ-stibido clusters [71]. The structure of $[Os_3(CO)_9(\mu^2\text{-}SbPh_2)_2(SbPh_3)]$ shows the $SbPh_3$ occupying an equatorial position on one osmium [72].

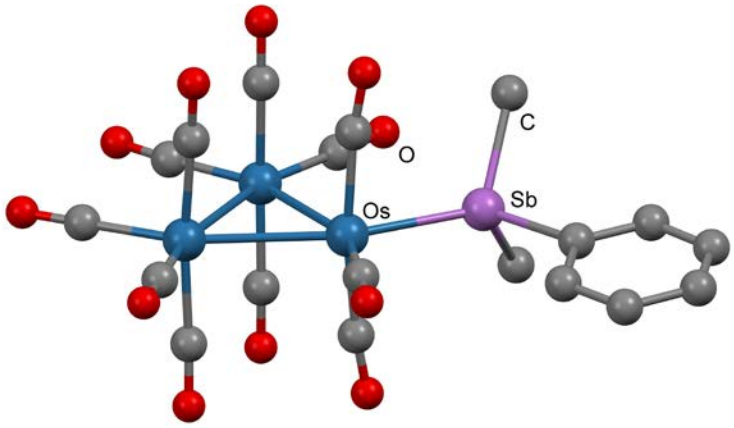

Fig.12: Structure of $[Os_3(CO)_{11}(SbMe_2Ph)]$, redrawn from Ref. 71.

$[Os_3(CO)_{10}(\mu^2\text{-}OEt)_2]$ reacts with Me_3NO and $SbPh_3$ in MeCN to give yellow $[Os_3(CO)_9(\mu^2\text{-}OEt)_2(SbPh_3)]$ [73]. Mixed ruthenium-osmium clusters have also attracted interest. $[RuOs_3(CO)_n(\mu\text{-}H)_2(SbPh_3)_x]$ (n = 12, x = 1; n = 11, x = 2) were made by reaction of $[RuOs_3(CO)_{13}(\mu\text{-}H)_2]$, Me_3NO and $SbPh_3$, and separated chromatographically [74,75,76]. Both complexes exist as isomers, for example, in $[RuOs_3(CO)_{12}(\mu\text{-}H)_2(SbPh_3)]$ the $SbPh_3$ can be on either a Ru or Os vertex. The red hexa-osmium cluster $[Os_6(CO)_{17}(\mu^5\text{-}Sb)(\mu^2\text{-}SbPh_2)_2(\mu\text{-}H)_2(\mu^3\text{-}\eta^2\text{-}C_6H_4)]$, also containing the μ^5-Sb unit, was made by thermolysis of $[Os_3(CO)_{10}(\mu\text{-}H)(\mu^2\text{-}SbPh_2)]$ followed by chromatographic separation from the multiple co-products [67].

The nitrido-bridged complexes, $[(Ph_3Sb)Cl_4Os{\equiv}N\text{-}IrCl(\eta^5\text{-}C_5Me_5)(SbPh_3)]$ and $[(Ph_3Sb)_2Cl_3Os{\equiv}N\text{-}IrCl(COD)]$, were prepared from $[OsNCl_3(SbPh_3)_2]$ and $[\{(\eta^5\text{-}C_5Me_5)IrCl_2\}_2]$ or $[\{Ir(COD)Cl\}_2]$, respectively [77]; the structure of the former is shown in Fig 13.

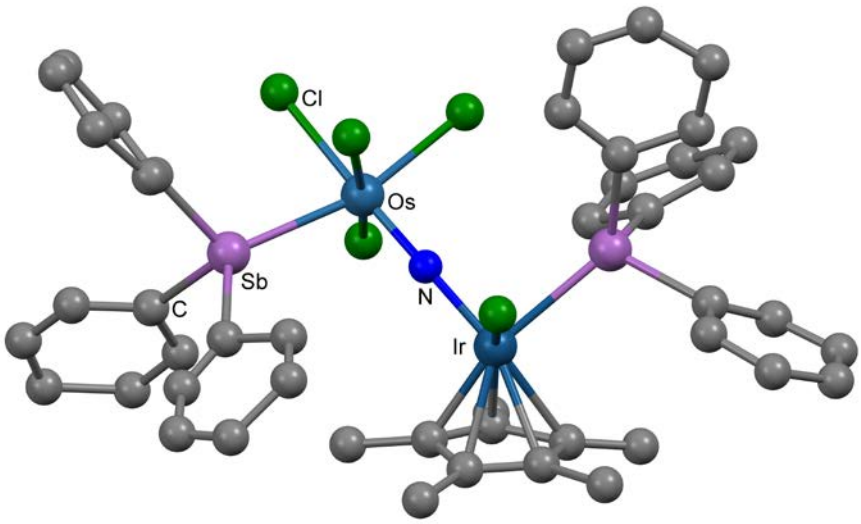

Fig. 13: The structure of $[(Ph_3Sb)Cl_4Os{\equiv}N\text{-}IrCl(\eta^5\text{-}C_5Me_5)(SbPh_3)]$, redrawn from Ref. 77.

The photoelectron spectrum (PES) of $[Co(CO)_2(NO)(SbMe_3)]$ has been measured and compared with those of the PMe_3 and $AsMe_3$ analogues [49].

The chemistry of the Rh-(μ-SbR_3)-Rh systems [78] has been summarised elsewhere [4] and a DFT study of the bonding is discussed in Section 8 [79]. Early studies on the reaction of $SbPh_3$ with $[\{Rh(CO)_2Cl\}_2]$ were contradictory, but it is now clear that two complexes exist, $[Rh(CO)(SbPh_3)_xCl]$, the yellow x = 2, and the red x = 3, and that the complexes are in equilibrium in many solvents 1,2]. In $MeNO_2$ solution in the presence of $SbPh_3$ both complexes convert into orange *mer-trans*-$[Rh(SbPh_3)_3(Ph)Cl_2]$ [80]. The kinetics of substitution of $SbPh_3$ in *trans*-$[Rh(CO)(SbPh_3)_xCl]$ by $(2,4\text{-}^tBu_2C_6H_3O)_3P$ have been explored [81]. The reaction of $RhCl_3$ with $SbPh_3$ is known to give both *mer*-$[Rh(SbPh_3)_3Cl_3]$ and *mer-trans*-$[Rh(SbPh_3)_2(Ph)Cl_2]$ [2]; the mechanism of this reaction has been explored by UV-visible spectroscopy and DFT calculations [82]. The structures of *mer*-$[Rh(SbPh_3)_3Cl_3]$ and of $[Rh(SbPh_3)(N,S\text{-tpym})_2(S\text{-tpym})]$ [Fig 14] formed in its reaction with 2-thio-1,3-pyrimidine (Htpym) are reported [83]. The $SbPh_3$ is coordinated to the Rh, but also is an acceptor towards one N donor atom of the S-tpym ligand (i.e. hypervalent).

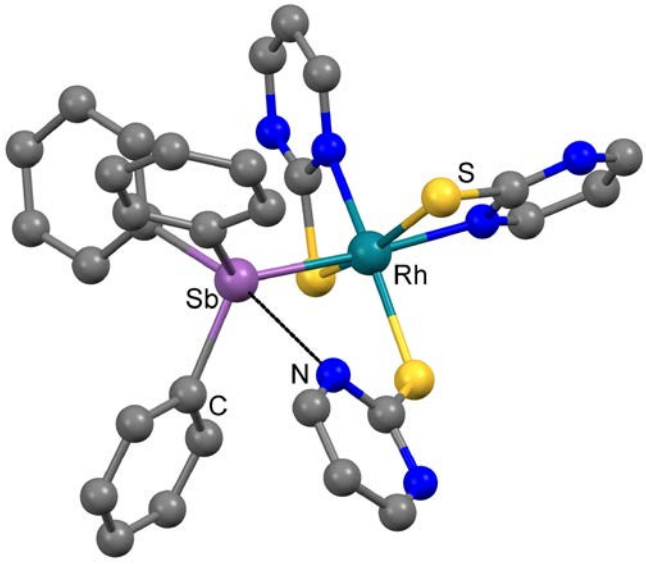

Fig.14: The structure of *mer*-$[Rh(SbPh_3)(N,S\text{-tpym})_2(S\text{-tpym})]$ showing the hypervalent interaction, redrawn from Ref. 83.

Red $[Cp^*Rh(SbPh_3)Cl_2]$ and orange $[Cp^*Ir(SbPh_3)Cl_2]$ were made in quantitative yield from $[\{Cp^*MCl_2\}_2]$ (M = Rh, Ir) and $SbPh_3$ in CH_2Cl_2 solution; structures of both were reported [84].

$[Rh(\eta^4\text{-diene})_2(Sb^iPr_3)]Y$ (diene = butadiene, isoprene, 2,3-dimethylbutadiene, Y = BF_4, CF_3SO_3) have been characterised [85].

In the nickel(0) complexes $[Ni_2(P_2C_{12}H_{20})_3(SbPh_3)_2]$ ($P_2C_{12}H_{20}$ = (XIX) in Fig. 15), the diphosphanes bridge the two metal centres and the stibines occupy *trans* axial positions [86].

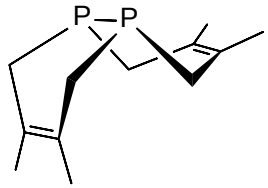

Fig. 15: Structure of the bicyclic diphosphane, $P_2C_{12}H_{20}$ (XIX).

The reaction of NiI_2 with tertiary stibines in fluorobenzene solution gave violet square planar *trans*-$[NiI_2(SbR_3)_2]$ (R_3 = $^iPr_3$, $^iPr_2Ph$) and trigonal bipyramidal $[NiI_2(SbR_3)_3]$ (R_3 = Me_2Ph, $MePh_2$) [87]. The X-ray structures of all four were reported (Fig. 16) and are the first structures of a nickel(II) halide with tertiary stibine ligands. Both types of complex are diamagnetic despite the relatively weak ligand field generated by these donor ligand combinations, and ^1H, $^{13}C\{^1H\}$ NMR and UV/visible spectra were reported. The *trans*-$[NiI_2(Sb\,^iPr_3)_2]$ in Et_2O takes up CO to form trigonal bipyramidal $[NiI_2(CO)(Sb\,^iPr_3)_2]$, the structure of which shows axial stibines. Heating copper coated silicon wafers with the *trans*-$[NiI_2(Sb\,^iPr_3)_2]$ in fluorobenzene, resulted in the formation of a Cu-Ni alloy deposit on the wafers [87].

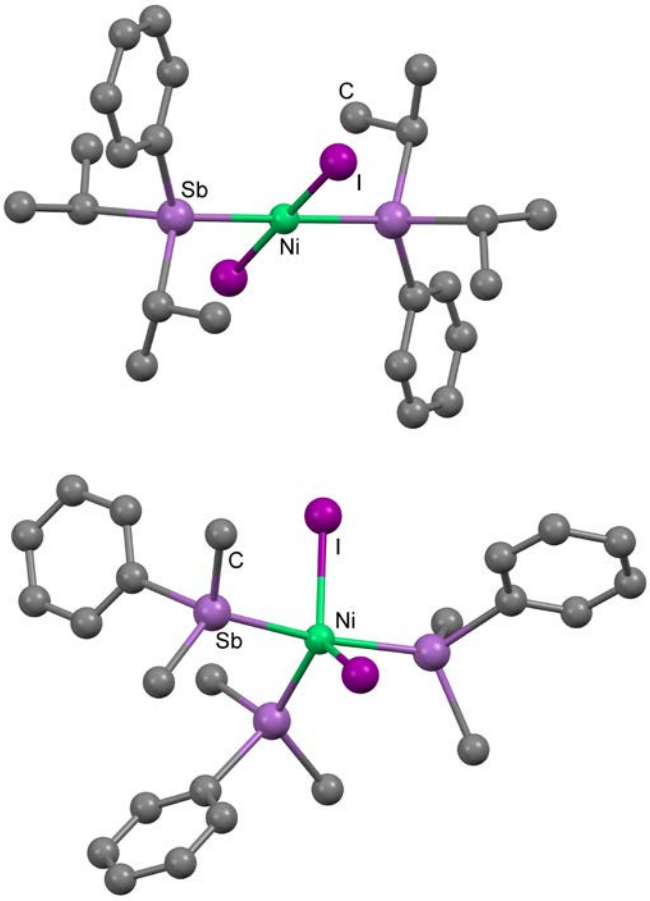

Fig. 16: Structures of *trans*-$[NiI_2(Sb^iPr_2Ph_3)_2]$ and $[NiI_2(SbMe_2Ph)_3]$, redrawn from Ref. 87.

The complex, *trans*-[Ni(3,5-$C_6Cl_2F_3$)$_2$($SbPh_3$)$_2$], dissolves in wet acetone with displacement of the stibine and formation of *cis*-[Ni(3,5-$C_6Cl_2F_3$)(Me_2CO)$_{2-x}$(H_2O)$_x$] (x = 0, 1, 2); similar chemistry occurs with AsR_3 ligands, although displacement of the arsine is only partial [88].

The use of organonickel-$SbPh_3$ complexes as catalysts for olefin oligomerisation or polymerisation has attracted considerable recent effort. While the catalysis is discussed further in Section 9, here we describe the nickel(II) complexes. Complexes of the type [Ni(C_6F_5)$_2$(ER_3)$_2$] (ER_3 is most often $SbPh_3$, although sometimes AsR_3) and [Ni($C_6Cl_2F_3$)$_2$($SbPh_3$)$_2$] are used because of the ready displacement of the pnictine [89-94]. The complexes [Ni(η^3-C_3H_5)($SbPh_3$)$_2$]Y (Y = B{3,5-(CF_3)$_2C_6H_3$}$_4$], [Al{OC(CF_3)$_3$}$_4$]) were prepared as yellow-red crystals by reaction of [{Ni(η^3-C_3H_5)(μ-Cl)}$_2$], $SbPh_3$ and NaY in Et_2O [95]. Nickel indenyl complexes [Ni(η^5-R_n-Ind)($SbPh_3$)$_2$]BF_4 (R_n = H, 1-Me, 2-Me, 1-$SiMe_3$, 1,3-Me_2) [Fig 17] were made by protonation of [Ni(η^5-R_n-Ind)$_2$] with the stoichiometric amount of HBF_4 in the presence of two equivalents of $SbPh_3$ and [Ni(η^5-Ind)($AsPh_3$)($SbPh_3$)$_2$]BF_4 from [Ni(η^5-Ind)($AsPh_3$)Cl], $TlBF_4$ and $SbPh_3$ [96,97].

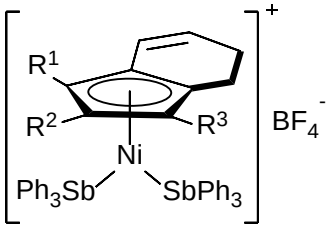

R_n = H, 1-Me, 2-Me, 1-$SiMe_3$, 1,3-Me_2

Fig.17: Nickel indenyl complexes, redrawn from Ref. 96.

Cationic and neutral nickel-allyl species, [Ni(η^3-$CH_2C(R)CH_2$)($SbPh_3$)$_3$][B{3,5-(CF_3)$_2C_6H_3$}$_4$] (R=CH_3, H), [Ni(η^3-CH_2CHCH_2)(PPh_3)(L)][B{3,5-(CF_3)$_2C_6H_3$}$_4$] (L=$SbPh_3$, $AsPh_3$) and [Ni(η^3-$CH_2C(R)CH_2$)Br($SbPh_3$)] (R=CH_3, H), are also active catalysts [98].

Arguably, the most unexpected new stibine complex reported is the dark purple [Pd_4(μ^3-$SbMe_3$)$_4$(κ^1-$SbMe_3$)$_4$], obtained from [Pd_2Cl_4($SbMe_2Cl$)$_4$] and 8 equivalents of MeLi in thf [34]. The X-ray structure revealed a Pd_4 tetrahedron with each palladium carrying a terminal $SbMe_3$ and with one $SbMe_3$ ligand capping each triangular face [Fig. 18].

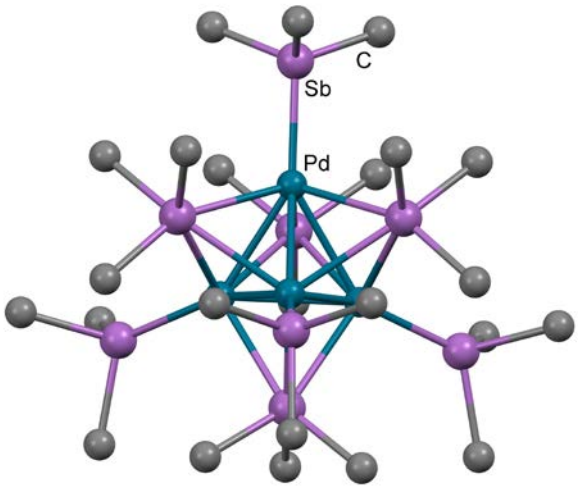

Fig. 18: View of $[Pd_4(\mu^3\text{-}SbMe_3)_4(\kappa^1\text{-}SbMe_3)_4]$, redrawn from Ref. 34.

The triply-bridging mode for $SbMe_3$ is unprecedented for any monodentate tertiary pnictine ligand. NMR spectroscopic data (^1H, $^{13}C\{^1H\}$) confirm the structure is retained in solution. Electron counting shows this is a 56 electron cluster, four short of the predicted valence electron count for a tetrahedron, although electron deficient clusters are well known for Pd and Pt, attributed to the large energy gap between the p- and d-orbitals for these metals [99]. DFT calculations, supported by energy decomposition analysis, show significant donor and acceptor contributions to the bonding of both the terminal and bridging stibines to the Pd_4 core.

Enthalpies of ligand substitution for the reaction:

$$cis\text{-}[Pd(C_6Cl_2F_3)_2(thf)_2] + 2L \rightarrow cis\text{-}[Pd(C_6Cl_2F_3)_2L_2] + 2thf$$

where L = a range of pnictines, including PPh_3, $AsPh_3$, $SbPh_3$, $PMePh_2$, PMe_3, $AsMePh_2$, were determined; the smallest value was for $SbPh_3$ [100]. Neutral *trans*-$[Pd(C_6F_5)L_2X]$ and cationic *trans*-$[Pd(C_6F_5)L_2(MeCN)]BF_4$ (X = Cl, Br; L = $SbPh_3$, $AsPh_3$, $As(C_6Cl_2F_3)Ph_2$, $AsCyPh_2$, $AsMePh_2$, PPh_3) complexes have been tested for norbornene polymerisation and copolymerisation with 5-norbornene-2-carboxaldehyde [101]. The neutral complexes have little activity, but the cationic arsine and stibine are very effective for palladium-catalysed norbornene polymerisation, the complex with $As(C_6Cl_2F_3)Ph_2$, being the best, indicating that steric bulk is an important factor.

A series of complexes of Pd(II) containing $SbPh_3$ and N-heterocyclic carbenes, *trans*-$[Pd(NHC)(SbPh_3)Cl_2]$ (NHC = N,N'-bis-(2,4,6-trimethylphenyl)imidazol-2-ylidene, N,N'-bis-(2,6-di(iso-propyl)phenyl)imidazol2-ylidene, N,N'-bis-(2,4,6-trimethylphenyl)imidazolidin-2-ylidene, N,N'-bis-(2,6-di(isopropyl)phenyl)imidazolidin-2-ylidene)), have been prepared from $[\{Pd(\mu\text{-}Cl)Cl(NHC)\}_2]$ and $SbPh_3$ in CH_2Cl_2 solution [102]. The X-ray structures of all four were determined; one example is shown in Fig. 19.

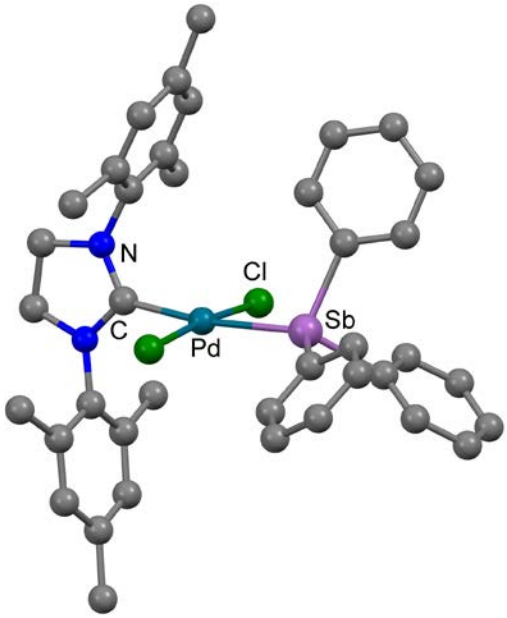

Fig. 19: Structure of *trans*-[Pd(N,N'-bis-(2,4,6-trimethylphenyl)imidazol-2-ylidene)($SbPh_3$)Cl_2], redrawn from Ref. 102.

Related Pd-allyl complexes [Pd(NHC)(allyl)($SbPh_3$)]ClO_4 were obtained from [Pd(NHC)(allyl)Cl], $AgClO_4$ and $SbPh_3$, and characterised by ^1H, $^{13}C\{^1H\}$ NMR spectroscopy and by X-ray structural studies [103]. Both series of complexes show high catalytic activity (Section 9). The complexes [Pd(S-Phoz)(L)Cl] (S-Phoz = 2-(2-thiophenyl)-4,4-dimethyloxazoline, L = N,N'-bis-(2,4,6-trimethylphenyl)imidazolidin-2-ylidene, PPh_3, $AsPh_3$, $SbPh_3$) were prepared and evaluated as catalysts for the coupling of p-bromoacetophenone with phenylboronic acid; the activity as a function of the neutral donor ligand was lowest for L = $SbPh_3$ [104].

A variety of other palladium systems with pnictine co-ligands have been tested as catalysts for cross-coupling reactions. The stibine is almost always $SbPh_3$ and it should be noted that $SbPh_3$ is not a "typical" or "representative" stibine, but is often more weakly coordinated than alkylstibines (which may or may not be beneficial in specific chemistry), and Sb-Ph bonds cleave readily in some systems. Examples studied include sulfur-containing palladocycles, [{FcC(S)OEt}PdCl(ER_3)] (Fc = ferrocenium, ER_3 = PPh_3, PMe_3, $SbPh_3$) (XX)[105] and [Pd($C_6H_4CH{=}NC_6H_2R$)LCl] (L = $AsPh_3$, $SbPh_3$) (XXI) [106]. Air stable half-sandwich compounds, [(η^5-C_5H_5)Pd(C_6F_5)L] (L = ^{t}BuNC, PPh_3, PMe_2Ph, $AsPh_3$, $SbPh_3$), were examined as norbornene polymerisation catalysis after activation with methylaluminoxane [107]. The structure of chloro{1-[(dimethylamino)methyl]ferrocenyl}-(triphenylstibine) palladium(II) (XXII) has been determined [108].

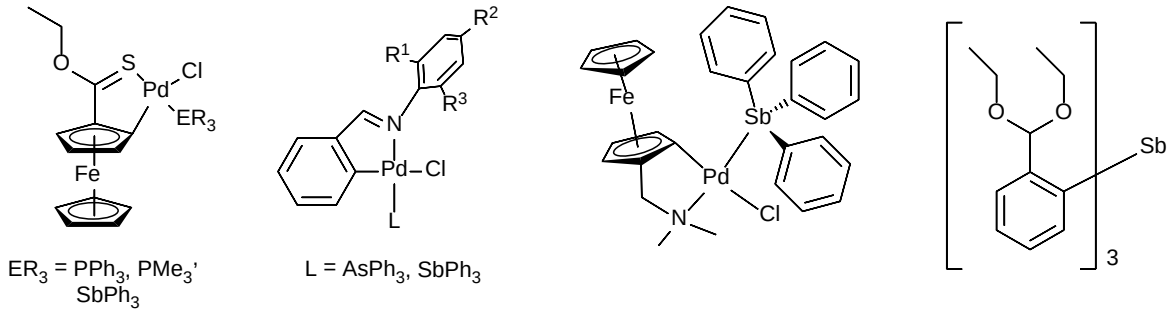

XX XXI XXII XXIII

Fig. 20: Structures of some palladocycles and the substituted stibine.

Palladium tropylium complexes, $[Pd_3(C_7H_7)_2(L)_3][BF_4]_2$ (L = $SbPh_3$, PPh_3, $AsPh_3$) (Fig. 21), have been prepared [109].

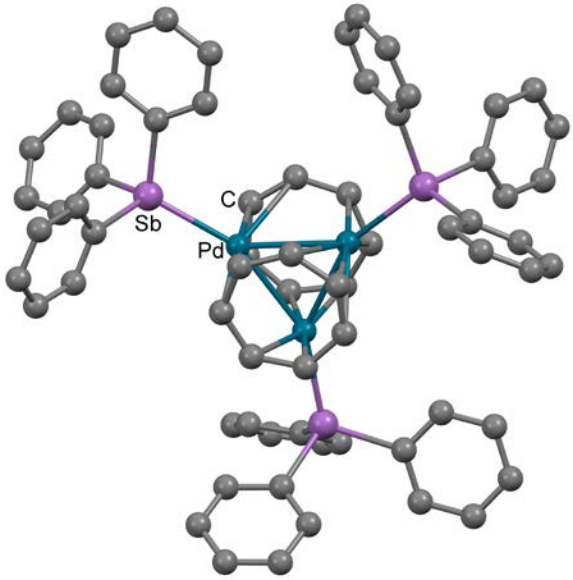

Fig. 21: Structure of $[Pd_3(C_7H_7)_2(SbPh_3)_3]^{2+}$, redrawn from Ref. 109.

Tertiary monostibine complexes of platinum(II) halides have been thoroughly investigated in earlier works [1,2] and few new complexes have been described. Worthy of mention here is *cis*-$[Pt(dmso)(SbPh_3)Cl_2]$, obtained by reaction of $[Ph_4Sb]Cl$ and $K_2[PtCl_4]$ in dmso solution [110], while reaction of $[PtCl_2([9]aneS_3)]$ ([9]aneS$_3$ = 1,4,7-trithiacyclononane) with one equivalent of $SbPh_3$ and $[NH_4][PF_6]$ produces $[PtCl([9]aneS_3)(SbPh_3)][PF_6]$, whilst with two equivalents of $SbPh_3$ the product is $[Pt([9]aneS_3)(SbPh_3)_2][PF_6]_2$ [111]. The X-ray structure of the former is a square pyramid with a long apical Pt-S bond (2.787(2) Å), whereas the $[Pt([9]aneS_3)(SbPh_3)_2][PF_6]_2$ has a very distorted five-coordinate geometry, more akin to a trigonal bipyramid (Fig 22) [111]. Upon standing in nitromethane solution, $[Pt([9]aneS_3)(SbPh_3)_2][PF_6]_2$ decomposes to $[Pt([9]aneS_3)(Ph)(SbPh_3)][PF_6]$,

which also has a highly distorted five-coordinate cation geometry [112].

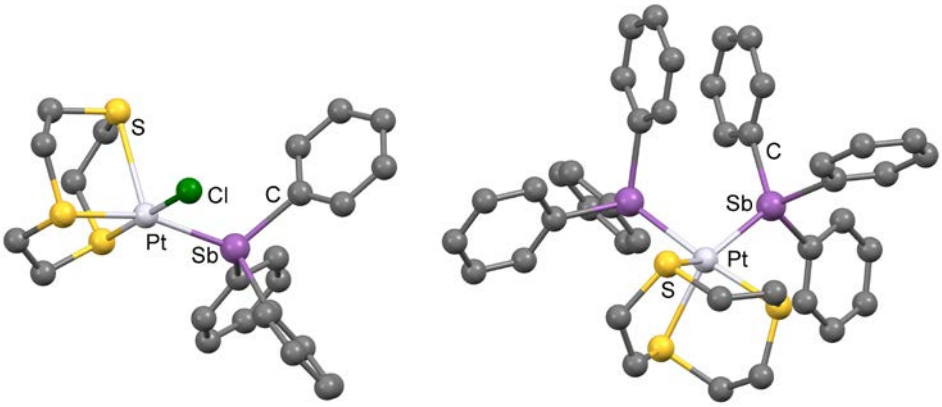

Fig. 22: Structures of $[Pt([9]aneS_3)(SbPh_3)Cl]^+$ and $[Pt([9]aneS_3)(SbPh_3)_2]^{2+}$, redrawn from Ref. 111.

Displacement of the pyridine in *trans*-$[Pt(NHC)(py)I_2]$ (NHC = 3-benzyl-1-methyl-1H-imidazol-3-ium, 3-(anthracen-9-ylmethyl)-1-methyl-1H-imidazol-3-ium or 1,3-dimethyl-1H-benzoimidazol-3-ium) by one equivalent of EPh_3 (E = P, As, Sb) gave *cis*-$[Pt(NHC)(EPh_3)I_2]$, whereas with two equivalents of EPh_3 the products were *trans*-$[Pt(NHC)(EPh_3)_2I]I$ [113]. The isomers present were confirmed by single crystal X-ray studies, and all exhibited higher cytotoxicity than cisplatin. The synthesis and structure of *trans*-$[PtCl_2L_2]$ (L = tris(2-diethylacetyl-formylphenyl)stibine (XXIII)) has been described [114].

The Pt(IV) complexes, *fac*-$[PtMe_3I(SbR_3)_2]$ (R_3 = Ph_3, Ph_2Me, $PhMe_2$) were obtained by refluxing $PtMe_3I$ with the stibine in $CHCl_3$ [115].

4.3 Groups 11-12

Two series of stibine complexes of CuI have been prepared by reaction of the ligands with CuI in fluorobenzene [116,117]. These were the cuboidal $[Cu_4(SbR_3)_4(\mu^3\text{-}I)_4]$ (R_3 = $^iPr_3$, $^tBu_3$, Cy_3, $^iPr_2Ph$, $^tBu_2Ph$) and the dimeric $[Cu_2(SbR_3)_4(\mu^2\text{-}I)_2]$ (R_3 = $^iPr_2Ph$, Me_2Ph, Ph_3). Structures of all seven complexes were determined and confirm that the dimers are formed by the less sterically bulky ligands, whilst ligands with larger steric requirements produce cuboids, with Sb^iPr_2Ph producing both types; examples are shown in Fig. 23. The thermoluminescence of the cuboid structures was examined in detail along with DFT calculations and the X-ray data, which show that short Cu-Cu bonds and high crystallographic symmetry of the Cu_4 core favour NIR emission [117].

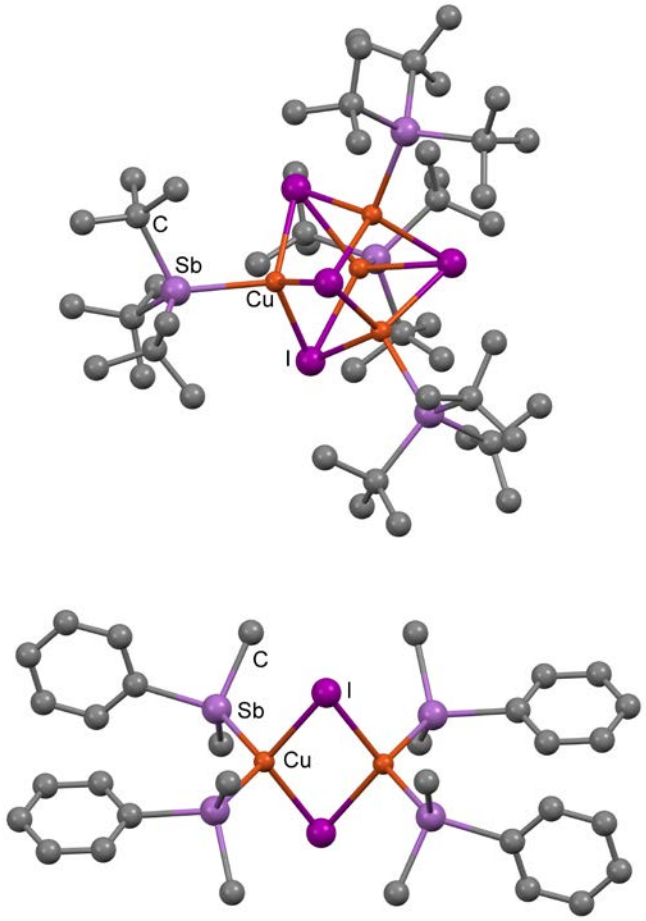

Fig. 23: Structures of cuboidal $[Cu_4(Sb^tBu_3)_4(\mu^3\text{-}I)_4]$ and the dimeric $[Cu_2(SbMe_2Ph)_4(\mu^2\text{-}I)_2]$, redrawn from Ref. 117.

$[Cu(R_3\text{-tacn})(SbPh_3)]SbF_6$ were formed by decomposition of the stibine sulfide complexes, $[Cu(R_3\text{-tacn})(Ph_3SbS)]SbF_6$ (R = Me, Et, ^{i}Pr), in the presence of added $[Cu(R_3\text{-tacn})(MeCN)]SbF_6$ (the other product is $[Cu_2(R_3\text{-tacn})_2(\mu^2\text{-}S_2)][PF_6]_2$) [118]. The phosphaalkene complex $[CuCl(Sb^iPr_3)\{P(^tBu)C(NMe_2)_2\}]$ has also been reported [119].

The self-assembly reaction between $AgNO_3$, $SbPh_3$ and $[\beta\text{-}Mo_8O_{26}]^{4-}$ in DMF led to the formation of $[\beta\text{-}\{Ag(SbPh_3)(DMF)\}_2Mo_8O_{26}]^{2-}$, which contains six-coordinate silver [120]. Potential anti-cancer drugs containing silver and $SbPh_3$ have been reported [121,122].

Treatment of [Au(tht)Cl] (tht = tetrahydrothiophene) with the sterically bulky $Sb(2,4,6\text{-}Me_3C_6H_2)_{3-n}Ph_n$) (n = 2,1,0) ligands gave linear $[Au\{Sb(2,4,6\text{-}Me_3C_6H_2)_{3-n}Ph_n)\}Cl]$ irrespective of the metal : ligand ratio used, whilst from $[Au(tht)_2]ClO_4$ and a 1 : 2 ratio, the products were the linear $[Au\{Sb(2,4,6\text{-}Me_3C_6H_2)_{3-n}Ph_n\}_2]ClO_4$ complexes [123]. The stibine $Sb(2,4,6\text{-}Me_3C_6H_2)Ph_2$ alone, gave a trigonal planar *tris* complex $[Au\{Sb(2,4,6\text{-}Me_3C_6H_2)Ph_2\}_3]ClO_4$. The complexes are rather unstable in solution, often depositing gold mirrors, but crystals were obtained in several cases,

including [Au{Sb(2,4,6-$Me_3C_6H_2)_3$)}Cl], [Au{Sb(2,4,6-$Me_3C_6H_2)_{3-n}Ph_n$}$_2$]ClO_4 (n = 0, 1) and [Au{Sb(2,4,6-$Me_3C_6H_2$)Ph_2}$_3$]ClO_4 (Fig. 24) [123].

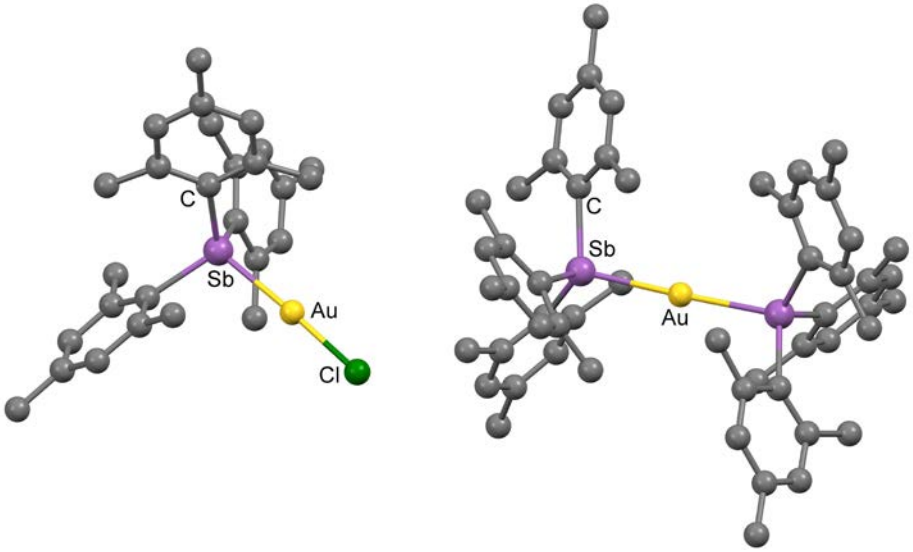

Fig. 24: Structures of [Au{Sb(2,4,6-$Me_3C_6H_2)_3$)}Cl] and [Au{Sb(2,4,6-$Me_3C_6H_2)_3$}$_2$]$^+$, redrawn from Ref. 12.

Structures were also determined for the ligands Sb(2,4,6-$Me_3C_6H_2)_3$ and Sb(2,4,6-$Me_3C_6H_2$)Ph_2. DFT calculations replicated the experimental geometries and metrics, with the C-Sb-C angle widening on coordination (Section 8).

The only new stibine complex reported in Group 12 is the [Hg{Sb(C_6H_3(2,6-$OMe)_2)_3$}I_2], obtained by combining the stibine and HgI_2 in acetone. This species adopts a trigonal planar geometry at mercury [124].

4.4 Groups 13-14

New stibine complexes of the p-block elements are mostly with Group 13 halides and alkyls for which the fundamental behaviour and trends are now clear. Trialkylstibine complexes of the boron halides are very moisture sensitive and decompose in both the solid state and in solution in halocarbons in a few hours to a few days depending on the halide present; stability falls I > Br > Cl >>F [125]. Bubbling BF_3 into solutions of SbR_3 (R = Et, ^{i}Pr) in n-hexane precipitated white powders in poor yield, identified by IR, ^{1}H, ^{19}F and ^{11}B NMR spectroscopy as [BF_3(SbR_3)]. The solids fume in air and have a significant vapour pressure of BF_3 at ambient temperatures. There is a clear trend in stability compared with complexes of lighter pnictines: [BF_3(PMe_3)] > [BF_3($AsMe_3$)] >> [BF_3(SbR_3)] [125,126]. Complexes with BCl_3, [BCl_3(SbR_3)], are slightly more stable, but still degrade in hours at ambient temperatuures, although a crystal structure of [BCl_3(Sb^{i}Pr$_3$)] was obtained. The [BX_3(SbR_3)] (X = Br, I) are very moisture sensitive and the solids degrade in a few days; X-ray crystal structures were obtained for all four complexes and reveal a *pseudo*-tetrahedral geometry about both B and Sb

(Fig. 25) and show small differences in d(B-Sb) with an overall decrease Cl > Br > I, consistent with the expected Lewis acidity trend. The experimental and computational data show that the C-Sb-C angles widen on coordination of the stibines (Section 8), providing evidence that this effect is not limited to d-block complexes [125]. In contrast, the reaction of the triaryl stibine, $SbPh_3$, with BCl_3 in either C_6D_6 or CD_2Cl_2 was shown by *in situ* ^{11}B NMR spectroscopy to produce $PhBCl_2$, with no evidence for simple adduct formation. With BBr_3 or BI_3 in *situ* ^{11}B NMR data showed transient formation of $[BX_3(SbPh_3)]$, which decomposed rapidly with scrambling of substituents at B and Sb.

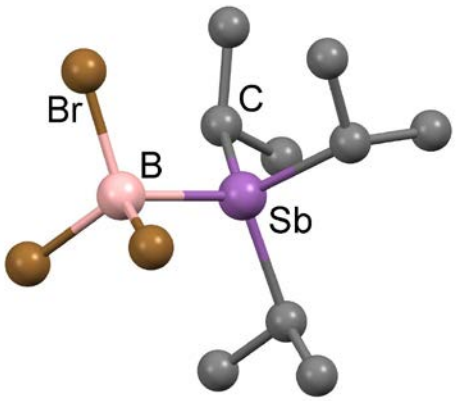

Fig. 25: Structure of $[BBr_3(Sb^iPr_3)]$, redrawn from Ref. 125.

For the $BF_3/SbPh_3$ system ^{19}F NMR spectra showed only very weak interactions in solution and no complex could be isolated (substituent scrambling is not expected here given the strength of the B-F bond) [125].

The reactions of BX_3 (X = Cl, Br) with a variety of stibines, followed by treatment by 1,3-propanediol and MeOH to give arylboronates has been described, however, the work did not attempt to identify adduct formation, which is presumably the first step of the sequence of reactions [127].

Reaction of AlX_3 (X = Cl, Br, I) with SbR_3 (R = Et, ^{i}Pr) produced $[AlX_3(SbR_3)]$ as extremely moisture sensitive, low melting solids or waxes, but in contrast to the boron complexes, these are stable over time both as the solid and in solution as long as they are protected from moisture [125]. AlF_3 is an inert polymer, which does not complex with soft donor ligands, including pnictines [128]. The $[AlCl_3(SbR_3)]$ are soluble in CH_2Cl_2 without reaction, but $[AlX_3(SbR_3)]$ (X = Br, I) react with the solvent by Cl/X exchange to form $[AlX_{3-n}Cl_n(SbR_3)]$, readily identified in the ^{27}Al NMR spectra. The low melting points of $[AlX_3(SbR_3)]$ hindered attempts to produce crystals for X-ray analysis, but the structure of $[AlI_3(Sb^iPr_3)]$ was obtained, and showed the expected pseudo-tetrahedral geometry at aluminium [125]. The structure of $[Al^tBu_3(SbMe_3)]$, made from Al^tBu_3 and $SbMe_3$ in n-pentane, has been determined [129] and the structure of $[Al^tBu_3(Sb^iBu_3)]$, formed as a by-product of the reaction of Al^tBu_3 with $Sb_2{}^iBu_4$, reported [130].

Gallium and indium trihalides form complexes, [$MX_3(SbR_3)$] (M = Ga, In; X = Cl, Br, I; R = Et, ^{i}Pr, ^{n}Bu), by combination of the constituents in n-hexane or CH_2Cl_2 [125,131]. The solids are much less moisture sensitive than the boron or aluminium complexes, although they still hydrolyse in solution. In contrast to the cases with PR_3 or AsR_3, which form both 4- and 5-coordinate adducts with indium halides, there was no evidence for [$InX_3(SbR_3)_2$] complexes from *in situ* ^{115}In NMR spectroscopic studies [131]. Structures were determined for nine representative examples, all containing the expected tetrahedral environment at the metal centre (Fig. 26), and showed d(M-Sb) increased with halide Cl < Br < I (the reverse order to the boron halides above). The indium chloride complexes [$InCl_3(SbR_3)$] (R = Et, ^{i}Pr, ≠ ^{n}Bu) show hypervalent Cl···Sb interactions between neighbouring molecules (Fig. 27).

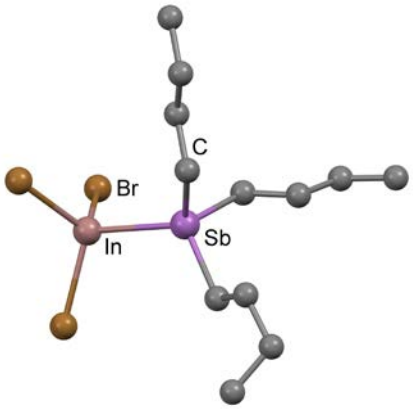

Fig. 26: Structure of [$InBr_3(Sb^{n}Bu_3)$], redrawn from Ref. 131.

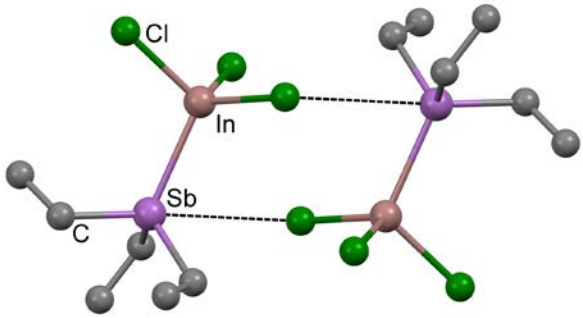

Fig. 27: Structure of [$InCl_3(SbEt_3)$] showing hypervalent interactions, redrawn from Ref. 125.

The absence of hypervalent interactions in solid [$InCl_3(Sb^{n}Bu_3)$] shows that the hypervalency only provides a small energy contribution, and this may be outweighed by crystal packing or steric factors.

The structure of [$GaCl_3(SbMe_3)$] has also been reported [132]. Attempts to use [$GaCl_3(SbR_3)$] or [$InCl_3(SbR_3)$] (R = Et, ^{n}Bu) as low pressure chemical vapour deposition reagents for GaSb or InSb films were unsuccessful, with deposition of elemental antimony observed instead [131]. Pseudo-

tetrahedral stibine adducts of Ga^tBu_3, $[Ga^tBu_3(SbR_3)]$ (R_3 = Me_3, $Et_2{}^tBu$, Ph_3) [133-136], have been prepared and characterised spectroscopically and by X-ray diffraction (Fig. 28). The d(Ga-Sb) bonds appear to be ~ 0.2-0.3 Å longer than those in $[GaCl_3(SbR_3)]$ [125], consistent with reduced Lewis acidity of the gallium alkyls, although the sterically bulky R-groups also contribute to the lengthening of the bonds. Notably, thermal decomposition of the trialkylgallium complexes gives GaSb films or nanowires.

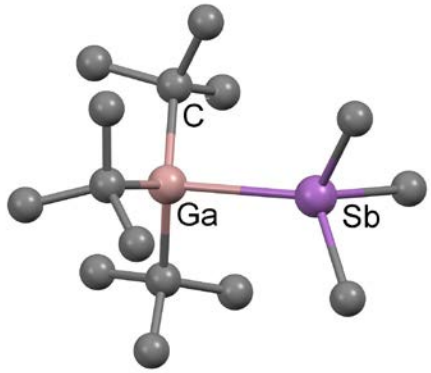

Fig. 28: Structure of $[Ga^tBu_3(SbMe_3)]$ redrawn from Ref. 134.

The addition of SbR_3 (R = Et, ^iPr) to SnX_4 (X = Br, Cl) in CH_2Cl_2 results in immediate formation of R_3SbX_2 and an insoluble grey solid, probably SnX_2 [137]. Similarly, the reaction of $SnCl_4$, $SbEt_3$ and trimethylsilyl triflate, $Me_3SiO_3SCF_3$, results in redox chemistry, with $[Et_3SbCl(O_3SCF_3)]$ as one product obtained in ~ 30% yield [137].

5. Monodentate bismuthine complexes

Triorganobismuthine complexes remain relatively elusive, although the detailed characterisation of some trialkylbismuthine complexes is notable. The reaction of $[M(CO)_5(thf)]$ (M =Cr, W), prepared *in situ* by photolysis of $M(CO)_6$ in thf, with BiR_3 (R = Me, $^tBu_3$) produced white, air-sensitive $[M(CO)_5(BiR_3)]$ [37,43]. The structures of both were determined (Fig. 29) and show that coordination causes the C-Bi-C angles to open [8,43] (analogous to the SbR_3 case), and that the cone angles of the bismuthines determined from the X-ray data are slightly smaller than those of lighter pnictines (for a given R group) due to the longer M-Bi bonds. DFT calculations indicate that the ligand donor properties of $SbMe_3$ and $BiMe_3$ are surprisingly similar, with the latter only slightly more weakly binding [37], although the fragility of the Bi-C bond remains a problem in some other systems.

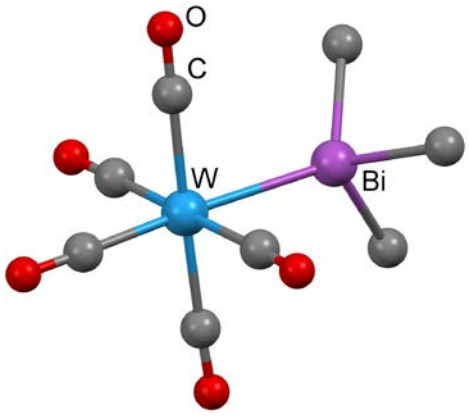

Fig. 29: Structure of $[W(CO)_5(BiMe_3)]$, redrawn from Ref. 37.

The complexes, $[M(CO)_5\{BiPh_2(o\text{-}C_6H_4OMe)\}]$ (M = Cr, W), have been prepared and are very rare examples of unsymmetrical tertiary bismuthine complexes [138]. The kinetics of the formation of $[W(CO)_5(BiPh_3)]$ from $[W(CO)_5(Me_3SiC{\equiv}CSiMe_3)]$ and $BiPh_3$ have been studied [139].

Red $[Mn(\eta^5\text{-CpMe})(CO)_2(Bi^tBu_3)]$ (CpMe = C_5H_4Me) and $[Fe(CO)_4(Bi^tBu_3)]$ were prepared from the ligand and $[Mn(\eta^5\text{-CpMe})(CO)_3]$ or $[Fe_2(CO)_9]$, respectively, and their structures determined [37,43]. The reaction of $BiMe_2Ph$ with $[CpFe(CO)_2(thf)]BF_4$ in CH_2Cl_2, irrespective of the reaction times or temperature (-78°C to ambient), gave 'scrambled' mixtures of $[CpFe(CO)_2(BiPh_{3-n}Me_n)]BF_4$ (n = 0, 1, 2, 3), as determined by ES^+ mass spectrometry and *in situ* ^1H and $^{13}C\{^1H\}$ NMR spectroscopy [13]. In contrast, $[CpFe(CO)_2\{BiPh_2(o\text{-}C_6H_4OMe)\}]BF_4$ was successfully prepared from $[CpFe(CO)_2(thf)]BF_4$ and $BiPh_2(o\text{-}C_6H_4OMe)$ and its structure determined (Fig. 30) [13]. This is the first crystallographically authenticated complex containing an unsymmetrical tertiary monobismuthine. Slow scrambling of the R-substituents on bismuth was observed in solution in CH_2Cl_2. The crystal structures of three polymorphs of $[CpFe(CO)_2(BiPh_3)]BF_4$ have been obtained [13]. Unstable yellow $[Os_3(CO)_{11}(BiPh_3)]$ was isolated from reaction of $[Os_3(CO)_{11}(cyclooctene)]$ and $BiPh_3$; the X-ray structure reveals the $BiPh_3$ occupying an equatorial position on one osmium [140].

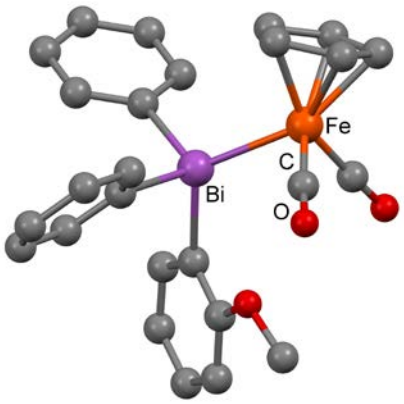

Fig. 30: Structure of $[CpFe(CO)_2\{BiPh_2(o\text{-}C_6H_4OMe)\}]^+$, redrawn from Ref. 13.

6. Distibine Complexes

The 1,8-naphthalene distibines (I, Scheme 1) and the binaphthyl distibines (II, Scheme 1) readily displace norbonadiene (nbd) from $[Mo(CO)_4(nbd)]$ to form beige or orange-brown *cis*-$[Mo(CO)_4(distibine)]$ (distibine = I or II) [11]. The structure of $[Mo(CO)_4$(II; R = Me)] (Fig. 31) shows a Sb-Mo-Sb angle of ~ 84°, which is remarkably small for a seven-membered chelate ring, and most likely attributable to the sterically bulky and rather rigid backbone present.

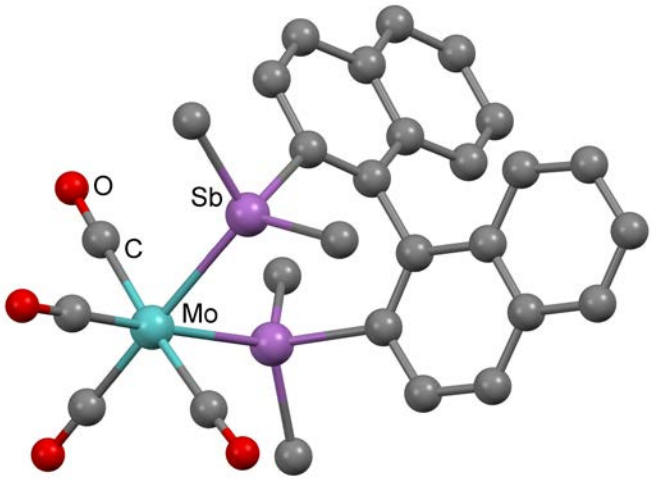

Fig. 31: Structure of $[Mo(CO)_4$(II, R = Me)], redrawn from Ref. 11.

Similar complexes of the enantiomers of the DIOP based ligands (III, Scheme 1) were also described [11]. The wide-angle distibine, $\{CH_2(o\text{-}C_6H_4CH_2SbMe_2)\}_2$, forms *cis*-$[W(CO)_4\{CH_2(o\text{-}C_6H_4CH_2SbMe_2)\}_2]$ on reaction with $[W(CO)_4(pip)_2]$, the X-ray structure of which shows the presence of an 11-membered chelate ring [10]. Two polymorphs of the complex were identified which differ in the orientation of the ligand backbone (Fig. 32) [10].

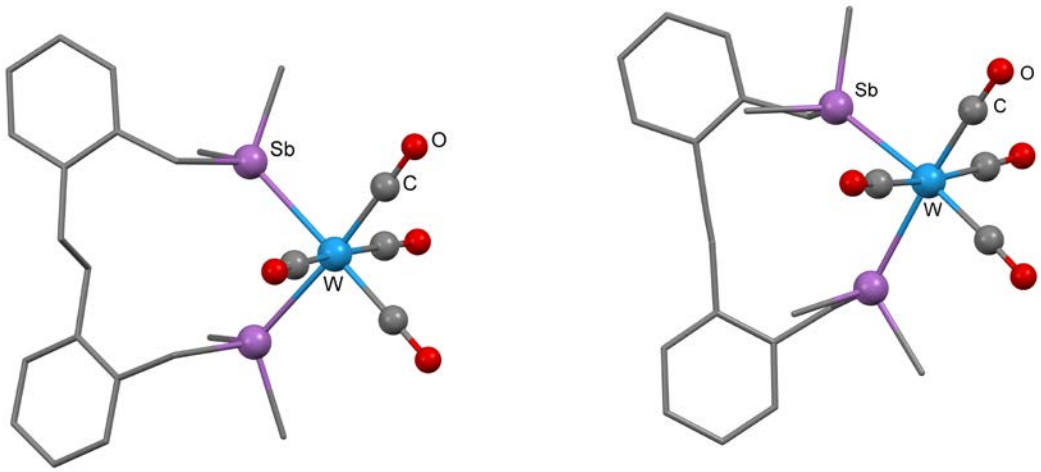

Fig. 32: Structures of two polymorphs of *cis*-[W(CO)$_4${CH$_2$(*o*-C$_6$H$_4$CH$_2$SbMe$_2$)}$_2$], redrawn from Ref. 10.

The X-ray structure of the dinuclear [{CpFe(CO)$_2$}$_2${μ^2-Ph$_2$Sb(CH$_2$)$_3$SbPh$_2$)] has been reported [13].

The distibine, Ph$_2$Sb(CH$_2$)$_3$SbPh$_2$, reated with [Rh$_2$(CO)$_4$Cl$_2$] to produce [Rh{Ph$_2$Sb(CH$_2$)$_3$SbPh$_2$}$_2$(CO)][Rh(CO)$_2$Cl$_2$], which on treatment with further distibine and [NH$_4$][PF$_6$] was converted to [Rh{Ph$_2$Sb(CH$_2$)$_3$SbPh$_2$}$_2$(CO)][PF$_6$], with a trigonal bipyramidal cation and an equatorial carbonyl [141]. The corresponding [Rh(distibine)$_2$(CO)][Rh(CO)$_2$Cl$_2$],] (distibine = Me$_2$Sb(CH$_2$)$_3$SbMe$_2$ or *o*-C$_6$H$_4$(CH$_2$SbMe$_2$)$_2$) were isolated similarly at low temperatures, and identified by a combination of IR, ^{1}H NMR spectroscopy and ES$^+$ mass spectrometry, but are unstable in solution at room temperature [141]. Treatment of [Rh$_2$(COD)$_2$Cl$_2$] with R$_2$Sb(CH$_2$)$_3$SbR$_2$ (R = Me, Ph) or *o*-C$_6$H$_4$(CH$_2$SbMe$_2$)$_2$ gave the 18e electron, five-coordinate [Rh(COD){distibine}Cl]. In the presence of AgBF$_4$, the four coordinate planar 16e cations [Rh(COD)(distibine)]BF$_4$ can be isolated. Using the precursor bearing the more readily displaced cyclooctene (COE), [Rh$_2$(COE)$_4$Cl$_2$], the [Rh(distibine)$_2$]BF$_4$ are formed [141]. An alternative synthesis of [Rh{Ph$_2$Sb(CH$_2$)$_3$SbPh$_2$}$_2$(CO)]Cl is from CO and [Rh{Ph$_2$Sb(CH$_2$)$_3$SbPh$_2$}$_2$]$^+$ in acetone solution, and under a CO atmosphere a dicarbonyl species is formed (identified by its IR spectrum, but not isolated). The latter seems unlikely to be the 20e [Rh{Ph$_2$Sb(CH$_2$)$_3$SbPh$_2$}$_2$(CO)$_2$]$^+$ and may be [Rh{κ^2-Ph$_2$Sb(CH$_2$)$_3$SbPh$_2$}{κ^1-{Ph$_2$Sb(CH$_2$)$_3$SbPh$_2$}(CO)$_2$]$^+$, since the reaction reverses when the CO atmosphere is removed. [Rh{Ph$_2$Sb(CH$_2$)$_3$SbPh$_2$}$_2$(CO)]$^+$ is oxidised by Br$_2$ to [Rh{Ph$_2$Sb(CH$_2$)$_3$SbPh$_2$}$_2$Br$_2$]$^+$, but does not react with MeI. The reaction of [Rh{Ph$_2$Sb(CH$_2$)$_3$SbPh$_2$}$_2$(CO)]$^+$ with HCl gas in CH$_2$Cl$_2$ gives a mixture of products, which include [Rh{Ph$_2$Sb(CH$_2$)$_3$SbPh$_2$}(H)Cl$_2$] and [Rh{Ph$_2$Sb(CH$_2$)$_3$SbPh$_2$}{PhClSb(CH$_2$)$_3$SbPhCl}Cl$_2$]Cl. The structure of the latter reveals it to be the first complex of a bidentate halostibine, and that the Cl$^-$ ion

forms a strong hypervalent interaction with both antimony atoms in the halostibine (Fig 33). Rhodium(I) complexes [Rh(COD)(distibine)Cl] (distibine = I, II, Scheme 1 R = Ph) have also been characterised [11] .

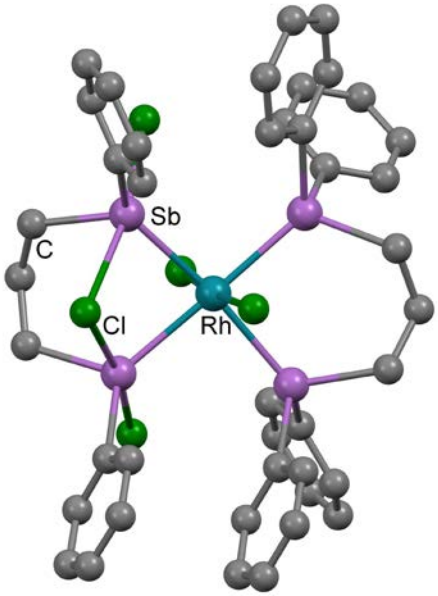

Fig. 33: Structure of [Rh{$Ph_2Sb(CH_2)_3SbPh_2$}{$PhClSb(CH_2)_3SbClPh$}Cl_2]Cl, redrawn from Ref. 141.

The [Ir(COD)(distibine)][BF_4] (distibine = $Ph_2Sb(CH_2)_3SbPh_2$, *o*-$C_6H_4(CH_2SbMe_2)_2$) and [Ir{$Ph_2Sb(CH_2)_3SbPh_2$}$_2$]BF_4 were made analogously to the rhodium complexes described; the latter takes up CO in acetone solution to form a dicarbonyl, but the CO is lost on removing the solvent [141].

Square planar [$PtCl_2$(distibine)] (distibine = I, II, III; Scheme 1) have been prepared and characterised; those with Ph substituents are very poorly soluble in common solvents [11]. The wide-angle distibine {CH_2(*o*-$C_6H_4CH_2SbMe_2$)}$_2$ forms a planar [$PtCl_2${CH_2(*o*-$C_6H_4CH_2SbMe_2$)}$_2$], whose X-ray structure reveals a weakly associated dimer (Fig. 34) assembled via a Pt···Pt interaction of 3.176(1) Å and hypervalent Sb···Cl links [10].

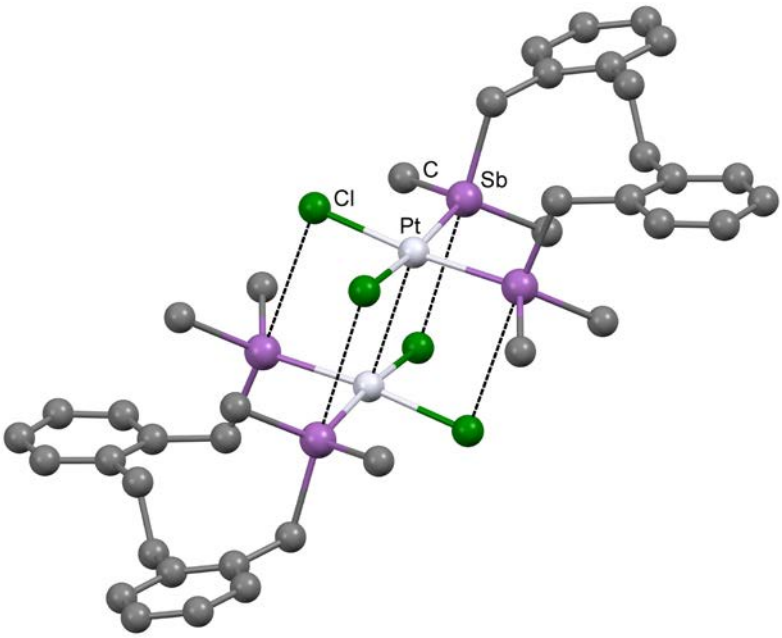

Fig. 34: Structure of [Pt{CH_2(*o*-$C_6H_4CH_2SbMe_2$)}$_2Cl_2$] dimer, redrawn from Ref. 10.

Yellow [$PtMe_2$(distibine)] (distibine = $R_2Sb(CH_2)_3SbR_2$, R = Me, Ph, *o*-$C_6H_4(CH_2SbMe_2)_2$) are readily prepared from [$PtMe_2(SMe_2)_2$] and the distibine in benzene [115]. However the $R_2SbCH_2SbR_2$ (R = Me, Ph) produce dimers, [$Me_2Pt(\mu^2$-$R_2SbCH_2SbR_2)_2PtMe_2$]. Platinum(IV) distibines, *fac*-[$PtMe_3I$(distibine)], obtained from reaction of $PtMe_3I$ with the ligands in chloroform [115], are much more stable than the corresponding [$PtCl_4$(distibines)], which decompose in a few days in the solid state and very rapidly in solution, with formation of Pt(II) and organoantimony dihalides [142]. The [$PtMe_2\{Ph_2Sb(CH_2)_3SbPh_2\}$] oxidatively adds MeI to form [$PtMe_3I\{Ph_2Sb(CH_2)_3SbPh_2\}$] and on heating the latter reductively eliminates ethane. The structure of [$PtMe_3I\{Me_2Sb(CH_2)_3SbMe_2\}$] is shown in (Fig. 35) [115].

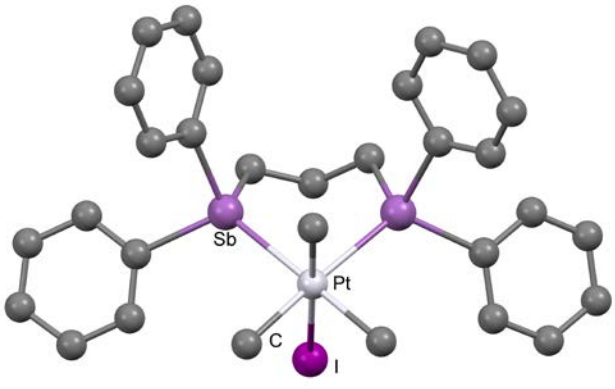

Fig. 35: Structure of [$PtMe_3I\{Me_2Sb(CH_2)_3SbMe_2\}$], redrawn from Ref. 115.

The distibinomethane complexes, [($PtMe_3I)_2(\mu^2$-$R_2SbCH_2SbR_2$)], are dimers with both iodide and distibine bridges (Fig. 36).

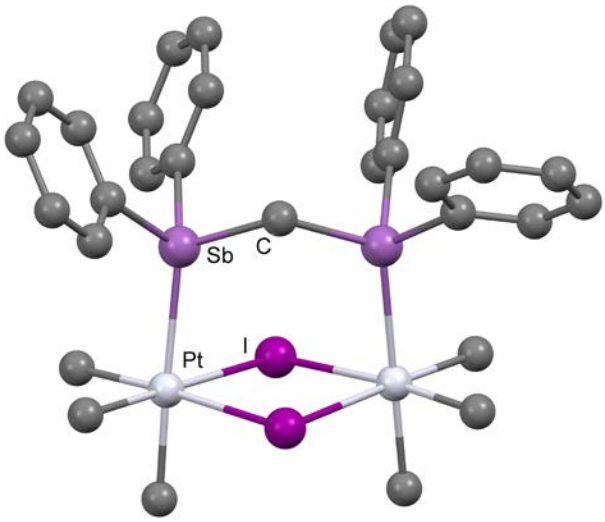

Fig. 36: Structure of $[(PtMe_3I)_2(\mu^2\text{-}Ph_2SbCH_2SbPh_2)]$, redrawn from Ref. 115.

Evaporation of a mixture of CuI and $Ph_2SbCH_2SbPh_2$ in MeCN gave a few crystals with the composition $[(CuI)_3(Ph_2SbCH_2SbPh_2)_2(MeCN)]\cdot MeCN$ whose structure revealed a "step" polymer with the distibine bridging alternate pairs of copper atoms [143].

7. Mixed donor polydentates containing stibine or bismuthine donor groups

7.1. Ligands containing neutral O, S or N donor atoms

The ligands $O(CH_2CH_2SbR_2)_2$ (R = Me, Ph) react with $[M(CO)_5(thf)]$ (M = Cr, W) in a 1:2 molar ratio in thf to give a mixture of $[\{M(CO)_5\}_2\{O(CH_2CH_2SbR_2)_2\}]$ and *cis*-$[M(CO)_4\{O(CH_2CH_2SbR_2)_2\}]$ [138]. The pentacarbonyl dimers can be obtained pure by using excess $[M(CO)_5(thf)]$, while the tetracarbonyls are formed cleanly using $[Cr(CO)_4(nbd)]$ or $[W(CO)_4(pip)_2]$. The pentacarbonyl complexes decompose slowly in solution to the tetracarbonyls and $M(CO)_6$ and crystal structures could not be obtained, although the spectroscopic data are in accord with the proposed structures [138]. Crystal structures of both tetracarbonyl complexes showed the expected Sb_2-coordination and eight-membered chelate rings, but disorder in the backbone prevented identification of any hypervalent interaction(s) involving the oxygen.

The ligand, $O(CH_2CH_2BiPh_2)_2$, reacted with $[M(CO)_5(thf)]$ (M = Cr, W) to give $[\{M(CO)_5\}_2\{O(CH_2CH_2BiPh_2)_2\}]$, but in contrast to the antimony analogues, there was no evidence for tetracarbonyl formation [138]. This possibly reflects the slightly less basic nature of the bismuthine.

Hypervalent interaction with one antimony was observed in the structure of $[\{CpFe(CO)_2\}_2\{O(CH_2CH_2SbMe_2)_2\}][BF_4]_2$, with Sb···O = 3.184(8) Å (Fig. 37), and is also evident in the IR spectra of both $[\{CpFe(CO)_2\}_2\{O(CH_2CH_2SbR_2)_2\}][BF_4]_2$, which show inequivalent

$CpFe(CO)_2$ carbonyl groups in the solid state; the inequivalence is not evident in the solution IR spectra [13].

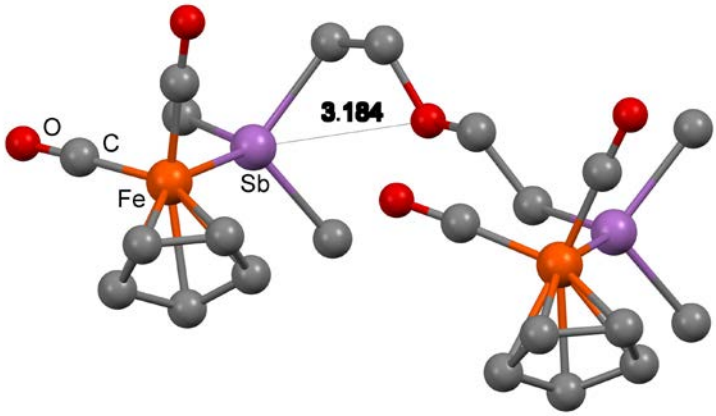

Fig.37: Structure of $[\{CpFe(CO)_2\}_2\{O(CH_2CH_2SbMe_2)_2\}]^{2+}$, redrawn from Ref. 13.

Red $[\{CpFe(CO)_2\}_2\{O(CH_2CH_2BiPh_2)_2\}][BF_4]_2$ was made similarly and fully characterised spectroscopically, although it decomposes rapidly at room temperature [13]. The complexes, $[RhCl_2\{O(CH_2CH_2SbR_2)_2\}_2]Cl$ and $[PtCl_2\{O(CH_2CH_2SbR_2)_2\}]$ (R = Me, Ph), contain Sb_2-coordinated ligands [12]. Tetrahedral $[Cu\{O(CH_2CH_2SbR_2)_2\}_2]BF_4$ and the light-sensitive $[Ag\{O(CH_2CH_2SbR_2)_2\}_2]BF_4$, containing Sb_4-coordination at the metal centres and which exhibit weak hypervalent O···Sb to both antimony centres, were also reported. [12].

In contrast to the Sb_2O ligands, which show no tendency to coordinate to metal centres via the ether oxygen, the $S(CH_2\text{-}2\text{-}C_6H_4SbMe_2)_2$ behaves as an Sb_2S-donor ligand in *fac*-$[M(CO)_3\{S(CH_2\text{-}2\text{-}C_6H_4SbMe_2)_2\}]$ (M = Cr, Mo), formed from the ligand and $[M(CO)_3(MeCN)_3]$; the X-ray structure of the Cr complex was determined 138]. No reaction occurred between $[M(CO)_3(MeCN)_3]$ and the $S(CH_2\text{-}2\text{-}C_6H_4BiR_2)_2$ (R = Me, Ph) in MeCN at room temperature, and the ligands fragmented on heating the solution [138]. The *fac*-$[Mn(CO)_3\{S(CH_2\text{-}2\text{-}C_6H_4SbMe_2)_2\}][CF_3SO_3]$ was obtained using $[Mn(CO)_3(acetone)_3][CF_3SO_3]$. Both the $S(CH_2\text{-}2\text{-}C_6H_4SbR_2)_2$ and $S(CH_2\text{-}2\text{-}C_6H_4BiR_2)_2$ ligands form $[\{Cp_2Fe(CO)_2\}_2(ligand)][BF_4]_2$ in which they function as Sb_2- and Bi_2-donors [13].

The halostibine, $(2\text{-}Me_2NCH_2C_6H_4)PhClSb$, which contains a short hypervalent intramolecular Sb-N bond, forms the ionic palladium(II) complex $[Me_2N(H)CH_2C_6H_5][PdCl_3\{SbClPh(C_6H_4CH_2NMe_2\text{-}2)]$, which has a planar anion and with the pendant arm nitrogen still interacting with the antimony [144]. The related $Sb(2,4,6\text{-}Me_3C_6H_2)_2(C_6H_4CH_2NMe_2)$ forms a conventional (SbN-coordinated) *cis*-$[PdCl_2(ligand)]$ complex [144].

The potentially tridentate Sb_2N-donor ligand, $MeN(CH_2\text{-}2\text{-}C_6H_4SbMe_2)_2$ (V, Scheme 1), reacts with $[Cr(CO)_4(nbd)]$, $[W(CO)_4(pip)_2]$ or $Mo(CO)_6$ + $NaBH_4$ to form the tetracarbonyl complexes *cis*-

[M(CO)$_4${MeN(CH$_2$-2-C$_6$H$_4$SbMe$_2$)$_2$}] cleanly, which were fully characterised spectroscopically. X-ray crystal structures of all three complexes confirmed the Sb$_2$-coordination, but whilst the isomorphous Mo and W complexes show one hypervalent N···Sb interaction (Fig. 38), in the chromium complex the N···Sb are too long for a significant interaction and the (different) backbone conformation does not allow a close approach required for hypervalency (Fig. 39) [14,138]. In the orange [{Cr(CO)$_5$}$_2${MeN(CH$_2$-2-C$_6$H$_4$BiPh$_2$)$_2$}], spectroscopic data are consistent with the Bi$_2$-coordinated ligand bridging two pentacarbonylchromium groups; the corresponding tungsten complex is unstable and could not be isolated in a pure form [138].

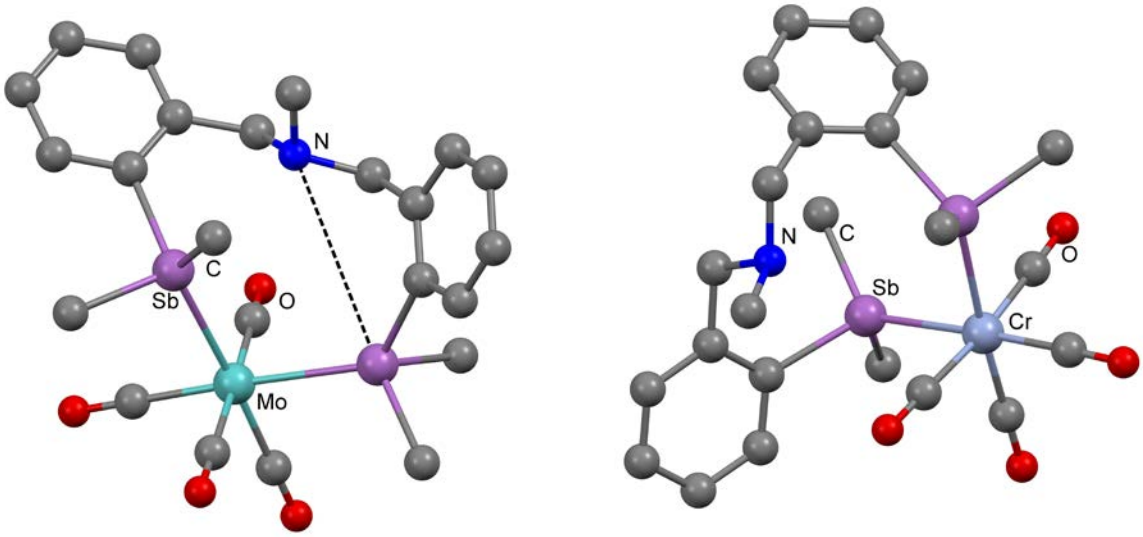

Fig. 38: Structure of *cis*-[Mo(CO)$_4${MeN(CH$_2$-2-C$_6$H$_4$SbMe$_2$)$_2$}] and Fig. 39: structure of *cis*-[Cr(CO)$_4${MeN(CH$_2$-2-C$_6$H$_4$SbMe$_2$)$_2$}], redrawn from Ref. 14 and 138.

Tridentate coordination (Sb$_2$N) of MeN(CH$_2$-2-C$_6$H$_4$SbMe$_2$)$_2$ is achieved in *fac*-[Mn(CO)$_3${MeN(CH$_2$-2-C$_6$H$_4$SbMe$_2$)$_2$}][CF$_3$SO$_3$] [14,138] and confirmed by a crystal structure. In solution in CDCl$_3$ a second (minor) species is present, believed to be *fac*-[Mn(CO)$_3${κ^2-MeN(CH$_2$-2-C$_6$H$_4$SbMe$_2$)$_2$}(CF$_3$SO$_3$)] where a coordinated triflate has displaced the weakly bound tertiary amine donor.

The structure of the complex [{CpFe(CO)$_2$}$_2${MeN(CH$_2$-2-C$_6$H$_4$SbMe$_2$)$_2$}][BF$_4$]$_2$, shows no hypervalent interaction, but in contrast, the IR spectra of [{CpFe(CO)$_2$}$_2${MeN(CH$_2$-2-C$_6$H$_4$BiPh$_2$)$_2$}][BF$_4$]$_2$ contain four υ(CO) stretches both in the solid and in solution, indicating a hypervalent N···Bi coordination to one bismuth, which (most unusually) persists in solution [13]. Other complexes of MeN(CH$_2$-2-C$_6$H$_4$SbMe$_2$)$_2$ include, [Cu{MeN(CH$_2$-2-C$_6$H$_4$SbMe$_2$)$_2$}$_2$[BF$_4$] (Sb$_4$

coord.), *fac*-[PtMe$_3$I{MeN(CH$_2$-2-C$_6$H$_4$SbMe$_2$)$_2$}] (Sb$_2$N coordination) and [RhCl$_2${MeN(CH$_2$-2-C$_6$H$_4$SbMe$_2$)$_2$}$_2$]Y (Y = Cl, BF$_4$) (Sb$_4$Cl$_2$? coordination). [14].

Two complexes of the linear tetradentate CH$_2$(CH$_2$N(Me)CH$_2$-2-C$_6$H$_4$SbMe$_2$)$_2$ (VI, Scheme 1) have been obtained [14]; neither has been characterised by X-ray crystallography, but the coordination based upon spectroscopic data are [Cu{CH$_2$(CH$_2$N(Me)CH$_2$-2-C$_6$H$_4$SbMe$_2$)$_2$}$_2$]BF$_4$ (tetrahedral Sb$_4$), [RhCl$_2${CH$_2$(CH$_2$N(Me)CH$_2$-2-C$_6$H$_4$SbMe$_2$)$_2$}]Cl (octahedral Sb$_2$N$_2$Cl$_2$).

The potentially tripodal tetradentate NSb$_3$-donor ligand, N(CH$_2$-2-C$_6$H$_4$SbMe$_2$)$_3$ (IX, Scheme 1), has a marked preference to behave as an Sb$_3$ donor [15], and its complexes include [{CpFe(CO$_2$}$_3${N(CH$_2$-2-C$_6$H$_4$SbMe$_2$)$_3$}[BF$_4$]$_3$, where each antimony is coordinated to a different iron centre, and *fac*-[Mn(CO)$_3${N(CH$_2$-2-C$_6$H$_4$SbMe$_2$)$_3$}][CF$_3$SO$_3$], where it is a chelating tridentate (Sb$_3$ coord.). Treatment of the latter with Me$_3$NO in MeCN solution removes one carbonyl group, but rather than coordinate the apical amine, the X-ray structure reveals the product is [Mn(CO)$_2${N(CH$_2$-2-C$_6$H$_4$SbMe$_2$)$_3$}(MeCN)][CF$_3$SO$_3$]; the failure to coordinate the apical N-donor may be due to the steric effects of the semi-rigid linking groups (Fig. 40) .

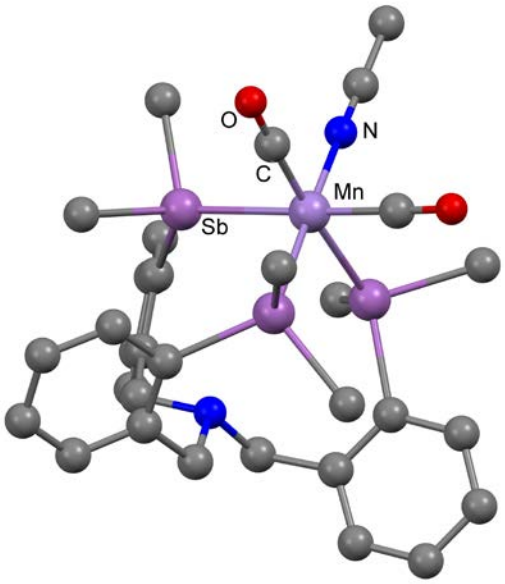

Fig. 40: Structure of [Mn(CO)$_2${N(CH$_2$-2-C$_6$H$_4$SbMe$_2$)$_3$}(MeCN)][CF$_3$SO$_3$], redrawn from Ref. 15.

The complexes, [Cu{N(CH$_2$-2-C$_6$H$_4$SbMe$_2$)$_3$}][BF$_4$] and [Ag{N(CH$_2$-2-C$_6$H$_4$SbMe$_2$)$_3$}][BF$_4$], which may contain either tetrahedral NSb$_3$ or trigonal Sb$_3$ coordination, were obtained, but unfortunately all attempts to obtain X-ray quality crystals were unsuccessful. The variable temperature ^{1}H and ^{13}C{^{1}H} NMR data indicate exchanging systems in solution, although the observation of a ^{63}Cu NMR resonance in the former complex may indicate the higher symmetry tetrahedral geometry is present [15]. Bromo-copper oligomers, [Cu$_4$Br$_4${N(CH$_2$-2-C$_6$H$_4$SbMe$_2$)$_3$}$_2$] and [Cu$_3$Br$_2${N(CH$_2$-2-C$_6$H$_4$SbMe$_2$)$_3$}][BF$_4$], were isolated and structurally characterised [15]. Tris-(2-N,N-

dimethylaminomethylferrocenyl)stibine (Fig. 41) forms a 1:1 complex with $PtCl_2$ in which it is coordinated as a bidentate (SbN) [145].

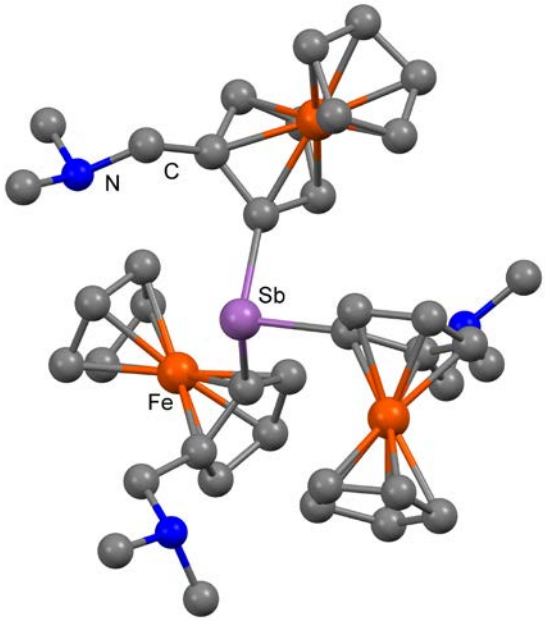

Fig. 41: Structure of tris-(2-N,N-dimethylaminomethylferrocenyl)stibine, redrawn from Ref 145.

A series of tris(2-pyridyl)bismuthines (X, Scheme 1) coordinate to Li^+, Ag^+, Cu^+ via the pyridyl nitrogens, whilst in some cases the bismuth behaves as a Lewis acid interacting with anions present; the chemistry can be modulated by substituents in the 3- or 6-positions on the heterocyclic rings [16,146]. Under some conditions, and with some metals, transfer of 2-pyridyl groups (Au(I) and Fe(II)) or coupling to form bipyridines (Cu(I) or Cu(II)) occurs.

7.2 Ligands containing neutral P donor atoms

Tri- and tetra-dentate phosphine ligands exemplified by $PhP(o\text{-}C_6H_4PPh_2)_2$ and $P(o\text{-}C_6H_4PPh_2)_3$ were developed in the 1960s, along with arsenic analogues, and their chemistry with late d-block halides explored in detail [147]. A few examples containing antimony or bismuth as the central donor were subsequently described, but received limited study, and did not appear to be significantly different. In the last decade the latter type has been revisited and it has been shown that in addition to hypervalent interactions, the metal coordinated stibine donor can be oxidised by one or two electrons to stiboranyl and stiborane groups, respectively, while remaining coordinated to the metal. The effect is to turn the electron pair donor stibine group into an electron acceptor from the metal in the stiborane. Similar but less extensive results involving bismuthine donors have also been reported. This ambiphilic behaviour in the Green nomenclature [148] converts an L-type ligand (stibine) into an X-type (stiboranyl) and then a Z-type (stiborane) ligand. (Green's scheme does not require assignment of formal oxidation states). The Z-ligand platforms have applications in catalysis, and in

some systems coordination of fluoride results in significant colour changes to the complexes making them potential fluoride anion sensors. Much of this elegant work has come from the Gabbaï group and has been described in two reviews [7,149]. In the present article the emphasis is on the hybrid stibine complexes, and the chemistry of the stiboranyls and stiboranes is not covered in detail. The metal centres involved to-date are from Groups 10 and 11.

The tripodal tetradentate Sb(*o*-$C_6H_4PPh_2)_3$ reacts with [$Ni(PPh_3)_4$] to form the Ni(0) complex, [Ni{Sb(*o*-$C_6H_4PPh_2)_3$}(PPh_3)], in which the tripod ligand is SbP_2-coordinated to a distorted tetrahedral nickel centre (Fig. 42) [150].

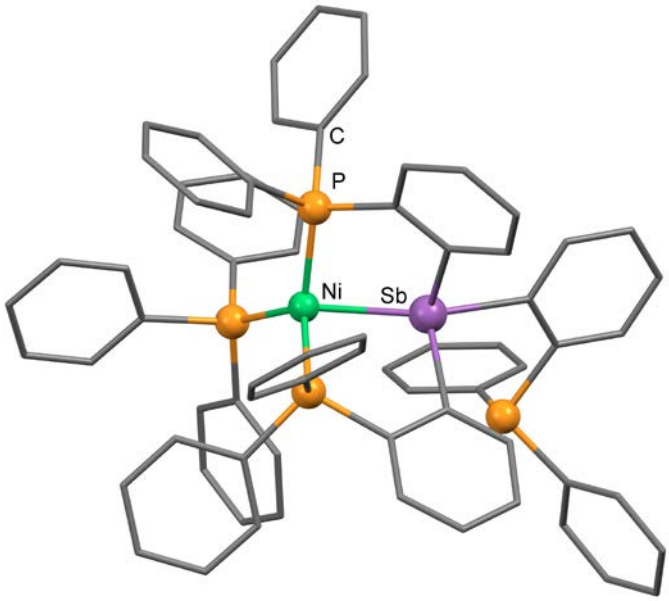

Fig. 42: Structure of [Ni{Sb(*o*-$C_6H_4PPh_2)_3$}(PPh_3)], redrawn from Ref. 150. Phenyl rings shown as planar hexagons for clarity.

Oxidation of this complex with $PhICl_2$ produced a purple complex in which the antimony, all three phosphine groups and a chlorine are coordinated to the nickel, but with the antimony also carrying a coordinated chlorine, i.e. [NiCl{Sb(Cl)(*o*-$C_6H_4PPh_2)_3$}] (Sb-Cl = 2.6835(9) Å) (Fig. 43) [150,151].

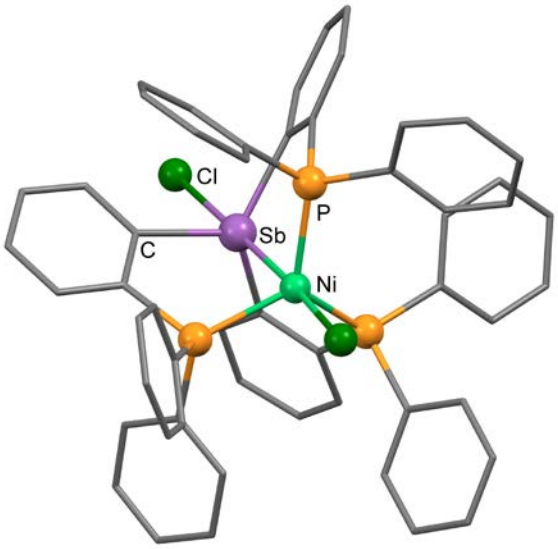

Fig. 43: Structure of [NiCl{Sb(Cl)(*o*-$C_6H_4PPh_2)_3$}], redrawn from Ref. 150.

Re-investigation of the series of complexes [NiCl{E(*o*-$C_6H_4PPh_2)_3$}]Cl (E = P, As, Sb) originally made by Venanzi [152,153] from $NiCl_2{\cdot}6H_2O$ and the pnictines, showed that the cases with E = P or As were trigonal bipyramidal Ni(II) species, as were the corresponding [NiCl{E(*o*-$C_6H_4PPh_2)_3$}]BPh_4, including the ligand with E = Sb; the structure of the [NiCl{Sb(*o*-$C_6H_4PPh_2)_3$}]BPh_4 was determined and confirmed the stibine group present (Fig. 44).

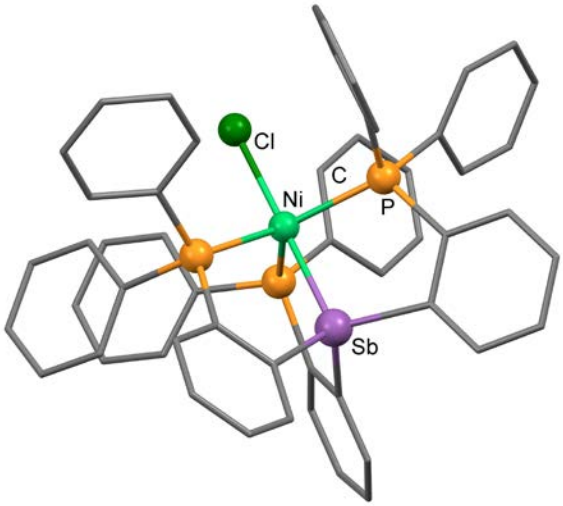

Fig. 44: Structure of [NiCl{Sb(*o*-$C_6H_4PPh_2)_3$}]$^+$, redrawn from Ref. 151.

Comparison of the structures shows that the large antimony atom is compressed onto the nickel (originally proposed by Venanzi to explain some anomalies in the electronic spectra) and the distortions at the antimony set up the geometry for coordination of the chlorine *trans* to the nickel [151]. The 'non-innocent' nature of the antimony in [NiCl{Sb(Cl)(*o*-$C_6H_4PPh_2)_3$}] was also explored by DFT calculations [151]. The Pd(II) complexes, [PdCl{Sb(*o*-$C_6H_4PPh_2)_3$}]BPh_4 and

[PdCl{SbPh(*o*-$C_6H_4PPh_2$)$_2$}]BPh_4, were obtained by combination of [$PdCl_2$(COD)], the appropriate pnictine and $NaBPh_4$; the X-ray crystal structures showed square planar palladium (SbP_2Cl-coordinated) [154]. Treatment of solutions of these complexes with [$^nBu_4N$]F produced the fluorostiboranyl complex, [PdCl{SbF(*o*-$C_6H_4PPh_2$)$_3$}], which had a trigonal bipyramidal geometry (SbP_3Cl donor set) (Fig. 45) and square planar [PdCl{SbPhF(*o*-$C_6H_4PPh_2$)$_2$}] (SbP_2Cl donor set), both confirmed by crystal structures.

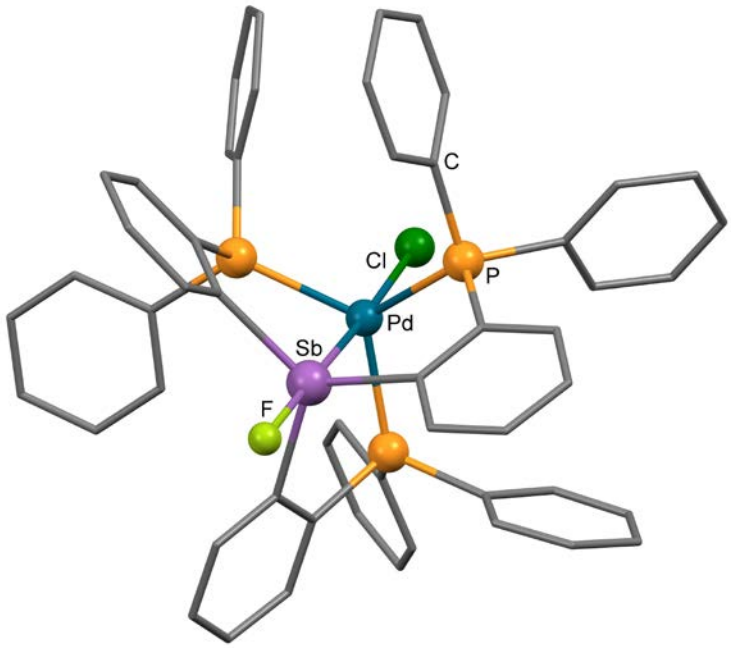

Fig. 45: Structure of [PdCl{SbF(*o*-$C_6H_4PPh_2$)$_3$}], redrawn from Ref. 154.

DFT calculations are consistent with Pd→Sb donation in the fluoro-complexes [154]. The substantial colour change that accompanies the formation of complex [PdCl{SbF(*o*-$C_6H_4PPh_2$)$_3$}] makes it suitable as an aqueous fluoride ion sensor [154]. Reaction of [$PtCl_2(SEt_2)_2$] with SbPh(*o*-$C_6H_4PPh_2$)$_2$ slowly forms the complex [PtCl{SbPhCl(*o*-$C_6H_4PPh_2$)$_2$}], with a planar platinum centre [155]. The complex [PtCl{SbCl(*o*-$C_6H_4PPh_2$)$_3$}] is formed analogously from the tetradentate pnictine and has a trigonal bipyramidal geometry [156]. Reaction of this complex with Ag[SbF_6] as a halide abstractor, cyclohexylisonitrile (CyNC), and a fluoride ion source, produced [Pt{Sb(*o*-$C_6H_4PPh_2$)$_3$}(CyNC)][SbF_6]$_2$, [Pt{SbF(*o*-$C_6H_4PPh_2$)$_3$}(CyNC)][SbF_6] and [Pt{SbF_2(*o*-$C_6H_4PPh_2$)$_3$}(CyNC)].

Most unexpectedly, the tetradentate Sb(*o*-$C_6H_4P^iPr_2$)$_3$ reacted with CuCl or AgCl in thf to form trimeric complexes, [Cu_3(μ^2-Cl)$_3${Sb(*o*-$C_6H_4P^iPr_2$)$_3$}] and [Ag_3(μ^2-Cl)$_3${Sb(*o*-$C_6H_4P^iPr_2$)$_3$}], whose structures revealed a central M_3(μ^2-Cl)$_3$ unit with each M coordinated to one phosphine group (Fig. 46) [157]. The stibine donor sits over the M_3 triangle and interacts with all three metal centres, a very

rare example of such an μ^3 mode. Multinuclear NMR spectroscopy suggests the structures persist in solution.

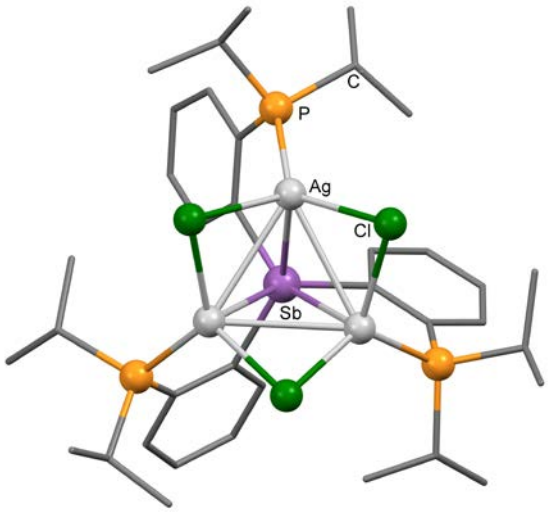

Fig. 46: Structure of $[Ag_3(\mu^2\text{-}Cl)_3\{Sb(o\text{-}C_6H_4P^iPr_2)_3\}]$, redrawn from Ref. 157.

Even more surprising is that similar behaviour was found with the bismuthine analogue, $Bi(o\text{-}C_6H_4P^iPr_2)_3$, with formation of $[Cu_3(\mu^2\text{-}Cl)_3\{Bi(o\text{-}C_6H_4P^iPr_2)_3\}]$ and $[Ag_3(\mu^2\text{-}Cl)_3\{Bi(o\text{-}C_6H_4P^iPr_2)_3\}]$, which not only have the unprecedented triply-bridging bismuth (Fig. 47), but appear to be the first bismuthine complexes of copper or silver [157].

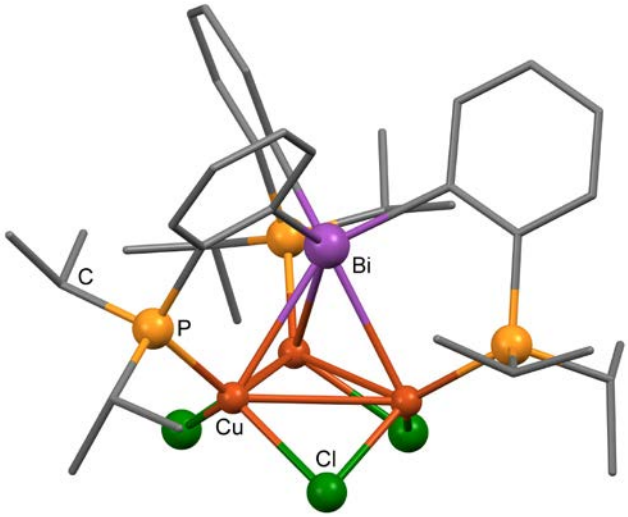

Fig 47: Structure of $[Cu_3(\mu^2\text{-}Cl)_3\{Bi(o\text{-}C_6H_4P^iPr_2)_3\}]$, redrawn from Ref. 157.

The coordination chemistry of gold with these ligands is quite different to that of the lighter congeners. The bidentate $Ph_2Sb(o\text{-}C_6H_4PPh_2)$ reacted with [AuCl(tht)] to form $[AuCl\{Ph_2Sb(o\text{-}C_6H_4PPh_2)\}]$ which has a T-shaped geometry with a long Au-Sb bond (3.051(1) Å (av)) (Fig. 48) [158].

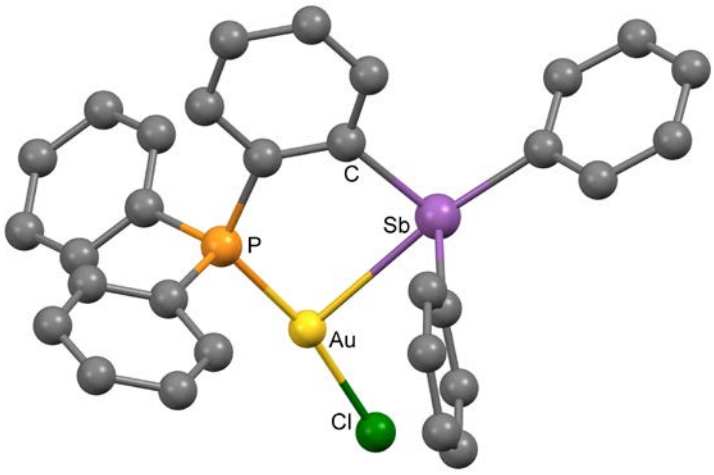

Fig. 48: Structure of [AuCl{$Ph_2Sb(o\text{-}C_6H_4PPh_2)$}], redrawn from Ref. 158.

Similarly, [AuCl{$PhSb(o\text{-}C_6H_4P^iPr_2)_2$}] has a trigonal pyramidal geometry with apical antimony [17]. The reaction of [AuCl(tht)] with $Sb(o\text{-}C_6H_4PPh_2)_3$ produced [AuCl{$Sb(o\text{-}C_6H_4PPh_2)_3$}], which has a distorted four-coordinate geometry (SbP_2Cl-donor set), again with a long Au-Sb bond (2.837(4) Å) [159]. Oxidation with $PhICl_2$ generates [AuCl{$SbCl_2(o\text{-}C_6H_4PPh_2)_3$}] in which the gold is still four-coordinate but the stiborane antimony is now in a distorted octahedral environment. In contrast to the stibine chemistry, the bismuthine-phosphine $Bi(o\text{-}C_6H_4PPh_2)_3$ reacts with [AuCl(thf)] to transfer an $o\text{-}C_6H_4PPh_2$ group to gold in [{$Au(o\text{-}C_6H_4PPh_2)$}$_2$] with formation of a chlorobismuthine ligand $ClBi(o\text{-}C_6H_4PPh_2)_2$ (below) [19]. The $BiR(o\text{-}C_6H_4PPh_2)_2$ (R = Me, C_6F_5) form square pyramidal platinum complexes [$PtCl_2${$BiR(o\text{-}C_6H_4PPh_2)_2$}] (Fig. 49) [20]. However, a detailed DFT and NBO analysis showed the Pt-Bi bond to be formed by donation from a filled Pt dz^2 orbital into a Bi-C σ* orbital [20].

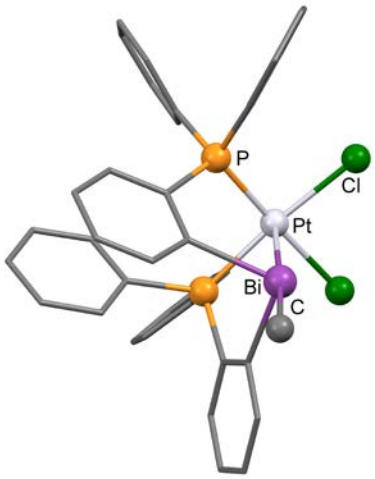

Fig. 49: Structure of [$PtCl_2${$BiMe(o\text{-}C_6H_4PPh_2)_2$}], redrawn from Ref. 20.

A new phosphine-bismuthine bidentate with a xanthene backbone, (Xan(PPh_2)($BiPh_2$)) (Fig. 50), reacted with the Pd(0) source [$Pd_2(dba)_3$] (dba = bis(dibenzylideneacetone)) to form the tetrahedral Pd(0) complex, [Pd{Xan(PPh_2)($BiPh_2$)}$_2$] [160]. The Pd-Bi bond lengths are Bi-Pd = 2.7342(11), 2.7845(11) Å, and DFT and NBO calculations are consistent with Bi→Pd donation [160]. In solution the complex decomposes in air to form a peroxopalladium(II) complex with the bismuthine functions uncoordinated.

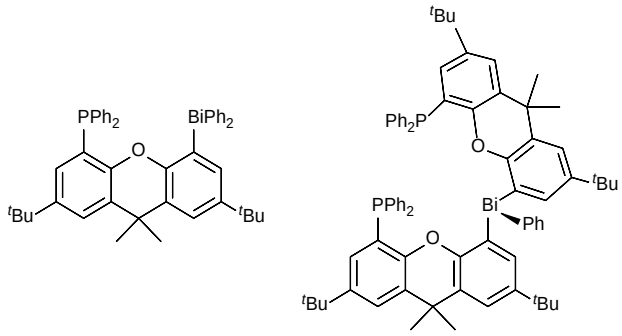

Fig. 50: Structures of Xan(PPh_2)($BiPh_2$) and PhBi(Xan(PPh_2)$_2$.

Unexpectedly, the Xan(PPh_2)($BiPh_2$) rearranges on reaction with [$Cu(MeCN)_4$][CF_3SO_3], $Ag(CF_3SO_3)$, and [$Au(PPh_3)(CF_3SO_3)$], transforming into the tridentate PhBi(Xan(PPh_2)$_2$ (Fig. 50) [161]. The resulting complexes, [Cu{PhBi(Xan(PPh_2)$_2$)}CF_3SO_3], [Ag{PhBi(Xan(PPh_2)$_2$)}CF_3SO_3], and [Au{PhBi(Xan(PPh_2)$_2$)}PPh_3][CF_3SO_3], have tetrahedral metal centres, coordinated to both phosphine groups, the bismuth and either the triflate anion or PPh_3 (Au) [161]. DFT calculations identified the bismuth as a σ-donor to the Group 11 metals [161].

In the last few years, ligands combining phosphine donor groups with a halostibine or halobismuthine group (Scheme 2, XV, XVI, XVII) have been explored by the Gabbaï and Limberg groups. The dichlorostibine, $SbCl_2$(*o*-$C_6H_4PPh_2$), made by comproportionation of $SbCl_3$ and Sb(*o*-$C_6H_4PPh_2$)$_3$, forms the gold complex [AuCl{$SbCl_2$(*o*-$C_6H_4PPh_2$)}], whose structure reveals a near linear Cl-Au-P unit with a weak perpendicular interaction to antimony [158]. In the complexes, [AuCl{SbCl(*o*-$C_6H_4PR_2$)$_2$}] (R = Ph, ^{i}Pr), the gold is in a trigonal pyramidal geometry (Fig. 51) with an apical antimony, and DFT calculations suggest the Au-Sb bond is best described as Au→Sb donation [17, 162].

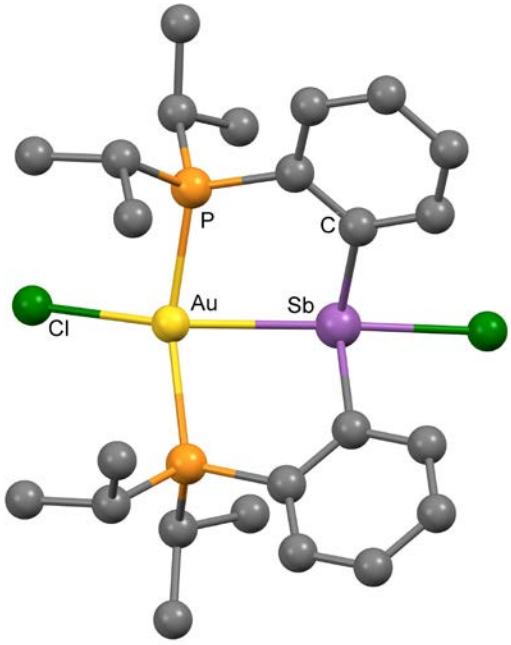

Fig. 51: Structure of [AuCl{SbCl(*o*-$C_6H_4P^iPr_2)_2$}], redrawn from ref. 17.

The Au-Cl bond is cleaved by Ag[SbF_6] to form [Au{SbCl(*o*-$C_6H_4P^iPr_2)_2$}][SbF_6], which has a T-shaped core with a further long interaction to a fluorine of the $[SbF_6]^-$ anion. The complexes are readily oxidised by $PhICl_2$ to the trichlorostiboranes [AuCl{$SbCl_3$(*o*-$C_6H_4PR_2)_2$}] and F/Cl exchange converts the Sb-Cl bonds into Sb-F (but does not exchange the Au-Cl) [17,162]. The platinum complex, [Pt{SbCl(*o*-$C_6H_4PPh_2)_2$}(CyNC)] $[CF_3SO_3]_2$ is also known [163].

Yellow [AuCl{BiCl(*o*-$C_6H_4PPh_2)_2$}] was formed by reaction of Bi(*o*-$C_6H_4PPh_2)_3$ with [AuCl(tht)] and has a square planar geometry about the gold, while the bismuth has a disphenoidal rather than the expected tetrahedral geometry, both of which suggest Au(III) and Au→Bi donation [19]. The [Au{BiCl(*o*-$C_6H_4PPh_2)_2$}Cl] was also made from preformed BiCl(*o*-$C_6H_4PPh_2)_2$ and [AuCl(PPh_3)] [18]. The product from the reaction of Bi(*o*-$C_6H_4PPh_2)_3$ with [$PdCl_2$(COD)] contained the chlorobismuthine ligand and a chelating *o*-$C_6H_4PPh_2$ in [PdCl{BiCl(*o*-$C_6H_4PPh_2)_2$}(*o*-$C_6H_4PPh_2$)] [19]. The geometry about the palladium is a distorted octahedron, more reminiscent of Pd(IV) than Pd(II) and DFT calculations support the presence of Pd→Bi donation. Reaction of [$PtCl_2$(COD)] with BiCl(*o*-$C_6H_4PPh_2)_2$ formed [$PtCl_2$BiCl(*o*-$C_6H_4PPh_2)_2$}] with the square pyramidal structure shown in (Fig. 52) [18]. The complex reacts with Ag(CF_3SO_3) to produce [$PtCl_2$Bi(CF_3SO_3)(*o*-$C_6H_4PPh_2)_2$}] [20]. Comparison of the structures of the series [$PtCl_2$BiX(*o*-$C_6H_4PPh_2)_2$}] (X = Cl, Me, C_6F_5, CF_3SO_3), supplemented by DFT and NBO calculations, shows that all contain Pt→Bi donation and that the extent of the donation increases with increasing electron withdrawing ability of the X group [20].

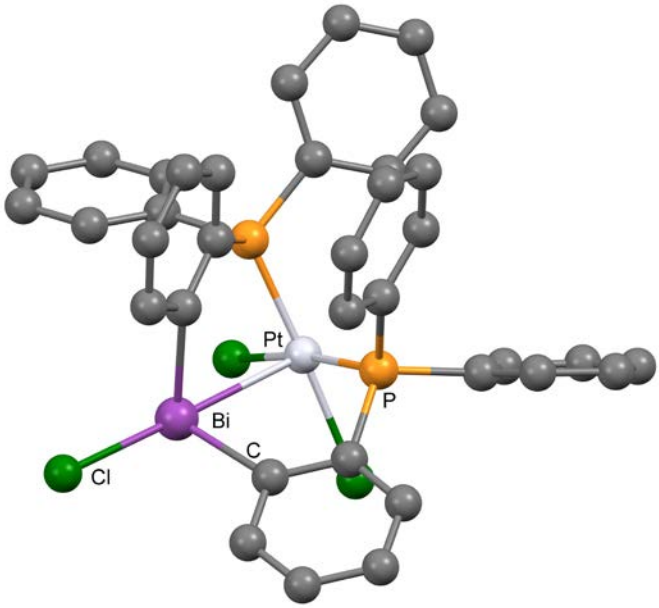

Fig. 52: Structure of [$PtCl_2${$BiCl(o\text{-}C_6H_4PPh_2)_2$}], redrawn from Ref. 18.

Different complexes of the type [MCl{$Bi(o\text{-}C_6H_4PPh_2)_2$}], are formed by combination of $BiCl(o\text{-}C_6H_4PPh_2)_2$ and [$M(PPh_3)_4$] (M = Pd, Pt), formally from the insertion of the Pd or Pt into the Bi-Cl bond (Fig. 53); the corresponding [PtX{$Bi(o\text{-}C_6H_4PPh_2)_2$}] (X = Br, I) were also isolated [164]. Two products were formed from $BiCl(o\text{-}C_6H_4PPh_2)_2$ and [Ir(acac)(COD)], identified as [Ir^{I}(acac){$BiCl(o\text{-}C_6H_4PPh_2)_2$}] and [$Ir^{III}$(acac)Cl{$Bi(o\text{-}C_6H_4PPh_2)_2$}], which are in equilibrium in solution [164].

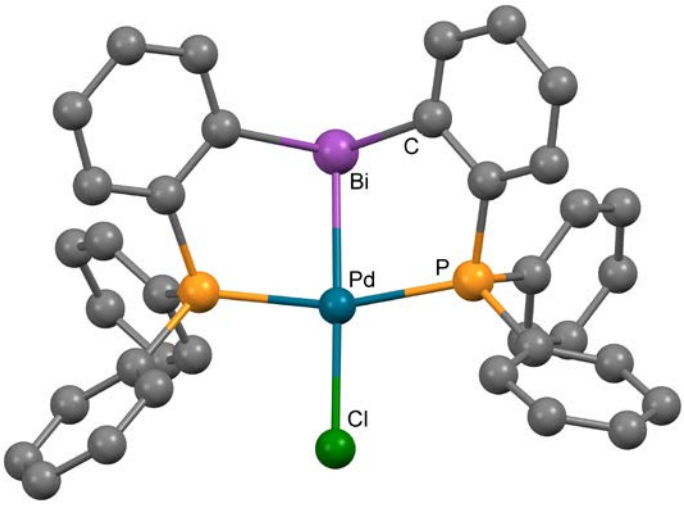

Fig. 53: Structure of [$PdCl${$Bi(o\text{-}C_6H_4PPh_2)_2$}], redrawn from Ref. 164.

8. Systematics of Structure and Bonding

The understanding of the nature of the bonds between metals and pnictines has evolved slowly over the past seventy years. The original view (the Chatt model) saw the phosphorus in a PR_3 ligand

forming a σ-bond to the metal utilising the lone pair in an sp^3 hybrid orbital and a π-acceptor bond with metal electron density transferred into phosphorus 3d orbitals [165]. For metal oxidation states of +2 or greater, the σ-interaction was dominant (and maybe exclusive), whilst in lower oxidation states a π-acceptor component seemed essential. Whilst quantification of the σ and π components proved elusive, the model was generally accepted and applied to the heavier pnictines essentially unchanged. When it became evident that the phosphorus 3d orbitals were too high in energy to form a significant π-bond, the Orpen-Connelly modification, which proposed that the acceptor orbitals were P-C σ* or a symmetry-allowed combination of P-C σ* and 3d orbitals, was introduced [166], and again this model was used for the heavier pnictines. Some differences as Group 15 was descended were noted, for example, the C-E-C angles in EPh_3 decreased down the group E = P 103°, As 100°, Sb 96°, Bi 94°, which resulted as the pnictogen s-p orbital energies diverged, resulting in the C-E bonds having greater p-character. By the 1990s, the accumulation of X-ray crystallographic data allowed these effects to be probed in more detail. Notably, a study of some 1292 examples (1860 fragments) of M-PPh_3 complexes from the CSD by Orpen [167] noted that the geometry of the PPh_3 was little changed on coordination to transition metal centres. That this largely unchanged geometry may not be replicated for stibine complexes was evident in some tungsten carbonyl complexes, e.g $[W(CO)_5(\kappa^1\text{-}Ph_2SbCH_2SbPh_2)]$, where the C-Sb-C angles of the coordinated antimony widen by ≤ ~8° upon coordination, whilst those at the unbound group are unchanged from those in the 'free' distibine [168].

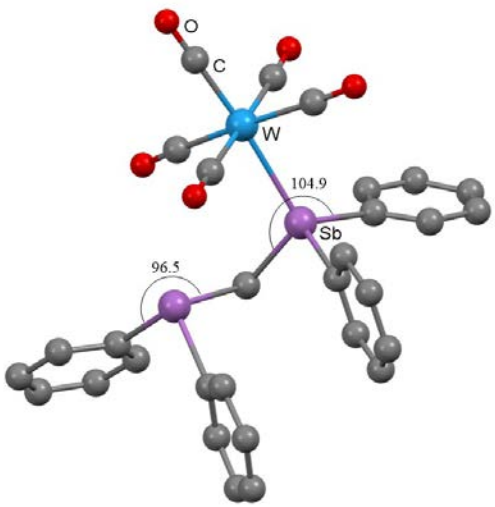

Fig. 54 Structure of $[W(CO)_5(\kappa^1\text{-}Ph_2SbCH_2SbPh_2)]$, redrawn from Ref. 168.

Study of the structures of 130 M-$SbPh_3$ examples taken from CSD showed that in all cases the C-Sb-C angles increased upon coordination and d(Sb-C) slightly shortened (the examples were mostly of late d-block or coinage metals) [2,169]. This was rationalised by proposing that on coordination the Sb-C orbitals had greater s-character and the donated "lone pair" higher p-character. Very few

structures of M-$BiPh_3$ were available, but these too showed a widening of the C-Bi-C angles on coordination, similarly explained, although the effect of coordination on d(Bi-C) was less clear [170].

In the last twenty years, structural data on stibine complexes of a wider range of metals has become available (Sections 2,4,6,7) and the development of DFT calculations has allowed accurate simulation of the structures and detailed exploration of the bonding. The widening of the C-Sb-C angles and some shortening of the Sb-C bonds appears to be found in all areas - notable recent examples are Au(I) complexes of $SbPh_{3-n}(C_6H_2Me_3)_n$ (n = 1-3) [123], trialkylstibine complexes of chromium and tungsten carbonyls [37], $SbEt_3$ and Sb^iPr_3 complexes of the group 13 trihalides [125]. The DFT calculations confirm that the changes on coordination are due to changes in the Sb 5s and 5p components of the Sb-M and Sb-C bonds. For example, NBO analysis of $[Au(SbPh_3)_n]^+$ (n = 2-4) shows that the Sb-C is ~ 10% Sb(5s) in $SbPh_3$, which increases to 15-20% in the complexes [123]. Similarly, the Sb(5s) contribution to Sb-C in the two trialkylstibines is ~11%, which increases to ~22-25% in the Group 13 trihalide complexes [125]. More X-ray structural data are also now available for bismuthines, and these show clearly that similar widening of the C-Bi-C angle and shortening of Bi-C bond effects are observed, and DFT calculations confirm this is due to changes in the bismuth 6s and 6p orbital contributions to Bi-C on coordination [8,37,43].

Of course it is also necessary to consider steric effects, and the Tolman cone angle model remains a valuable means of ranking steric contributions of the ligands, but increasingly the cone angles are refined from X-ray structural data [e.g. 43,87,123] rather than obtained by geometric calculations.

The data on halostibine complexes is limited, but shows similar changes in geometry about the antimony on coordination [28,30,35].

DFT methods have been used to explore the secondary bonding (hypervalency) of coordinated halostibines to halide ions in the series $[PdCl_2(SbMe_2Cl)_n]$ (n = 1-4) where the coordination about the antimony changes from pseudotetrahedral to approaching trigonal bipyramidal and shown to involve Cl(lone pair) → Sb-Cl σ* interaction [35]. The hypervalent Cl → Sb interaction occurs *trans* to an existing Sb-Cl bond, and has a significant orbital overlap rather than being simply electrostatic. X-ray crystal structures of $[Pd_2Cl_4(SbMe_2Cl)_4]\cdot$solv (solv = 2.4 C_6H_6, 2.2 CH_2Cl_2) show minimal differences in the core bond lengths and angles from the unsolvated form, but whilst the solvent molecules do not interact directly with the complex, the angles about the antimony centres have Cl···Sb···Sb···Cl torsion angles which vary from ~28° to ~3° [35]. The differences are ascribed to packing effects, but do show the relative weakness of the hypervalent interactions. Hypervalency in other systems also manifests itself in significant distortions about the coordinated antimony towards trigonal bipyramidal, typically with the hypervalent interaction *trans* to the Sb-X bond [5].

One notable difference between stibines and their lighter analogues is the very rare formation of stibine bridges between metal centres. Essentially three systems need consideration: $[Rh_2X_2(\mu^2\text{-}Sb^iPr_3)(\mu^2\text{-}CR_2)_2]$(X = C, Br, I, acac, O_2CMe, O_2CCF_3) (Fig. 55) [4,79], $[Pd_4(\mu^3\text{-}SbMe_3)_4(SbMe_3)_4]$ [34]], $[M_3(\mu^2\text{-}Cl)_3\{Sb(o\text{-}C_6H_4P^iPr_2)_3\}]$(M = Cu, Ag) [157], as well as the unique bismuthine examples, $[M_3(\mu^2\text{-}Cl)_3\{Bi(o\text{-}C_6H_4P^iPr_2)_3\}]$ [157].

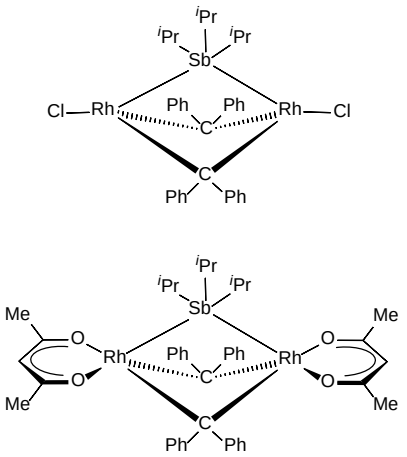

Fig. 55: Two rare examples of stibine bridges redrawn from Ref. 4.

The chemistry of $[Rh_2X_2(\mu^2\text{-}Sb^iPr_3)(\mu^2\text{-}CR_2)_2]$ has been reviewed by Werner [4] and is not described in detail here. It contains a significant number of examples, although these represent a narrow range of types. All contain two carbene bridges and a Rh-Rh interaction in addition to the bridging stibine; the terminal X-groups also influence the chemistry and stability significantly. Attempts to prepare complexes with bridging PR_3 or AsR_3 directly were unsuccessful, but metathesis of the stibine in some (but not all) $[Rh_2X_2(\mu^2\text{-}Sb^iPr_3)(\mu^2\text{-}CR_2)_2]$ with PR_3 produced $[Rh_2X_2(\mu^2\text{-}PR_3)(\mu^2\text{-}CR_2)_2]$ and eventually $[Rh_2X_2(\mu^2\text{-}AsMe_3)(\mu^2\text{-}CR_2)_2]$ were isolated. DFT calculations indicate that both strong σ-donation Sb→M and significant π-acceptance into the Sb-C σ* orbitals are important contributions to the stability. It seems that only in a very limited number of situations do the bonding energies favour μ^2-coordination over κ^1. DFT calculations on the $[Rh_2X_2(\mu^2\text{-}Sb^iPr_3)(\mu^2\text{-}CR_2)_2]$ systems showed Rh to be the best metal from Group 9 to form such complexes, but with Ir also a valid target, although the Ir complexes remain unknown [79]. Cobalt did not appear likely to form such complexes.

The complex containing the triply bridging $SbMe_3$, $[Pd_4(\mu^3\text{-}SbMe_3)_4(SbMe_3)_4]$ [34]], is presently unique both in being the only example of a μ^3 tertiary monopnictine and in having no other donor ligand types present (i.e. homoleptic $SbMe_3$ coordination). The crystal structure, which has a Pd_4 tetrahedron (Fig. 18) appears (from NMR studies) to be retained in solution and exchange between the μ^3- and κ^1 -$SbMe_3$ bonding modes does not occur at ambient temperatures on the NMR time-

scale. The κ^1-Sb-Pd distance is 2.520(av) Å, while the μ^3-Sb-Pd distance is 2.773(av) Å, with the bridging stibines effectively equidistant from each Pd atom on the triangular face.

In the $[M_3(\mu^2\text{-}Cl)_3\{Sb(o\text{-}C_6H_4P^iPr_2)_3\}]$ (M = Cu, Ag) [157] (Fig. 46) an equilateral triangle of Cu or Ag atoms with three μ^2-Cl ligands below the plane, and each copper/silver is coordinated to a terminal phosphine donor of the $Sb(o\text{-}C_6H_4P^iPr_2)_3$ ligand, which places the antimony symmetrically over the triangular face. The d(Cu-Sb) are longer, ~2.80 Å, than in copper complexes of tertiary stibines, ~ 2.5-2.6 Å. but still clearly a significant interaction. The bonding of the antimony to to M_3 unit was viewed as a four-centre two-electron system utilising the antimony 5s electron pair [157]. The bismuthine complexes are analogous, but DFT calculations indicate the bonding energy of the bismuth to the metals is significantly less, as would be anticipated.

The scarcity of reports to-date of bridging by stibine or bismuthine ligands makes it unlikely that many examples will exist and at present their experimental discovery remains rather serendipitous.

In Section 7.2 the oxidation of metal-stibine groups (L-type ligand) in polydentate stibine-phosphine ligands was described and the nature of the 'non-innocent' products, X- or Z-type ligands, identified by a combination of X-ray structural data and DFT calculations. A smaller number of cases of M→Bi donation were also discussed. The distribution of electron density in the bonding orbitals in the M-Sb or M-Bi framework in these complexes covers a significant range within the different series, and the results of the DFT calculations are often subtle and complex as detailed in the original publications [e.g. 7,17,19,20,151,154,160,162]. Currently this behaviour is limited to metals of Groups 10 and 11, as well as one Ir example, and it remains to be seen whether L-type antimony centres bonded to earlier transition metals can be oxidised in a similar manner to X- or Z-type without loss from the metal.

9. Applications

The aim of this section was not to provide comprehensive coverage, but rather to illustrate the types of new applications of stibine complexes being developed.

Transition metal phosphine complexes have played a central role in homogeneous catalysis for the last seventy years, but the development of active catalysts containing stibine ligands is much more recent. Organonickel complexes as olefin oligomerisation reagents have attracted significant recent effort [89-94]. The complexes $[Ni(C_6F_5)_2(SbPh_3)_2]$ and $[Ni(C_6Cl_2F_3)_2(SbPh_3)_2]$ have been used in the synthesis of polynorbornenes, where the ready displacement of the $SbPh_3$ leads to high yields of high molecular mass polymers; corresponding complexes of $AsPh_3$ or PPh_3 are much less successful [94]. Functionalised polymers with silicon or tin groups can be made by vinyl addition norbornene polymerisation with these catalysts [89,90,91]. Siloxane functionalised polynorbornenes have high

thermal stabilities and considerable potential for CO_2/N_2 separation as a route to CO_2 capture and sequestration from power stations [92].

The complexes, $[Ni(\eta^3\text{-}C_3H_5)(SbPh_3)_2]Y$ (Y = $B\{3,5\text{-}(CF_3)_2C_6H_3\}_4$], $[Al\{OC(CF_3)_3\}_4]$), catalyse the polymerisation of butadiene in aqueous solution or in aqueous emulsions [95]. Cationic and neutral nickel-allyl species, $[Ni(\eta^3\text{-}CH_2C(R)CH_2)(SbPh_3)_3][B\{3,5\text{-}(CF_3)_2C_6H_3\}_4]$ (R = CH_3, H); $[Ni(\eta^3\text{-}CH_2CHCH_2)(PPh_3)(L)][B\{3,5\text{-}(CF_3)_2C_6H_3\}_4]$ (L = $SbPh_3$, $AsPh_3$) and $[Ni(\eta^3\text{-}CH_2C(R)CH_2)Br(SbPh_3)]$ (R = CH_3, H) are active catalysts for styrene and α-methylstyrene conversion to dimers, trimers or higher oligomers depending upon the reaction conditions [98]. Nickel indenyl complexes, $[Ni(\eta^5\text{-}R_n\text{-}Ind)(SbPh_3)_2]BF_4$ (R_n = H, 1-Me, 2-Me, 1-$SiMe_3$, 1,3-Me_2) (Fig. 17) and $[Ni(\eta^5\text{-}Ind)(AsPh_3)(SbPh_3)_2]BF_4$ are also highly active in styrene oligomerisation [96,97].

Potential palladium(II) catalysts for co-polymerisation of norbornenes include neutral *trans*-$[PdX(C_6F_5)L_2]$ and cationic *trans*-$[Pd(C_6F_5)L_2(MeCN)]BF_4$ (X = Cl, Br; L = $SbPh_3$, $AsPh_3$, $As(C_6Cl_2F_3)Ph_2$, $AsCyPh_2$, $AsMePh_2$, PPh_3), where the cations show high activity [101]. The half-sandwich compounds, $[(\eta^5\text{-}C_5H_5)Pd(C_6F_5)L]$ (L = ^tBuNC, PPh_3, PMe_2Ph, $AsPh_3$, $SbPh_3$) were examined as norbornene and norbornene/5-vinyl-2-norbornene polymerisation catalysts after activation with methylaluminoxane, which found that complexes of the weaker bound pnictines were more active [107].

Palladium cross-coupling reagents containing $SbPh_3$ ligands include *trans*-$[PdCl_2(NHC)(SbPh_3)]$ (Hiyama coupling of aryls and Buchwald-Hartwig amination) [102]; $[Pd(NHC)(allyl)(SbPh_3)]ClO_4$ (Sonagashira coupling of alkynes and aryl bromides) [103]; $[\{FcC(S)OEt\}PdCl(ER_3)]$ (Suzuki-Miyaura coupling of aryl bromides and arylboronic acids) [105].

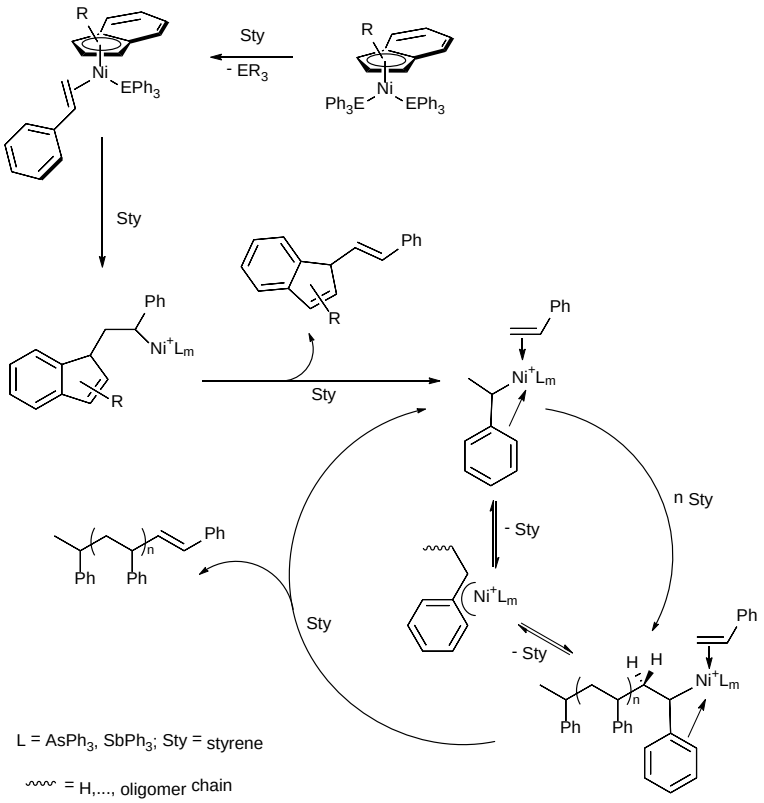

Fig. 56: Possible mechanistic pathway for the oligomerisation of styrene, redrawn from Ref. 96.

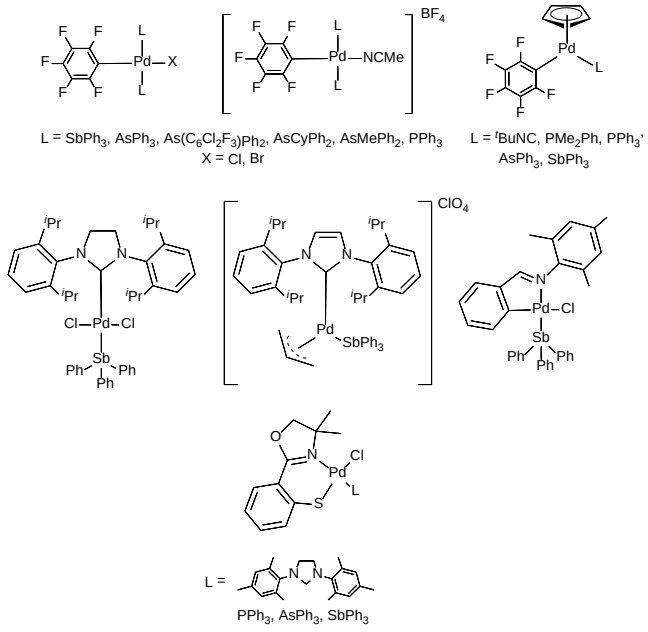

Fig. 57: Structure of some palladium cross-coupling reagents containing $SbPh_3$ ligands.

The complexes, [PdCl(S-Phoz)(L)] (S-Phoz = 2-(2-thiophenyl)-4,4-dimethyloxazoline, L = N,N'-bis-(2,4,6-trimethylphenyl)imidazolidin-2-ylidene, PPh_3, $AsPh_3$, $SbPh_3$) were evaluated as catalysts for the coupling of p-bromoacetophenone with phenylboronic acid in water; disappointingly in this case the activity as a function of the neutral donor ligand was lowest for L = $SbPh_3$ 104]. Microwave or infrared assisted cross-coupling reactions (Heck or Suzuki) using the sulfur-containing palladocycles,

[{FcC(S)OEt}PdCl(ER_3)] (Fc = ferrocenium; ER_3 = PPh_3, PMe_3, $SbPh_3$) (Fig. 20) were explored with IR radiation, which was found to be a highly efficient energy source [105].

The unusual stiborane complexes described in Section 7.2 have active catalytic properties based upon their Lewis acidity [7,17,158], although this chemistry falls outside the scope of the present article.

Trialkylstibine complexes of trialkyls of Group 13 (Al, Ga, In) have been explored in some detail as reagents for deposition of the metal antimonide semi-conductor films, and details of previous work are covered in several reviews [2,171,172]. Further studies of gallium complexes have been reported and the formation of GaSb films or nanowires described [133-136]. Disappointingly, attempts to use [$GaCl_3(SbR_3)$] or [$InCl_3(SbR_3)$] (R = Et, ^nBu) as low pressure chemical vapour deposition reagents for GaSb or InSb films were unsuccessful, with deposition of elemental antimony observed instead [131]. This contrasts with the successful generation of thin films of Ga_2Se_3 and Ga_2Te_3 using gallium trichloride complexes of selenoether and telluroether ligands [173].

The development of stibine complexes to deposit other metals has not received much attention. However the relatively weak M-Sb and Sb-C bonds may suggest this is a route worthy of some study. For example, heating a copper-coated silicon wafer with a fluorobenzene solution of [$Ni(Sb^iPr_3)_2I_2$] produced a layer of Cu-Ni alloy on the wafer, while the stibine scavenged the iodine as $^iPr_3SbI_2$ [87].

Copper cuboid clusters [$Cu_4I_4(SbR_3)_4$] have been described as possible thermoluminescent components for electronic devices [116,117].

As already described (Section 7.2) the yellow [PdCl{Sb(*o*-$C_6H_4PPh_2)_3$}]BPh_4 (planar SbP_2Cl coordination) reacts with a CH_2Cl_2 solution of [$^nBu_4N$]F to produce the deep orange fluorostiboranyl complex [PdCl{SbF(*o*-$C_6H_4PPh_2)_3$}], which had a trigonal bipyramidal geometry (SbP_3Cl coordination). The colour change, which is due to the changed palladium geometry, is the basis of a fluoride ion sensor. Whilst the insolubility do the Pd(II) complex prevents is use in pure water, even very dilute aqueous fluoride solutions layered with a CH_2Cl_2 solution of [PdCl{Sb(*o*-$C_6H_4PPh_2)_3$}]BPh_4 produce a detectable colour change [7,154].

10. Conclusions and Outlook

It is clear from a comparison of the chemistry of stibine ligands described above with that reported in the previous review [2], that the area has undergone major changes in the last 15 years, most notably in the chemistry of the mixed-donor polydentates (Section 7). Nonetheless significant unexplored areas meriting detailed studies remain. Trialkylstibines have been used much more widely and a range of new distibine ligands (Section 2) described. The ligand *o*-$C_6H_4(SbMe_2)_2$, which is the strongest coordinating distibine, still lacks a high yield synthesis that would encourage detailed study of its complexes. Despite producing a seven-membered chelate ring, the *o*-xylyl linked *o*-

$C_6H_4(CH_2SbMe_2)_2$ is at least a partial replacement. Only one tristibine, $MeC(CH_2SbPh_2)_3$, is known and a limited number of complexes were prepared in the 1990s [174]; $MeC(CH_2SbR_2)_3$ (R = alkyl) and linear tridentates are potential targets. A significant number of mixed-donor polydentates containing antimony in combination with O, N, S or P (E) donor groups have been prepared and their complexes examined in considerable detail (Sections 2 and 7). It is notable that some linkages, such as $-CH_2CH_2-$ do not form in distibines, but in hybrids the $-SbCH_2CH_2E-$ link appears relatively robust. There are no antimony macrocycles and very little work attempting their synthesis. A twelve-membered ring SbN_2 macrocycle (Scheme 1 VII) is known [14], but its coordination chemistry remains unexplored. The chemistry of the open-chain hybrids would suggest that mixed-donor macrocycles containing antimony may be more stable and easier to obtain than antimony-only examples. New bismuthine ligands have also been prepared and the reported chemistry of the mixed donor polydentates is a significant advance. Dibismuthines are few [2] and the ready scrambling of substituents on bismuth remains a major barrier. Thorough characterisation of some trialkylbismuthine complexes is also a notable advance.

For many years stibine coordination chemistry was mostly focused on late d-block metals in medium or low oxidation states or substituted metal carbonyl complexes. The last 15 years have seen considerable extention into other areas of the Periodic Table. In the p-block, earlier work was mostly focused on the adducts of the triel trialkyls as routes to metal-antimonide materials, but the recent work (Section 4.4) has shown that trialkylstibine complexes $[MX_3(SbR_3)]$ (M = Al, Ga, In; X = Cl, Br, I) are readily obtained in the absence of moisture and dioxygen, and less stable boron analogues have also been characterised. It should be possible to obtain cationic triel complexes with chelating distibines, which would have increased Lewis acidity; these may form spontaneously as in $[MX_2(L\text{-}L)_2][MX_4]$ (L-L = diphosphine or diarsine) [172,175]. Group 14 complexes look less likely. Stibines are chlorinated to R_3SbCl_2 by $SnCl_4$, and $GeCl_4$ [137], and although not reduced, neither SnF_4 or GeF_4 form complexes even with arsines [175]. In Group 12 there appear to be no reported complexes with zinc or cadmium halides, and few mercury examples, an area worth re-examination. The other major unexplored area is complexes of the early d-block metal halides. Although a small number of complexes of ScI_3 and YI_3 with chelating alkyl diphosphines have recently been reporterd [176], diarsine analogues did not form, and stibine complexes seem very unlikely. However, from Group 4 through Group 6 complexes of alkyl stibines and distibines with metal halides or oxide halides should be obtainable under carefully controlled conditions. The corresponding phosphine and arsine complexes have played significant roles in this area since the mid 20th century, and exploring stibine analogues would seem overdue. The recent synthesis of telluroether complexes of $NbCl_4$, $NbCl_5$ and

$TaCl_5$ [177] is a relevant analogy here, since telluroethers are readily halogenated to R_2TeX_2 and not normally considered as good ligands for high oxidation state metals.

Section 9 has described recent interest in developing catalysts based upon metal stibines for olefin oligomerization and a variety of cross-coupling reactions. Identifying the best combination of metal, stibine and co-ligands for optimal performance remains a challenge, but several active systems have been identified and much further work is to be expected. The use of $[MR_3(SbR_3)]$ (M = Al, Ga, In, R = alkyl) as synthons for MSb materials is well established [171, 172], but the relative weakness of the Sb-C bond may make other metal stibine complexes suitable precursors for LPCVD (low pressure chemical vapour deposition) or AACVD (aerosol assisted chemical vapour deposition) of metal-antimony materials as tin films or nanowires. With a few exceptions, e.g. [87], this area does not seem to have been examined.

The chemistry of the polydentate mixed-donor stibine-phosphine ligands described in Section 7.2 and in some cases the oxidation of the coordinated stibine to stiboranyl or stiborane groups, is a highlight of stibine coordination chemistry in the last 10 years, and further developments, including whether a wider range of metal-stibines will show this behaviour, will be eagerly awaited. The corresponding chemistry of some bismuthine-phosphine ligands, although currently less extensive, is even more surprising in the light of the limited chemistry of metal bismuthines and the perception that fission of the weak Bi-C bonds would be found in most systems.

Finally, we note that although new complexes with bridging stibines [34,79,157] and the first example of a triply-bridging bismuth centre [157] have been characterised, identification of some further examples may be expected if the metal/co-ligand fragment can provide the required electronic environment.

Acknowledgements

We thank the Engineering and Physical Sciences Research Council for funding (EP/P025137/1). The X-ray structures shown were drawn using data from the Cambridge structural database.

Statement of Interest

The authors have no to interests to declare.

References

[1] N. R. Champness, W. Levason, Coord. Chem. Rev. 133 (1994) 115.

[2] W. Levason, G. Reid, Coord. Chem. Rev. 250 (2006) 2565.

[3] W. Levason, G. Reid, Comprehensive Coordination Chemistry II, 1 (2003) 377.

[4] H. Werner, Angew. Chem. Int. Ed. 43 (2004) 938.

[5] S. L. Benjamin, G. Reid, Coord. Chem. Rev. 297-298 (2015) 168.

[6] C. I. Rat, C. Silvestru, H. J. Breunig, Coord. Chem. Rev. 257 (2013) 818.
[7] J. S. James, F. P. Gabbaï, Acc. Chem. Res. 49 (2016) 857.
[8] S. Schulz, A. Kuczkowski, D. Bläser, C. Wölper, G. Jansen, R. Haack, Organometallics, 32 (2013) 5445.
[9] W. Levason, M. L. Matthews, G. Reid, M. Webster, Dalton Trans. (2004) 51.
[10] M. D. Brown, W. Levason, G. Reid, M. Webster, Dalton Trans. (2006) 5648.
[11] M. Jura, W. Levason, G. Reid, M. Webster, Dalton Trans. (2008) 5774.
[12] M. F. Davis, M. Jura, W. Levason, G. Reid, M. Webster, J. Organomet. Chem. 692 (2007) 5589.
[13] S. L. Benjamin, L. Karagiannidis, W. Levason, G. Reid, M. C. Rogers, Organometallics 30 (2011) 895.
[14] M. Jura, W. Levason, G. Reid, M. Webster, Dalton Trans. (2009) 7811.
[15] S. L. Benjamin, W. Levason, G. Reid, Organometallics 32 (2013) 2760.
[16] A. Garcia-Romero, A. J. Plajer, D. Miguel, D. S. Wright, A. D. Bond, C. M. Alvarez, R. Garcia-Rodriguez, Inorg. Chem. 59 (2020) 7103.
[17] I.-S. Ke, F. P. Gabbaï, Inorg. Chem. 52 (2013) 7145.
[18] C. Tschersich, C. Limberg, S. Roggan, C. Herwig, N. Ernsting, S. Kovalenko, S. Mebs, Angew. Chem. Int. Ed. 51 (2012) 4989.
[19] T.-P. Lin, I.-S. Ke, F. P. Gabbaï, Angew. Chem. Int. Ed. 51 (2012) 4985.
[20] C. Tschersich, S. Hoof, N. Frank, C. Herwig, C. Limberg, Inorg. Chem. 55 (2016) 1837.
[21] C. Tschersich, B. Braun, C. Herwig, C. Limberg, Organometallics 34 (2015) 3782.
[22] A. J. Kosanovich, A. M. Jordan, N. Bhuvanesh, O. V. Ozerov, Dalton Trans. 47 (2018) 11619.
[23] W. Levason, G. Reid, Comprehensive Coordination Chemistry II 3 (2003) 465.
[24] W. Levason, M. E. Light, S. Maheshwari, G.Reid, W. Zhang, Dalton Trans. 40 (2011) 5291.
[25] S. L. Benjamin, J. Burt, W. Levason, G. Reid, M. Webster, J. Fluorine Chem. 135 (2012) 108.
[26] S. L. Benjamin, W. Levason, G. Reid, R. P. Warr, Organometallics 31 (2012) 1025.
[27] H. J. Breunig, E. Lork, O. Moldovan, R. Wagner, Z. Anorg. Allg. Chem. 634 (2008) 1397.
[28] H. J. Breunig, T. Borrmann, E. Lork, C. I. Rat, J. Organomet. Chem. 692 (2007) 2593.
[29] H. J. Breunig, M. Denker, K. H. Ebert, J. Organomet. Chem. 470 (1994) 87.
[30] S. L. Benjamin, W. Levason, M. E. Light, G. Reid, S. M. Rogers, Organometallics 33 (2014) 2693.
[31] Y.-Z. Li, R. Ganguly, W. K. Leong, Organometallics 33 (2014) 3867.
[32] Y.-Z. Li, W. K. Leong, J. Organomet. Chem. 812 (2016) 217.
[33] Y.-Z. Li, R. Ganguly, W. K. Leong, Y. Liu, Eur. J. Inorg. Chem. (2015) 3861.
[34] S. L. Benjamin, T. Krämer, W. Levason, M. E. Light, S. A. Macgregor, G. Reid, J. Am. Chem. Soc. 138 (2016) 6964.
[35] A. Jolleys, B. R. M. Lake, T. Krämer, S. L. Benjamin, Organometallics 37 (2018) 3854.
[36] S. L. Benjamin, W. Levason, G. Reid, M. C. Rogers, R. P. Warr, J. Organomet. Chem. 708-709 (2012) 106.
[37] H. J. Breunig, T. Borrmann, E. Lork, O. Moldovan, C. J. Rat, R. P. Wagner, J. Organomet. Chem. 694 (2009) 427.
[38] R. D. Adams, W. C. Pearl Jr, J. Organomet. Chem. 695 (2010) 937.

[39] R. D. Adams, G. Elpitiya, Polyhedron 103 (2016) 131.
[40] A. Antinolo, J.-C. Pérez-Flores, M. J. Hervás, S. Garcia-Yuste, M. I. Lopez-Solera, A. Otero, A. R. Fernadez-Pachero, M. T. Tercero-Morales, Organometallics 32 (2013) 862.
[41] S. L. Benjamin, Y-P. Chang, C. Gurnani, A. L. Hector, M. Huggon, W. Levason, G. Reid, Dalton Trans. 43 (2014) 16640.
[42] W. Levason, G. Reid, W. Zhang, J. Fluorine Chem. 172 (2015) 62.
[43] H. J. Breunig, E. Lork, C. I. Rat, R. P. Wagner, J. Organomet. Chem. 692 (2007) 3430.
[44] K. J. Asali, M. El-khateeb, Y. Foudeh, H. Abul-Futouh, J. Coord. Chem. 70 (2017) 3810.
[45] A. J. van Rensburg, M. Landman, M. M. Conradie, E. Erasmus, J. Conradie, Electrochimica Acta 246 (2017) 897.
[46] A. J. van Rensburg, M. Landman, P. H. van Rooyen, M. M. Conradie, E. Erasmus, J. Conradie, Polyhedron 133 (2017) 307.
[47] M. Landman, A. J. van Rensburg, P. H. van Rooyen, M. M. Conradie, J. Conradie, New J. Chem. 42 (2018) 7301.
[48] W. Levason, F. M. Monzittu, G. Reid, W. Zhang, Chem. Commun. 54 (2018) 11681.
[49] C. I. Pongor, Z. Gengeliczki, L. Szepes, F. Axe, B. Sztaray, Organometallics 29 (2010) 724.
[50] R. D. Adams, B. Captain, W.C. Pearl Jr, J. Organomet. Chem. 693 (2008) 1636.
[51] R. D. Adams, W. C. Pearl Jr, Organometallics 29 (2010) 3887.
[52] R. D. Adams, M. B. Hall, W. C. Pearl, Jr., X. Yang, Inorg. Chem. 48 (2009) 652.
[53] M. A. Shestopalov, Yu. V. Mironov, K. A. Brylev, V. E. Fedorov, Rus. Chem. Bull., 57, (2008) 1644.
[54] W. Wei, T. Zheng, J. Zhao, G. Zeng, Z. Shi, L. Zhu, J. Organomet. Chem. 777 (2015) 67.
[55] R. Boddhula, A. Ghosh, C. Wölper, S. M. Mobin, S. Giri, S. Chatterjee, J. Organomet. Chem. 851 (2017) 22.
[56] S. Ghosh, A. Rahaman, G. Orton, G. Gregori, M. Bernat, U. Kulsume, N. Hollingsworth, K. B. Holt, S. E. Kabir, G. Hogarth, Eur. J. Inorg. Chem. (2019) 4506.
[57] E. S. Donovan, H. M. Plummer, A. S. Parada, G. S. Nicol, G. A. N. Felton, Inorg. Chim. Acta 487 (2019) 387.
[58] M. El-khateeb, T. Obidate, M. Al-Noaimi, Phosphorus, Sulfur, Silicon Rel. Elem. 184 (2009) 585.
[59] M. El-khateeb, J. Mol. Struct. 1123 (2016) 300.
[60] M. El-khateeb, M. Harb, A. Mansour, S. Yousuf, Inorg. Chim. Acta 486 (2019) 694.
[61] M. El-khateeb, R. Kumar, S. Yousuf, J. Mol. Struct. 1211 (2020) 128092.
[62] M. El-khateeb, H. Abul-Futouh, H. Görls, W. Weigand, Monatsch. Chemie 150 (2019) 1461.
[63] M. El-khateeb, A. Mansour, I. Jibril, T. Ruffer, H. Lang, Polyhedron 133 (2017) 63.
[64] M. El-khateeb, M. Al-Noaimi, A. A. Al-Akhras, H. Gorls, W. Weigand, J. Coord. Chem. 65 (2012) 2510.
[65] O. bin Shawkataly, I. A. Khan, S. S. Sirat, C. S. Yeap, H. K. Fun, Acta Crystallog. Sect. E. 67 (2011) m177.
[66] O. bin Shawkataly, I. A. Khan, C. S. Yeap, H. K. Fun, Acta Crystallog. Sect. E. 66 (2010) m94.
[67] G. Chen, W. K. Leong, J. Cluster Sci. 17 (2006) 111.

[68] M. D. Randles, M. P. Cifuentes, G. J. Moxey, A. Zahl, R.van Eldik, M. G. Humphries, J. Organomet. Chem. 849-850 (2017) 63.
[69] V. M. Cornejo, J. O. Mancilla, S. L. Morales, J. A. O. Fortino, S. Hernandez-Ortega, L. Alexandrova, R. L. Lagadec, J. Organomet. Chem. 799-800 (2015) 299.
[70] Y.-Z. Li, R. Ganguly, W. K. Leong, Organometallics 33 (2014) 823.
[71] K. H. Chan, W. K. Leong, K. H. G. Mak, Organometallics 25 (2006) 250.
[72] Y.-Z. Li, R. Ganguly, W. K. Leong, J. Organomet. Chem. 820 (2016) 46.
[73] E. C. Morrison, W. K. Leong, J. Tan, J. Cluster Sci. 18 (2007) 753.
[74] L. J. Pereira, W. K. Leong, J. Organomet. Chem. 691 (2006) 1941.
[75] L. J. Pereira, W. K. Leong, J. Organomet. Chem. 691 (2006) 2448.
[76] L. J. Pereira, W. K. Leong, Polyhedron 25 (2006) 2392.
[77] D. Morrogh, S. Schwarz, C. Maichle-Mössmer, J. Strähle, Z. Anorg. Allgem. Chem. 632 (2006) 801.
[78] P. Schwab, N. Mahr, J. Wolf, H. Werner, Angew. Chem. Int. Ed. 33 (1994) 97.
[79] S. Schinzel, R. Müller, S. Riedel, H. Werner, M. Kaupp, Chem. Eur. J. 17 (2011) 7228.
[80] S. Otto, A. Roodt, Inorg. Chem. Commun. 11 (2008) 114.
[81] C. Hennion, K. J. Jonasson, O.F. Wendt, A. Roodt, Dalton Trans. 42 (2013) 14134.
[82] G. Tamasi, R. Cini, D. G. Musaev, K. Morokuma, Polyhedron 28 (2009) 3675.
[83] R. Cini, G. Tamasi, S. Defanzio, M. Corsini, F. Berrettini, A.Cavaglioni, Polyhedron 25 (2006) 834.
[84] B. A. Chambers, M. Buhl, P. S. Nejman, A. M. Z. Slawin, D. J. Woollins, P. Kilian, J. Organomet. Chem. 799-800 (2015) 70.
[85] M.Bosch, H. Werner, Organometallics 29 (2010) 5646.
[86] D. Tofan, C. C. Cummings, Chem. Sci., 3 (2012) 2474.
[87] W. V. Taylor, Z.-L. Xie, N. I. Cool, S. A. Shubert, M. J. Rose, Inorg. Chem. 57 (2018) 10364.
[88] J. A. Casares, P. Espinet, J. M. Martinez-llarduya, J. J. Mucientes, G. Salas, Inorg. Chem. 46 (2007) 1027.
[89] N. Belova, R. Nikiforova, L. Starannikova, K. R. Gmernicki, C. R. Maroon, B. K. Long, V. Shantarovich, Y. Yampolskii, Eur. Polymer J. 93 (2017) 602.
[90] N. Carrera, E. Gutierrez, R. Benavente, M. Mar Villavieja, A. C. Albeniz, P. Espinet, Chem. Eur. J. 14 (2008) 10141.
[91] S. Martınez-Arranz, A. C. Albeniz, P. Espinet, Macromolecules 43 (2010) 7482.
[92] K. R. Gmernicki, E. Hong, C. R. Maroon, S. M. Mahurin, A. P. Sokolov, T. Saito, B. K. Long, ACS Macro Letters 5 (2016) 879.
[93] J. A. M. de la Torre, A. C. Albeniz, Eur. J. Inorg. Chem. (2017) 2911.
[94] J. A. Casares, P. Espinet, J. M. Martín-Alvarez, J. M. MartínezIlarduya, G. Salas, Eur. J. Inorg. Chem. (2005) 3825.
[95] B. Korthals, A. Berkefeld, M. Ahlmann, S. Mecking, Macromolecules 41 (2008) 8332.
[96] C. S. B. Gomes, S. I. Costa, L. C. Silva, M. Jimenez-Tenorio, P. Valerga, M. C. Puerta, P. T. Gomes, Eur. J. Inorg. Chem. (2018) 597.

[97] C. S. B. Gomes, P. Krishnamoorthy, L. C. Silva, S. I. Costa, P. T. Gomes, M. Jimenez-Tenorio, P. Valerga, M. C. Puerta, Dalton Trans. 44 (2015) 17015.
[98] M. Jimenez-Tenorio, M. C. Puerta, I. Salcedo, P. Valerga, I. de los Rios, K. Mereiter, Dalton Trans.(2009) 1842.
[99] D. G. Evans, D. M. P. Mingos, J. Organomet. Chem. 240 (1982) 321.
[100] G. Salas, J. A. Casares, P. Espinet, Dalton Trans. 39 (2009) 8413.
[101] J. A. Casares, P. Espinet, G. Salas, Organometallics 27 (2008) 3761.
[102] J. Yang, P. Li, Y. Zhang, L. Wang, Dalton Trans. 43 (2014) 14114.
[103] J. Yang, J. Organomet. Chem. 883 (2019) 35.
[104] C. Holzer, A. Dupé, L. M. Peschel, F. Belaj, N. C. Mösch-Zanetti, Eur. J. Inorg. Chem. (2018) 568.
[105] J. A. Balam-Villarreal, C. I. Sandoval-Chavez, F. Ortega-Jimenez, R. A. Toscano, M. P. Carreon-Castro, J. G. Cortez, M. C. Ortega-Alfaro, J. Organomet. Chem. 818 (2016) 7.
[106] H. Wang, J. Yang, App. Organomet. Chem. 30 (2016) 262.
[107] F. Blank, J. K. Vieth, J. Ruiz, V. Rodriguez, C. Janiak, J. Organomet. Chem. 696 (2012) 473.
[108] D. Perez, P. Sharma, M. Sharma, S. Hernandez, Acta Crystallog.Sect. E. 69 (2013) m372.
[109] D. C. Babbini, F. L. Mulligan, H. R. Schulhauser, T. C. Sweigart, G. S. Nichol, S. K. Hurst, Inorg. Chem. 49 (2010) 4307.
[110] V. V. Sharutin, V. S. Senchurin, A. P. Pakusina, O. K. Sharutina, and B. B. Kunkurdonova, Russ. J. Gen. Chem. 80 (2010) 1753.
[111] G. J. Grant, D. A. Benefield, D. G. VanDerveer, Dalton Trans. 40 (2009) 8605.
[112] G. J. Grant, D. A. Benefield, D. G. VanDerveer, J. Organometal. Chem. 695 (2010) 634.
[113] M. Bouché, G. Dahm, A. Maisse-François, T. Achard, S. Bellemin-Laponnaz, Eur. J. Inorg. Chem. (2016) 2828.
[114] P. Sharma, D. Perez, N. Rosas, A. Cabrera, A. Toscano, J. Organometal. Chem. 691 (2006) 579.
[115] M. D. Brown, W. Levason, G. Reid, M. Webster, Dalton Trans. (2006) 1667.
[116] W. V. Taylor, U. H. Soto, V. M. Lynch, M. J. Rose, Inorg. Chem. 55 (2016) 3206.
[117] W. V. Taylor, C. X. Cammack, S. A. Shubert, M. J. Rose, Inorg. Chem. 58 (2019) 16330.
[118] L. Yang, J. Tehranchi, W. B. Tolman, Inorg. Chem. 50 (2011) 2606.
[119] L. Weber, J. Krümberg, H.-G. Stammler, B. Neumann, Z. Anorg. Allg. Chem. 632 (2006) 879.
[120] A. V. Chupina, V. Shayapov, A. S. Novikov, V. V. Volchek, E. Benassi, P. A. Abramov, M. N. Sokolov, Dalton Trans. 49 (2020) 1522.
[121] C. N. Banti, C. Papatriantafyllopoulou, M. Manoli, A. J. Tasiopoulos, S. K. Hadjikakou, Inorg. Chem. 55 (2016) 8681.
[122] E. I. Gkaniatsou, C. N. Banti, N. Kourkoumelis, S. Skoulika, M. Manoli, A. J. Tasiopoulos, S. K. Hadjikalou, J. Inorg. Biochem. 150 (2015) 108.
[123] V. R. Bojan, E. J. Fernandez, A. Laguna, J. M. Lopez-de-Luzuriaga, M. Monge, M. E. Olmos, R. C. Puelles, C. Silvestru, Inorg. Chem. 49 (2010) 5530.
[124] I. Egorova, V. Zhidkov, I. Zubakina, N. Rodianova, I. Eltsov, J. Organomet. Chem. 907 (2020) 121077.

[125] V. K. Greenacre, W. Levason, G. Reid, Organometallics 37 (2018) 2123.
[126] J. Burt, J. W. Emsley, W. Levason, G. Reid, I. S. Tinkler, Inorg. Chem. 55 (2016) 8852.
[127] S. Yasuike, K. Nakata, W. Qin, M. Matsumura, N. Kakusawa, J. Kurita, J. Organometal. Chem. 788 (2015) 9.
[128] R. Bhalla, J. Burt, A. L. Hector, W. Levason, S. K. Luthra, G. McRobbie, F. M. Monzittu, G. Reid, Polyhedron 106 (2016) 65.
[129] S. Schulz, A. Kuczkowski, M. Nieger, H. Saxell, J. Organometal. Chem. 695 (2010) 2281.
[130] D. Schuchmann, A. Kuczkowski, S. Fahrenholz, S. Schulz, U. Flörke, Eur. J. Inorg. Chem. (2007) 931.
[131] K. R. Cairns, V. K. Greenacre, L. A. Grose, W. Levason, G. Reid, F. Robinson, J. Organometal. Chem. 912 (2020) 121176.
[132] C. Hering, M. Lehmann, A. Schulz, A. Villinger, Inorg. Chem 51 (2012) 8212.
[133] A. Heckel, G. Bendt, L. John, C. Wölper, S. Schulz, App. Organomet. Chem. 32 (2018) e4430.
[134] S. Schulz, A. Kuczkowski, M. Nieger, J. Chem. Crystallogr. 40 (2010) 1163.
[135] S. Schulz, M. Schwartz, A. Kuczkowski, W. Assenmacher, J. Crystal Growth 312 (2010) 1475.
[136] D. Schuchmann, S. Schulz, U. Flörke, Acta Crystallogr. Sect. E 63 (2007) m1606.
[137] V. K. Greenacre, R. P. King, W. Levason, G. Reid, Dalton Trans. 48 (2019) 17097.
[138] S. L. Benjamin, W. Levason, G. Reid, M. C. Rogers, Dalton Trans. 40 (2011) 6565.
[139] E. Bayram, S. Ozkar, J. Organomet. Chem. 691 (2006) 3267.
[140] S. P. Oh, Y.-Z. Li, W. K. Leong, J. Organometal. Chem. 783 (2015) 46.
[141] M. D. Brown, W. Levason, G. Reid, M. Webster, Dalton Trans. (2006) 4039.
[142] D. J. Gulliver, W. Levason, K. G. Smith, J. Chem. Soc., Dalton Trans. (1981) 2153.
[143] C. Di Nicola, G. A. Koutsantonis, C. Pettinari, B. W. Skelton, N. Somers, A. H. White, Inorg. Chim. Acta 359 (2006) 2159.
[144] D. Copolovici, F. Isaia, H. J. Breunig, C. I. Rat, C. Silvestru, RSC Advances 4 (2014) 26569.
[145] D. Pérez, P. Sharma, N. Rosas, A. Cabrera, J. L. Arias, F. del Rio-Portilla, J. Vazquez, R. Gutierrez, A. Toscano, J. Organomet. Chem. 693 (2008) 3357.
[146] A. J. Plajer, A. L. Colebach, F. J. Ruzzoto, P. Pröhm, A. D. Bond, R. Garcia-Rodriguez, D. S. Wright, Angew. Chem. Int. Ed. 57 (2018) 6648.
[147] B. Chiswell in Transition Metal Complexes of Phosphorus, Arsenic and Antimony ligands, C. A. McAuliffe (ed) MacMillan, London 1973. Chapter 4.
[148] M. L. H. Green, J. Organomet. Chem. 500 (1995) 127.
[149] S. Sen, I.-S. Ke, F. P. Gabbaï, Inorg. Chem. 55 (2016) 9162.
[150] J. S. Jones, C. R. Wade, F. P. Gabbaï, Angew. Chem. Int. Ed. 53, (2014) 8876.
[151] J. S. Jones, C. R. Wade, M. Yang, F. P. Gabbaï, Dalton Trans. 46 (2017) 5598.
[152] J. W. Dawson, L. M. Venanzi, J. Amer. Chem. Soc. 90 (1968) 7229.
[153] B. R. Higginson, C. A. McAuliffe, L. M. Venanzi, Inorg. Chim. Acta 5 (1971) 37.
[154] C. R. Wade, I.-S. Ke, F. P. Gabbaï, Angew. Chem. Int. Ed. 51 (2012) 478.

[155] I.-S. Ke, J. S. Jones, F. P. Gabbaï, Angew. Chem. Int. Ed. 53 (2014) 2633.
[156] J. S. Jones, C. R. Wade, F. P. Gabbaï, Organometallics 34 (2015) 2647.
[157] I.-S. Ke, F. P. Gabbaï, Aust. J. Chem. 66 (2013) 1281.
[158] J. S. Jones, F. P. Gabbaï, Chem. Eur. J. 23 (2017) 1136.
[159] C. R. Casey, F. P. Gabbaï, Angew. Chem. Int. Ed. 50 (2011) 7369.
[160] K. Materne, B. Braun-Cula, C. Herwig, N. Frank, C. Limberg, Chem. Eur. J. 23 (2017) 11797.
[161] K. Materne, S. Hoof, N. Frank, C. Herwig, C. Limberg, Organometallics 36 (2017) 4891.
[162] H. Yang, F. P. Gabbaï, J. Amer. Chem. Soc. 137 (2015) 13425.
[163] D. You, F. P. Gabbaï, J. Amer. Chem. Soc.139 (2017) 6843.
[164] C. Tschersich, B. Braun, C. Herwig, C. Limberg, Organometallics 34 (2015) 3782.
[165] A. Pidcock in Transition Metal Complexes of Phosphorus, Arsenic and Antimony ligands, C. A. McAuliffe (ed) MacMillan, London 1973. Chapter 1.
[166] A. G. Orpen, N. G. Connelly, Organometallics 9 (1990) 1206.
[167] B. J. Dunne, R. B. Morris, A. G. Orpen, J. Chem. Soc., Dalton Trans. (1991) 653.
[168] A. M. Hill, N. J. Holmes, A. R. J. Genge, W. Levason, M. Webster, S. Rutschow, J. Chem. Soc., Dalton Trans. (1998) 825.
[169] N. J. Holmes, W. Levason, M. Webster, J. Chem. Soc., Dalton Trans. (1998) 3457.
[170] N. J. Holmes, W. Levason, M. Webster, J. Organometal. Chem. 584 (1999) 179.
[171] S. Schulz, Coord. Chem. Rev. 215 (2001) 1.
[172] J. Burt, W. Levason, G. Reid, Coord. Chem. Rev. 260 (2014) 65.
[173] K. George, C. H. de Groot, C. Gurnani, A. L. Hector, R. Huang, M. Jura, W. Levason, G. Reid, Chem. Mater. 25 (2013) 1829.
[174] A. F. Chiffey, J. Evans, W. Levason, M. Webster, Organometallics 15 (1996) 1280.
[175] J. Burt, W. Levason, M.E. Light, G. Reid, Dalton Trans. 43 (2014) 14600.
[176] M. Carravetta, M. Concistre, W. Levason, G. Reid, W. Zhang, Inorg. Chem. 55 (2016) 12890.
[177] Y.-P. Chang, W. Levason, G. Reid, Dalton Trans. 45 (2016) 18393.